Stockholm University

Catalytic and Electrocatalytic Transformations with Palladium and Nickel

Scope and mechanistic investigations

Alejandro Valiente Sánchez

Doctoral Thesis in Organic Chemistry at Stockholm University, Sweden 2021

Catalytic and Electrocatalytic Transformations with Palladium and Nickel

Scope and mechanistic investigations

Alejandro Valiente Sánchez

Academic dissertation for the Degree of Doctor of Philosophy in Organic Chemistry at Stockholm University to be publicly defended on Friday 10 December 2021 at 10.00 in Magnélisalen, Kemiska övningslaboratoriet, Svante Arrhenius väg 16 B and online via Zoom, public link is available at the department website.

Abstract

The work presented in this thesis is based on methodology development and mechanistic investigations using heterogeneous palladium and nickel catalysts. Following the introduction (Chapter 1), Chapter 2 presents a summary of the synthesis and characterization of the MOF-supported Pd catalysts (Pd @ MOF) that are used in this thesis. Chapters 3, 4 and 5 are based on the use of heterogeneous Pd @ MOF catalysts for CC bond forming reactions, whilst Chapter 6 deals with the use of nickel foam for hydrogenation reactions.

In Chapter 3, the speciation of the ligandless Suzuki-Miyaura reaction catalyzed by Pd @ MOF is investigated. Here, questions regarding the composition, structure and reactivity of leached palladium are studied by means of electrospray ionization mass spectrometry (ESI-MS), density-functional theory (DFT) calculations, nuclear magnetic resonance (NMR) spectroscopy and scanning-transmission electron microscopy (STEM). (Paper I)

The next chapter (Chapter 4) deals with the study of the Mizoroki-Heck reaction catalyzed by Pd @ MOF under working conditions. In this study, catalyst activation, catalyst deactivation and the role of the MOF support are studied. (Paper II)

Chapter 5 concerns the use of MOF-supported Pd (II) complexes for the aerobic homocoupling of boronic acids. A mild oxidation method for regenerating active catalytic palladium species, which enables its recyclability, is described. (Paper III)

The last chapter (Chapter 6) describes the use of a commercially available nickel foam for the stereoselective semireduction of alkynes using electrochemically generated hydrides from acidic water. As the method tolerates numerous functional groups, it could be applied to a large variety of alkynes. The use of deuterated solvents provided easy access to a library of deuterated *Z* -olefins. (Paper IV)

Keywords: *Organic Chemistry, Heterogeneous Catalysis, Metal-organic frameworks, Nickel, Palladium, Electrocatalysis, Cross-coupling, Hydrogenation.*

Stockholm 2021
http://urn.kb.se/resolve?urn=urn:nbn:se:su:diva-198076

ISBN 978-91-7911-668-2
ISBN 978-91-7911-669-9

Department of Organic Chemistry

Stockholm University, 106 91 Stockholm

CATALYTIC AND ELECTROCATALYTIC TRANSFORMATIONS WITH PALLADIUM AND NICKEL

Alejandro Valiente Sánchez

Stockholm University

Catalytic and Electrocatalytic Transformations with Palladium and Nickel

Scope and mechanistic investigations

Alejandro Valiente Sánchez

ISBN print 978-91-7911-668-2
ISBN PDF 978-91-7911-669-9

Cover image: Pd(II)@MIL-101-NH_2 and nickel foam, catalysts that were used in the work that is presented.
Credit: Alejandro Valiente Sánchez

Printed in Sweden by Universitetsservice US-AB, Stockholm 2021

A mis padres

"The way I see it, if you
want the rainbow, you
gotta put up with the rain"

Dolly Parton

Abstract

The work presented in this thesis is based on methodology development and mechanistic investigations using heterogeneous palladium and nickel catalysts. Following the introduction (Chapter 1), Chapter 2 presents a summary of the synthesis and characterization of the MOF-supported Pd catalysts (Pd@MOF) that are used in this thesis. Chapters 3, 4 and 5 are based on the use of heterogeneous Pd@MOF catalysts for C–C bond forming reactions, whilst Chapter 6 deals with the use of nickel foam for hydrogenation reactions.

In Chapter 3, the speciation of the ligandless Suzuki-Miyaura reaction catalyzed by Pd@MOF is investigated. Here, questions regarding the composition, structure and reactivity of leached palladium are studied by means of electrospray ionization mass spectrometry (ESI-MS), density-functional theory (DFT) calculations and scanning-transmission electron microscopy (STEM). **(Paper I)**

The next chapter (Chapter 4) deals with the study of the Mizoroki-Heck reaction catalyzed by Pd@MOF under working conditions. In this study, catalyst activation, catalyst deactivation and the role of the MOF support are studied. **(Paper II)**

Chapter 5 concerns the use of MOF-supported Pd(II) complexes for the aerobic homocoupling of boronic acids. A mild oxidation method for regenerating active catalytic palladium species, which enables its recyclability, is described. **(Paper III)**

The last chapter (Chapter 6) describes the use of a commercially available nickel foam for the stereoselective semireduction of alkynes using electrochemically generated hydrides from acidic water. As the method tolerates numerous functional groups, it could be applied to a large variety of alkynes. The use of deuterated solvents provided easy access to a library of deuterated *Z*-olefins. **(Paper IV)**

Populärvetenskaplig sammanfattning

Från mitt perspektiv är världen en massiv reaktionskolv, och allt liv i den är en fantastisk och förvirrande ”produkt” genererad till följd av kemiska reaktioner som påbörjades för miljontals år sedan. Livets principer börjar och slutar med kemiska omvandlingar, och vi hittar ett av de mest uppenbara exemplen i vår kropps bränslekälla. Kläderna som vi har på oss är i de flesta fall gjorda av polymerer som produceras genom kemiska reaktioner. Många av de läkemedel som vi använder dagligen har utvecklats av kemister i ett laboratorium. Gödningsmedel tillverkas på samma sätt, och deras effekt i grödor möjliggjorde ökningen av världens befolkning. Dessa exempel är bara en liten del av historien. För att uttrycka det enkelt: livet är kemi och vi är omgivna av det. Kemister är som ingenjörer i atomskala eftersom de monterar kemiska startmaterial som kan jämföras med LEGO® byggstenar, med storleken på några ångström (1 ångström = 0,0000000001 meter). För att montera ihop dessa byggstenar krävs i många fall en katalysator, vilket är en substans som utlöser en reaktion. Detta blev fokus för forskargrupper över hela världen sedan katalys upptäcktes på 1800-talet, och det möjliggjorde livet som vi känner det idag.

Vår grupp arbetar med utvecklingen av nya katalysatorer, och samtidigt försöker vi förstå hur de fungerar. Dessa mekanistiska undersökningar utgör fokus för den större delen av denna avhandling (kapitel 2 och 3). Att förstå vilka byggstenar som är inblandade i varje individuellt steg i den kemiska processen, med så stor noggrannhet som möjligt, är viktigt eftersom detta är en förutsättning för utvecklingen av nya och effektivare katalysatorer; för att förbättra något, måste man först veta hur det fungerar.

Parallellt med mekanistiska undersökningar är vår grupp mycket engagerad i hållbarhet och utvecklingen av återvinningsbara katalysatorer för att minimera det kemiska avfallet. I denna avhandling identifieras processer som leder till katalysatordeaktivering, samtidigt som enkla metoder att regenerera katalysatorer undersöks (kapitel 4).

Vi har nyligen börjat utforska hur man kan använda elektricitet och tidiga övergångsmetaller för att transformera byggstenar baserade på kol. I det sista kapitlet i denna avhandling (kapitel 5) utvecklade vi en metod som kombinerar el och vatten som reaktanter, och en nickelplatta som katalysator, för att producera molekyler som oljesyra, en naturlig komponent som förekommer i exempelvis olivolja och frukter.

List of publications
This thesis is based on the following publications:

Paper I

Tetrameric Aryl Palladium Bromide Intermediates Leading to Facile Transmetalation in Suzuki-Miyaura Cross-Couplings with Pd@MIL-101-NH_2
Alejandro Valiente, Cheuk-Wai Tai, Mårten Ahlquist, Belén Martín-Matute.
Manuscript

Paper II

Probing the Evolution of Palladium Species in Pd@MOF Catalysts During the Heck-Mizoroki Coupling Reaction: an Operando X-ray Absorption Spectroscopy Study
Ning Yuan,† Vlad Pascanu,† Zhehao Huang, Alejandro Valiente, Niclas Heidenreich, Sebastian Leubner, A. Ken Inge, Jakob Gaar, Norbert Stock, Ingmar Persson, Belén Martín-Matute, Xiaodong Zou.
J. Am. Chem. Soc. **2018**, *140*, 8206–8217.

Paper III

Aerobic Homocoupling of Arylboronic Acids Catalyzed by Regenerable Pd(II)@MIL-88B-NH_2(Cr)
Alejandro Valiente, Sergio Carrasco, Amparo Sanz-Marco, Cheuk-Wai Tai, Antonio Bermejo Gómez, Belén Martín-Matute.
ChemCatChem. **2019**, *11*, 3933–3939.

Paper IV

Electrochemical Proton Reduction over a Nickel Foam for *Z*-Stereoselective Semihydrogenation/deuteration of Functionalized Alkynes
Alejandro Valiente, Pablo Martínez Pardo,† Gurpreet Kaur,† Magnus Johansson and Belén Martín-Matute.
Accepted for publication in ChemSusChem. DOI: 10.1002/cssc.202102221

Not included in this thesis:
Luminescence Properties of a Family of Lanthanide Metal-Organic Frameworks
Hani Nasser Abdelhamid, Magdalena Wilk-Kozubek, Ahmed M.El Zohryc, Antonio Bermejo Gómez, Alejandro Valiente, Belén Martín-Matute, Anja-Verena Mudring, Xiaodong Zou.
Microporous Mesoporous Mater. **2019**, *279*, 400–406.

† *These authors contributed equally to the publication*

Other documents based on this work

This document is partly based on the author´s half time report titled "Carbon-Carbon coupling reactions catalyzed by palladium supported on metal-organic frameworks". By chapters, the contribution of the half time report in this thesis is as follows:

The introduction was significantly modified as consequence of the new chapters that were introduced, being only *ca.* 50% of sections 1.1 and 1.2 based on the half time report (pages 1 - 5). The literature references of this part were also updated. The rest of the introduction, sections 1.3 and 1.4 (pages 8-14), are new.

Among the chapters including discussion of experimental results (Chapters 2-6), only Chapter 5 is *ca.* 80% as it was presented in the half time report. The references have been updated to reflect the latest developments in this field of research. Chapters 2, 3, 4 and 6 are presented in this thesis for the first time.

Abbreviations

Abbreviations and acronyms are in agreement with the standards in the field.*

ATA	2-Aminoterephthalic acid
BDC	1,4-Benzenedicarboxylate
BF	Bright field
BET	Brunauer-Emmett-Teller
BINAP	2,2′-Bis(diphenylphosphino)-1,1′-binaphthyl)
BPO	Benzoyl peroxide
COD	1,5-Cyclooctadiene
DIPT	Diisopropyl tartrate
DOPA	Dihydroxyphenylalanine
EDG	Electron donating group
EWG	Electron withdrawing group
ESI-MS	Electrospray ionization mass spectrometry
EXAFS	Extended X-ray absorption fine structure
HAADF	High-angle annular dark-field
HER	Hydrogen evolution reaction
HKUST	The Hong Kong University of Science and Technology
IUPAC	International Union of Pure and Applied Chemistry
ICP-OES	Inductively Coupled Plasma Optical Emission Spectrometry
MIL	Matériaux de l′Institut Lavoisier
MOF	Metal-organic Framework
n.d.	Not determined
n.r.	No reaction
NP	Nanoparticle
OER	Oxygen evolution reaction
ppm	Parts per million
ppb	Parts per billion
PSM	Post-synthetic modification
Py	Pyridine
RHE	Reversible hydrogen electrode
QEXAFS	Quick scanning extended X-ray absorption fine structure
SBU	Secondary building unit
SHOP	Shell higher olefin process
STEM	Scanning-transmission electron microscopy
TON	Turn-over number
wt%	Weight percent
XAS	X-Ray absorption spectroscopy
XRPD	X-Ray powder diffraction

** Petronella, K. M. Abbreviations List, The ACS Guide to Scholarly Communication. 2020 (DOI:10.1021/acsguide.50308)*

Table of Contents

1. Introduction

1.1. Catalysis and transition metals

In 1835, J. Berzelius reported for the first time[1] the existence of a "catalytic force" of yet unknown nature that was defined later by Ostwald[2] (Nobel Prize in Chemistry in 1909). A catalyst is a substance that enhances the rate of a chemical reaction by enabling alternative reaction pathways of lower activation energy without being consumed (Figure 1).[3] The overall process is called catalysis, and it is a purely kinetic phenomenon as it does not affect the overall thermodynamics of the transformation.

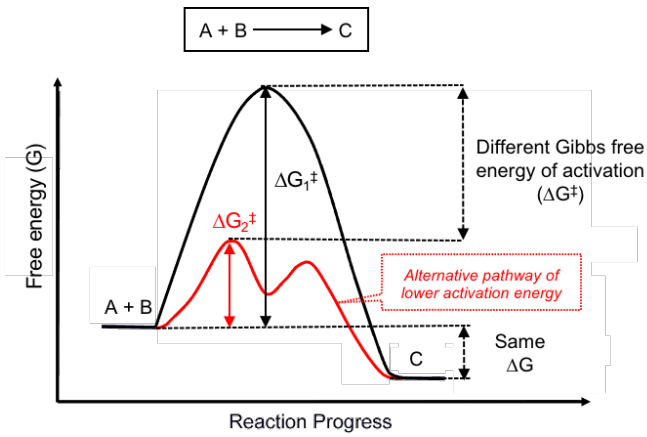

Figure 1. Simplified depiction of the reaction coordinate for a catalyzed (red) and uncatalyzed (black) reaction.

Catalysts come in a multitude of forms, varying from atoms, molecules or polymeric structures (as zeolites or enzymes) to solid surfaces. Enzymes in yeast were used for fermentation to make alcoholic beverage and bread since the beginning of human history, without any notion of catalysis. But since its beginning as a research field, catalysis has had an enormous influence in our society. The Haber-Bosch catalytic process for the synthesis of ammonia is one of the most important examples, whose impact on fertilizer production and crops allowed the global population to increase from 1.6 billion in 1900 to 7.9 billion by 2021.[4,5] The development of this iron-catalyzed process was awarded with the Nobel Prize in Chemistry to Haber in 1918. One of the first

important examples of the use of transition metals in catalysis are the hydrogenation methods developed by Sabatier. His work was recognized with the 1912's Nobel Prize in Chemistry together with Grignard, for the development of organomagnesium compounds.[6]

As versatile as these reagents are, their applicability in organic synthesis is limited. The highly polarized $M^{\delta+}$–$C^{\delta-}$ bond makes the majority of these reagents excellent nucleophiles, but they are also very basic.[7] In the case of transition metals, the presence of *d* electrons in the valence shell and the accessibility to multiple oxidation states makes them suitable to act as electron sinks or sources in the transformation of organic molecules. The discovery of the properties of transition metals was the beginning of a revolution in organic synthesis, as it provided chemists with tools to make transformations that were previously unachievable. Over 80% of the chemically manufactured products, such as fuels, polymers, fibers or pharmaceuticals among others, are synthesized involving at least one catalytic step.[8,9] Some of the most important catalytic transformations in organic chemistry, of which several were recognized with the Nobel Prize, are summarized in Figure 2.[10]

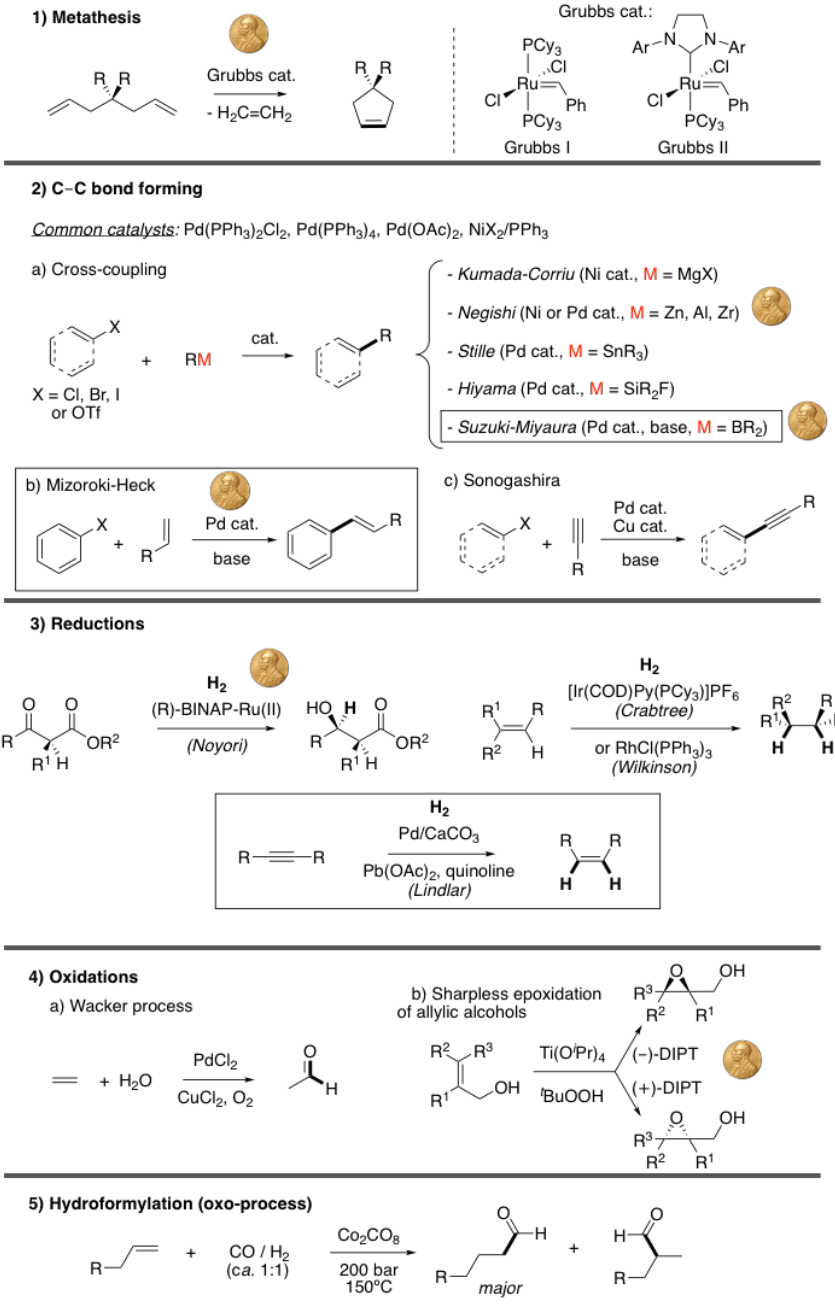

Figure 2. Relevant transition-metal catalyzed transformations in organic chemistry. In squares, reactions that are studied in this thesis.

1.2. Heterogeneous catalysis

Following Ostwald's original criteria,[2] heterogeneous catalysis refers to systems in which the catalyst and the reactant are not in the same phase, unlike homogeneous catalysis where they both operate in the same phase. One major advantage of heterogeneous catalysis is the ease of separation and reuse of the catalyst (see Table 1 for comparison). Despite the growth of homogeneous catalysis, heterogeneous catalysis is still of great significance in industrial processes.[9]

Table 1. General comparison of homogeneous and heterogeneous catalysts.

	Homogeneous	**Heterogeneous**
Advantages	- High activity and selectivity - High tunability - Good mechanistic insight	- High activity and selectivity - High stability - Easy separation and reusability
Limitations	- Tedious product separations - Expensive catalyst recovery	- Low tunability / active site control - Limited mechanistic insight - Surface poisoning
Relevant industrial processes	- Oligomerization of olefins (*e.g.* metathesis, SHOP) - Adiponitrile synthesis - Hydrogenations (*e.g.* metolachlor, L-DOPA) - CO reactions (*e.g.* Monsanto, Oxo-process)	- NH_3 synthesis (Haber-Bosch) - CH_3OH synthesis - Fisher-Tropsch process - Cracking and hydrocracking - Xylene oxidation - Hydrodesulfurization of diesel fuel

The heterogenization of molecular complexes combines the advantages of both heterogeneous and homogeneous catalysts, resulting in catalysts of molecular nature but operationally heterogeneous.[11] This has diminished the gap between homogeneous and heterogeneous catalysis. However, there are cases where this distinction can become certainly ambiguous: metal NPs and clusters. These species do not have molecular nature but they are often completely soluble (operating in the same phase as the reactants). Thus, the accuracy of the classification stands or falls on determining when a growing metal cluster in solution becomes a new phase, which can be challenging.[12] As alternative to the phase criteria, Schwartz[13] and Finke[14] proposed homogeneous and heterogeneous as mechanistic categories, depending on whether the catalytically active species are uniform single metal species or adjacent atoms in a solid surface. In this case, the classification heavily relies on determining the nature

of the true active catalytic centers. The implementation of *operando* spectroscopic techniques allows for an accurate information about the evolution and dominant form(s) of the catalyst.[15] Nevertheless, it must be combined with other techniques to convincingly determine the nature of the active catalyst, and in some cases it might not be conclusive. For example, the rhodium-catalyzed hydrogenation reported by Finke and co-workers, where Rh_4 clusters were found to be the active species, is a case where no clear distinction could be made.[16] In the context of this thesis, the term heterogeneous catalysis will be applied to catalysts supported on a non-soluble matrix, namely metal-organic frameworks (MOFs), regardless of the nature of the catalytically active species.

1.2.1. Metal-organic frameworks (MOFs)

According to IUPAC recommendations, MOFs are defined as *"coordination networks*[a] *with organic ligands whose structure contain potential voids"* (Figure 3).[17]

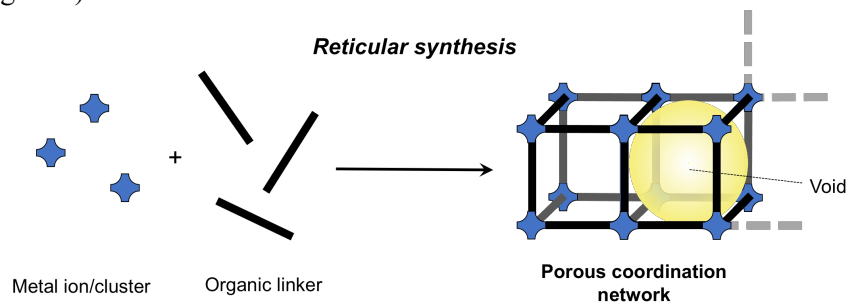

Figure 3. Schematic illustration of the assembly of a MOF.

Prussian Blue, a pigment from the 18th century, is one of the oldest known porous materials and it is considered by some the first member of the MOF family. But the origin of MOFs as an emerging area can be traced back to the work of Saito in the late 1950s, who reported the first examples of coordination networks based on Cu(I) centers linked by dinitriles as adiponitrile.[18–20] Later, in 1986, similar open structures with copper(I) and dinitrile linkers were reported by Hünig.[21] However, it was not until the early 1990s that the field began to grow in the wake of seminal papers by the group of Robson,[22–24] followed by significant developments from the groups of Kitagawa,[25,26]

[a] Coordination polymers in two- or three-dimensions

Moore[27,28] and Yaghi[29–33] (who coined the term MOF) among others.[34–36] By the end of the decade, the approach pioneered by Saito had a turning point with the debut of two stable MOFs after removing the guest solvent molecules: MOF-5[32,33] and HKUST-1.[36] These MOFs were developed by Yaghi and Williams respectively, and they broke internal surface area records with up to 2300 square meters per gram of material.

MOFs are chemically tunable and, due to their porosity, they usually display high internal surface areas. The existence of a carbon-based subunit is a remarkable feature, as organic chemistry tools can be applied for a precise linker design. This has enabled the synthesis of a huge diversity of functional MOFs with tailor-made properties.[37–39] Because of these properties, MOFs are suitable for a wide variety of applications, as gas storage, sensing, drug delivery and, importantly, catalysis.[40]

In the latter case, MOFs can be used in 3 different ways, depending on where the active catalytic sites are located: in the metal nodes, the organic linkers or hosted in the pores.[41–44] A significant part of the work presented in this thesis is focused on the use of MOFs as supports for Pd complexes and NPs. Specifically, we centered our attention in two Cr(III)-based MOFs developed by Férey and co-workers: MIL-101(Cr)[45] and MIL-88B(Cr)[46] (Figure 4). These materials are polymorphs assembled from terephthalic acid (BDC) and chromium trimers, sharing the formula $[Cr_3F(H_2O)_2O(BDC)_3]\cdot nH_2O$ but with network topologies and features that are totally different. In MIL-101(Cr), the secondary building units (SBUs) interconnect to form a rigid and highly porous zeotype structure[47] with cages of 29 and 34 Å and a BET surface area of 4100 square meters per gram. On the contrary, the SBUs in MIL-88B form a flexible hexagonal structure based on channels and cages that can expand or contract in response to the environment, reaching a maximum aperture of 15.6 Å (125% swelling amplitude in MeOH).[48]

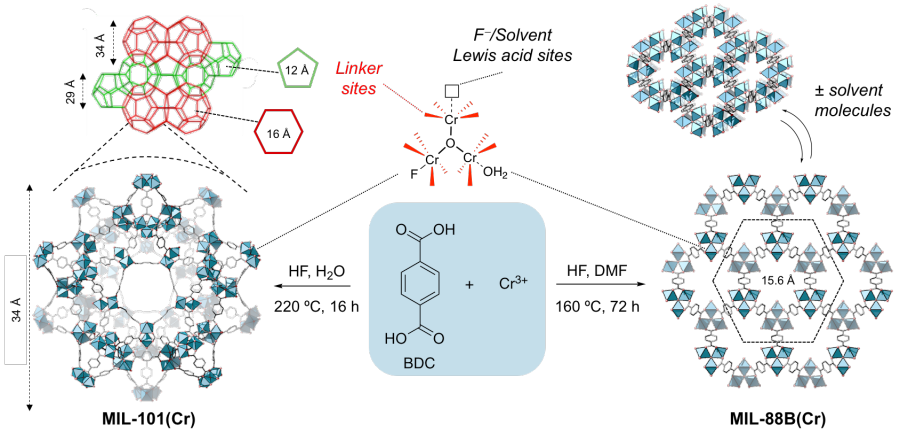

Figure 4. Synthesis of MIL-101(Cr) and MIL-88B(Cr).[45,48,49]

MOFs have been widely used in catalysis as supports for metal NPs.[50] For example, non-functionalized (pristine) MIL-101(Cr) was previously used as support for Pd NPs (Pd@MIL-101) in different of transformations,[51,52] where the work from Jiang and co-workers in 2010 represents the first application of this catalyst on the Suzuki-Miyaura cross-coupling. The introduction of $-NH_2$ groups in MOFs was reported to have a beneficial effect in the stabilization of NPs and limiting metal leaching.[53] Taking this into consideration, our group has reported the synthesis of Pd NPs on MIL-101-NH_2(Cr) and determined an optimal Pd loading in the composite of 8 wt% for outstanding catalytic performance in the Suzuki-Miyaura reaction.[54,55] Furthermore, our group has also studied the effect of the added base on the MOF structure during the cross-coupling reaction.[56] The versatility of Pd@MIL as catalysts is very large, and our group has also explored the applicability of these materials in aerobic oxidation,[57] C–H activation,[58] carbonylation[59] reactions and continuous-flow set-ups.[55,57] The synthesis of Pd@MOF catalysts is described in more detailed in Chapter 2.

Currently, the number of reported MOF structures stands at *ca.* 100000 according to the Cambridge Structural Database (in contrast to *ca.* 250 known zeolites).[b] Until recently, MOFs were believed to be synthetic materials exclusively but Friščić and Krivovichev reported two rare organic minerals, stepanovite and zhemchuzhnikovite, as naturally occurring MOFs.[60]

[b] According to the Database of Zeolite Structures (IZA structure commission).

1.3. Mechanistic investigations in C–C bond forming reactions: the Suzuki-Miyaura and Mizoroki-Heck reactions

Detailed investigations into the evolution of a catalyst under working conditions are essential to understand relevant aspects of the mechanism, such as the nature of the active species and factors controlling reactivity or possible deactivation pathways. In the context of homogeneous catalysis, this can be achieved by means of solution specific techniques but it becomes notoriously challenging in heterogeneous systems such as MOF-supported catalysts.

An important part of this thesis is focused on studying the speciation of palladium complexes and nanoparticles supported on MOFs. In this sense, MOFs are often considered to be "mere" spectators because they do not have an active role in the catalytic cycle. However, they might play an important role in the stabilization of NPs by keeping a certain degree of dispersion, what can have remarkable effects on catalyst's activity.[61] Even considering the aforementioned role, supported NPs are classified within the spectrum of dynamic systems,[62] also termed "cocktails" of catalysts by Ananikov.[63] This concept refers to a pool of interconverting active species with random composition that make noticeable contributions to product formation (Figure 5), which adds a layer of complexity to mechanistic investigations.[64]

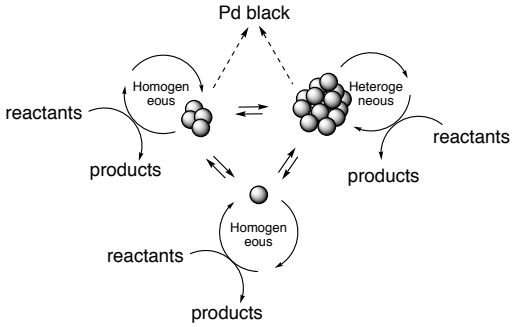

Figure 5. Depiction of the "cocktail" of catalysts concept. Figure adapted from the literature.[64]

For instance, systems lacking ancillary ligands and where either pre-formed or *in situ* generated NPs are in dynamic equilibrium with multiple species are within this category. Ligandless systems have been so largely investigated that the same phenomena has been termed in different ways, among which homeopathic catalysis, leaching and redeposition or nanoparticle reservoir are quite extended.[63] A significant part of the work presented in this thesis is focused on the study of two "cocktail"-type systems: the Suzuki-Miyaura (Chapter 3)

and the Mizoroki-Heck reactions (Chapter 4) catalyzed by Pd@MOF. The catalytic cycles for both of these reactions are markedly different, although they have one elementary step in common: the oxidative addition (Figure 6). Even if the steps involved in product formation are well defined for both processes, the composition and structure of the catalytic intermediates involved is still under debate due to the challenging detection of transient ligandless species. To a large extent this is due to their very low concentration in the reaction mixture, to their limited stability, and to the dynamic interconversion into other species. On the other hand, catalytic intermediates in systems involving dative ligands have reached a better understanding due to the greater control over the reacting centers. More than two decades before cross-couplings were recognized with the Nobel Prize in Chemistry, the research on these two reactions underwent an explosive growth and remains among the most studied palladium-catalyzed transformations.[65–69] In the rest of this section, a summary of relevant mechanistic investigations is presented.

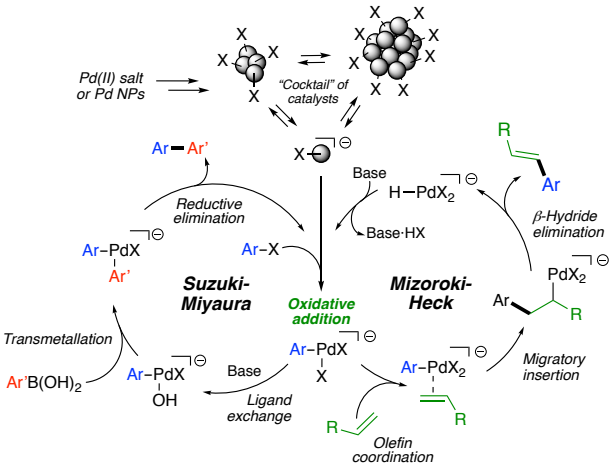

Figure 6. Catalytic cycles for the ligandless Suzuki-Miyaura and Mizoroki-Heck reactions.[69]

1.3.1. The Suzuki-Miyaura cross-coupling

A key aspect in the development of the Suzuki-Miyaura cross-coupling has been the understanding of the specific role of the base in the transmetallation step, and the nature of all the intermediates involved.[70,71] Relevant investigations have been performed by the groups of Schmidt,[72] Hartwig,[73] Jutand and Amatore[74–77] in both ligandless and phosphine-containing systems. These

studies agreed that the base is involved in a key halide exchange step by an oxygen centered nucleophile that enables the transmetallation (Figure 6).

For a long time, the transmetallation step was assumed to involve palladium-oxygen-boron linkages. In 2016, Denmark and co-workers reported the first definitive evidence for this connectivity in phosphine-containing pre-transmetallation intermediates (Figure 7a), that were thoroughly characterized by NMR spectroscopy.[78] Recently, the group of Bissember went one step further confirming the structure of the pre-transmetallation intermediates crystallographically by using phosphine-containing boronic acids that enabled the synthesis of kinetically stable species (Figure 7b).[79]

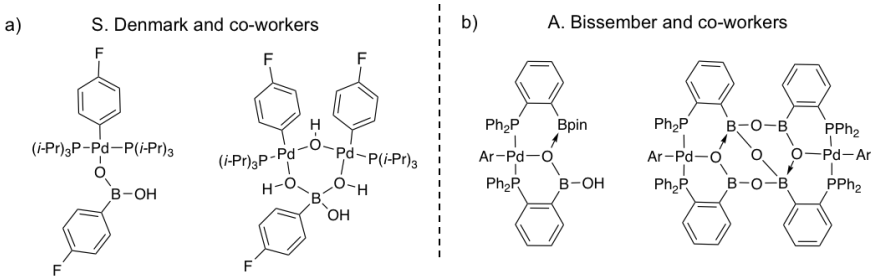

Figure 7. Pre-transmetallation intermediates characterized by NMR spectroscopy and X-Ray crystallography.[78,79]

Besides the aforementioned techniques, electrospray ionization mass spectrometry (ESI-MS) has also been used for the characterization of reaction intermediates. This technique can provide accurate information about the composition of charged species at a given reaction time.[80–84] Generally, there are three approaches that can enable the detection of ionic intermediates: using groups that easily can be ionized, charge-tagged starting materials, or tunning ligand electronics.[85]

In 1994, Canary and co-workers reported the first speciation study on the Suzuki-Miyaura reaction using ESI-MS, where the introduction of 3-bromopyridine provided easy access to $[M+H^+]$ ions.[86] This approach allowed the characterization of post oxidative addition and transmetallation intermediates, providing an accurate snapshot of the catalyst composition (Figure 8a).

Introduction of charge-tagged species in the ligands allowed Neto and co-workers to study ligand exchange processes by ESI-MS in Pd complexes that were used for Suzuki-Miyaura and Mizoroki-Heck couplings.[87] Charge-

tagged ligands have been used to study the speciation of other C–C bond forming reactions, as the Sonogashira coupling.[88] More recently, McIndoe and co-workers monitored the formation of cationic post-oxidative addition intermediates in the Suzuki-Miyaura reaction by real-time ESI-MS, introducing a charge-tagged aryl iodide (Figure 8b).[89]

Electron-poor phosphine ligands have been used for the stabilization and identification of anionic intermediates in cross-coupling reactions (Figure 8c). In 2017, Koszinowski and co-workers reported the composition of a series of molecular Pd(0) and Pd(II)-ate complexes stabilized by tris(3,5-bis(trifluoromethyl)phenyl)phosphine.[90] In a more recent work, the same authors used this approach to investigate the catalytic cycle of cross-coupling reactions involving Grignard reagents and extended the scope of known palladate(0) anions.[91] The detection of single atom Pd complexes was usual in the cases discussed above, although dimers can be also common (*vide infra*).

Corma and co-workers studied Pd speciation in ligandless cross-couplings using ESI-MS and catalytically active Pd(0) clusters of low nuclearity (3 or 4 atoms) were characterized.[92] Whether the active species in "cocktail-type" systems involve single atoms, clusters or a solid surface has been extensively debated.[12] In this regard, Fairlamb and Lee demonstrated for the first time that the Suzuki-Miyaura cross-coupling can be catalyzed on the surface of Pd NPs of *ca.* 1.8 nm. Together with the work from Corma and co-workers, this evidenced that the pool of catalytically active Pd species in ligandless systems is not ruled by a single speciation.

State of the art mechanistic investigations on the Suzuki-Miyaura reaction were performed recently by means of a high-resolution single-molecule model.[93] Guo and co-workers immobilized a single Pd catalyst molecule between nanogapped graphene electrodes and detected electrical signals associated to each of the elementary steps involved in the process.

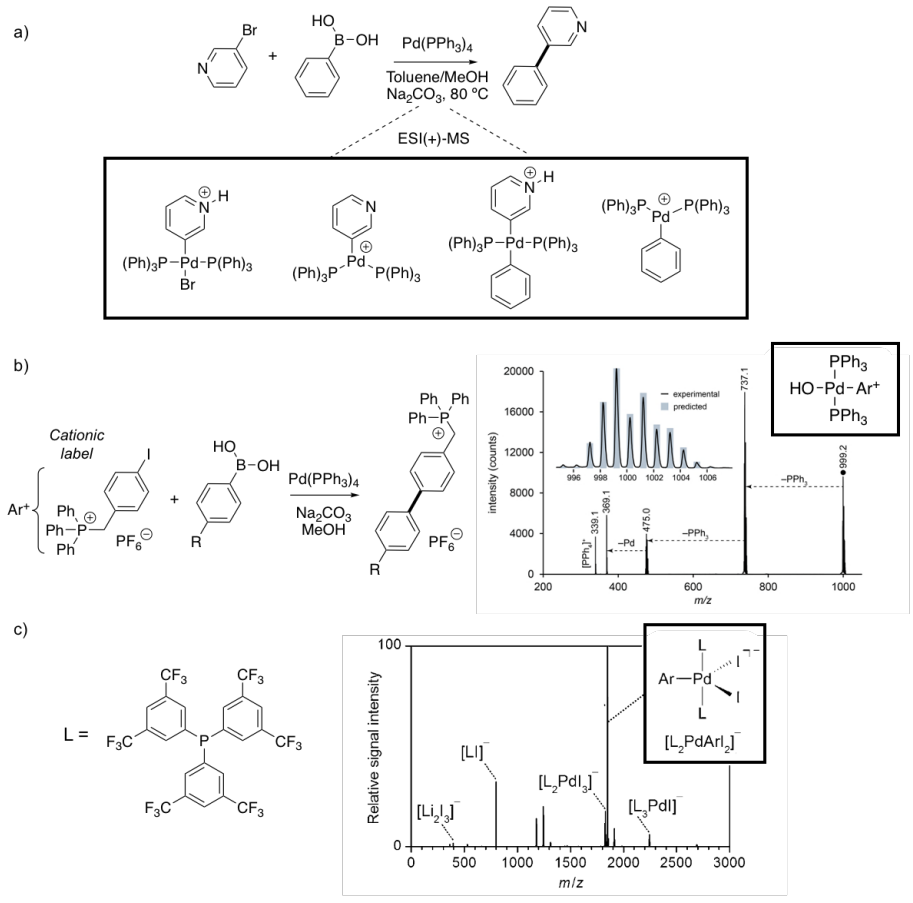

Figure 8. (a) Arylpalladium species detected by Canary and co-workers[86]; (b) use of cationic aryl iodide for the detection of reaction intermediates[89]; (c) use of electron-poor phosphine ligands to stabilize and characterize anionic intermediates.[90]

1.3.2. The Mizoroki-Heck reaction

Among those reactions that are mechanistically related to cross-couplings, the Mizoroki-Heck reaction is by far the most studied.[68,71,94] The original investigations by Heck[95,96] and Mizoroki[97] were mostly based on the use of ligandless Pd(II) pre-catalysts, but systems including phosphine ligands were used later.[98] Amatore, Jutand and co-workers performed seminal investigations on the $Pd(OAc)_2/PPh_3$ system that highlighted the importance of anionic species in the reaction mechanism.[99–102]

Jeffery showed the importance of stabilizing Pd NPs in the Mizoroki-Heck reaction by using tetraalkylammonium salt additives.[103,104] However, Beletskaya,[105] Reetz,[106] and de Vries[107] demonstrated that when the amount of Pd is very low (*e.g.* 0.0005 mol%), additives are no longer needed because Pd black formation is prevented by the high dilution and the high substrate/Pd ratio (therefore, keeping small Pd NPs and clusters).[108]

The use of MS techniques was useful to determine the composition of reaction intermediates,[108,109] but the constant advances in the time resolution of *in situ* XAS methods has provided crucial evidence about the nature of Pd species under working conditions. In 2002, Neisius and co-workers monitored the evolution of $Pd(OAc)_2$ using XAS techniques and identified catalytic intermediates corresponding to oxidative addition species (Figure 9) and isolated $[Pd_2I_6][NEt_3H]_2$ from the reaction mixture.[110]

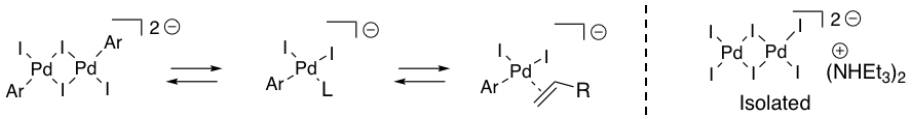

Figure 9. Intermediates proposed and isolated by Neisius and co-workers.[110]

In 2011, Grunwaldt, Baiker and co-workers reported an investigation on the Mizoroki-Heck reaction catalyzed by Pd/Al_2O_3 using XAS techniques (QEXAFS), where Pd evolution was monitored and molecular complexes like $[Pd_2Br_6]^{2-}$ and $[Pd_2Br_4]^{2-}$ were identified.[111] This investigation concluded that the reaction is catalyzed by *in situ* generated molecular Pd(0) whose leaching from NPs was rate determining step. However, NPs were proposed to have a more active role in the catalytic cycle even if there was no direct evidence of adsorbed species on their surface.

In 2006, de Vries proposed a general catalytic cycle that combined the results from many studies where ligandless systems were used, including anionic intermediates in analogy to those suggested by Amatore and Jutand (Figure 10).[108] Here, Pd NPs or $(H_2O)PdOAc^-$ (detected by MS) were proposed as catalytically active species for the oxidative addition step. After completion of a turnover, the resulting Pd(0)-ate complex can redeposit on Pd NPs, form off-cycle species or engage in a new cycle.

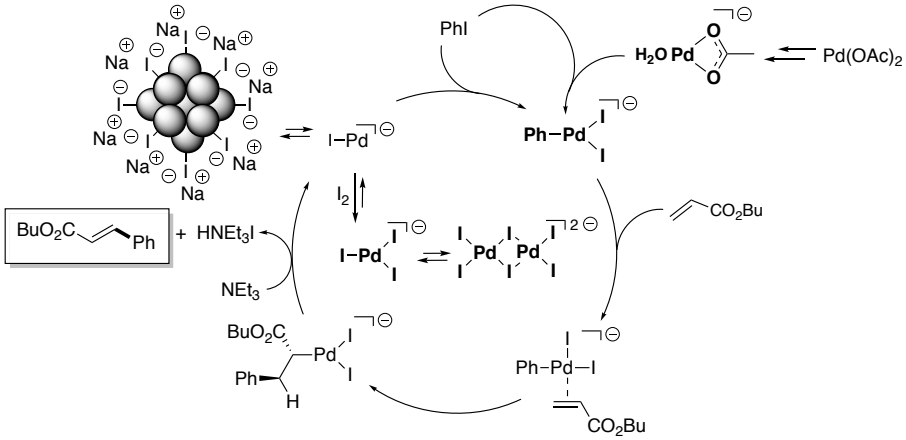

Figure 10. "Unifying" catalytic cycle for high temperature Mizoroki-Heck reactions, adapted from the literature.[108] In bold, species that were characterized by XAS or MS.

1.4. Catalytic and electrocatalytic semihydrogenation of alkynes

The stereoselective synthesis of alkenes is a relevant process in the manufacturing of a variety of natural products, pharmaceuticals and materials, among others.[112,113] The most common synthetic strategies involve the formation of a C–C double bond through olefination or metathesis, cross-coupling reactions, halide elimination or semireduction of alkynes. The latter is one of the few methods that provide *Z*-alkenes in high selectivity, where palladium catalysts are the most commonly used under a hydrogen atmosphere (*e.g.* Lindlar: $Pd/CaCO_3$ and $Pb(OAc)_2$ with quinoline)[114] (Figure 11).[113,115–117]

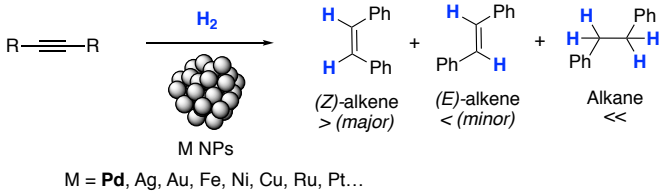

Figure 11. Semihydrogenation of alkynes catalyzed by metal NPs.

The use of earth abundant elements for hydrogenations (*e.g.* nickel), is a desirable alternative to noble metals. Under a hydrogen gas atmosphere, methods based on nickel catalysts typically involve high pressure and temperatures.[118–125] The use of transfer hydrogenation protocols with hypophosphorous acid or formic acid is an alternative to the use of hydrogen gas (Figure 12, a and b).[126–128] Bai and co-workers reported a different approach based on

low loadings of a nickel salt in alcoholic solutions of sodium borohydride, where *in situ* generated Ni NPs of *ca.* 6.2 nm were proposed as active species.[129] The latter catalytic system is one of the few that displays remarkable activity at atmospheric pressure and r.t., however it comes at the cost of using sodium borohydride as the reducing agent.

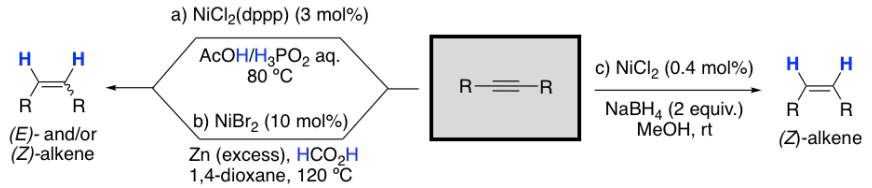

Figure 12. Ni-catalyzed methods for the semireduction of alkynes.[127–129]

Electrochemical methods have allowed the replacement of hydrogen gas or strong reductants by water (alcohols or amines), representing significant advantages from the economic, operational and environmental point of view. The large majority of these systems are based on palladium catalysis.[130]

In 2018, Berlinguette and co-workers reported the electrochemical reduction of 1-hexyne in a 3-chamber cell, where the hydrogenation and cathodic chambers are separated by a dense palladium membrane (Figure 13a).[131] According to the authors, the electrochemically generated hydrides from sulfuric acid can permeate through the palladium cathode to hydrogenate 1-hexyne in the neighboring chamber.

One year later, Ge and co-workers reported another protocol were *in situ* generated Pd NPs were active catalysts for the semihydrogenation reaction in the presence of methanol and other hydrogen sources (*i.e.* dimethylamine and tetrabutylammonium cations, Figure 13b).[132] Applying a constant current of 100 mA, a variety of *Z*-olefins were obtained in good yields and excellent selectivity.

In 2020, Zhang and co-workers reported a remarkable example of this chemistry using a Pd-P alloy as cathode and water as hydrogen source in alkaline media (Figure 13c).[133] Under the working conditions, the rate determining cleavage of O–H bonds in water generates adsorbed hydrogen over the Pd-P cathode that was identified as the catalytically active species of the transformation. Furthermore, the use of deuterated solvents provided with a facile route to semideuterated *Z*-alkenes, which otherwise can be difficult to access.[134,135]

During the current year, the same authors published a similar work this time using a selenium-dopped nickel foam as cathode under basic conditions for the semihydrogenation of terminal alkynes (Figure 13, d).[136] In this case, the authors proposed a mechanism starting with an electron transfer to the coordinated alkyne forming radical anion **I**, which is protonated by water forming radical **II** and finally affording the product upon coupling with the adsorbed hydrogen. This work represents one of the first electrocatalytic examples using a nickel foam and water as starting materials for this transformation.

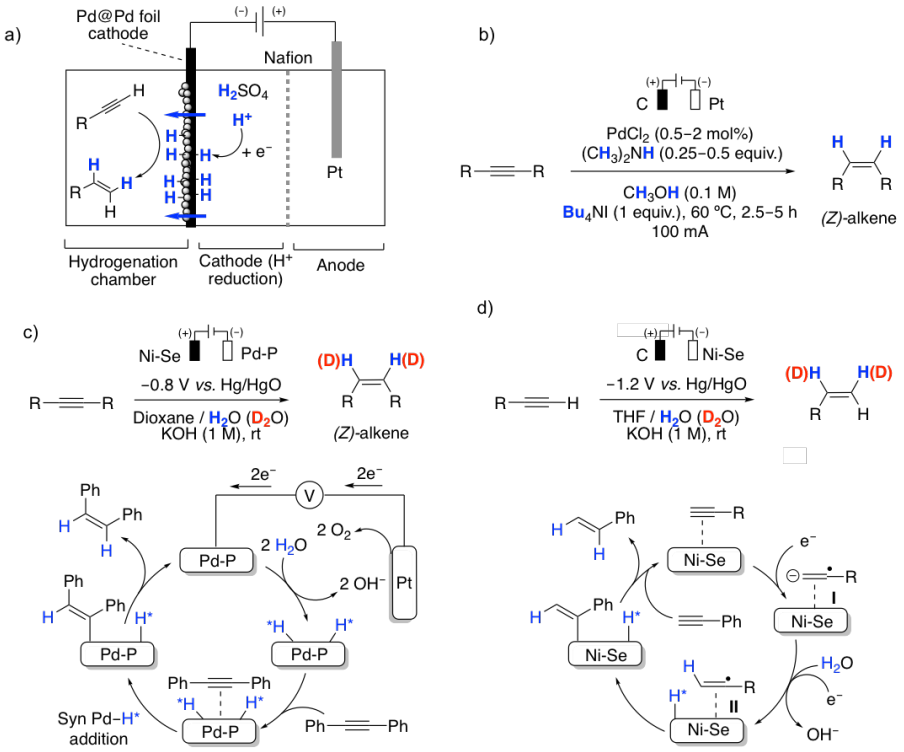

Figure 13. Different methodologies for the electrochemical semihydrogenation of alkynes. Schemes and mechanisms adapted from the literature. [131–133, 136]

Nickel foam (Figure 14a) is a commercially available material with high porosity and electric conductivity that has been widely investigated as electrocatalyst for the hydrogen evolution reaction (HER) in both alkaline and acidic media.[137–139] This material consists of metallic nickel that under ambient conditions forms surface oxide layers of *ca.* 1-2 nm thickness. This passive layer contains mainly α-nickel(II) hydroxide [α-$Ni(OH)_2$] with an underlayer of nickel(II) oxide (NiO), therefore resulting in a three layer structure Ni/NiO/α-$Ni(OH)_2$ (Figure 14a) that can greatly affect its catalytic properties.[140] Under cathodic potentials,

the α-Ni(OH)$_2$ phase can be reduced and act as catalytically active centers for the hydrogen evolution, forming adsorbed hydrogen (M–H*) in the so called Volmer step (Figure 14b).[141]

Importantly, even if the HER can be performed under acid or basic conditions, the corrosion stability of nickel foam is markedly different in each case. Under basic conditions, as in the semihydrogenation reported by Zhang and co-workers (*vide supra*),[136] the nickel foam does not suffer corrosion. Nevertheless, it dissolves under acidic conditions releasing H_2 and Ni^{2+} at potentials above the equilibrium potential (–0.245 V *versus* RHE).[139,142] In this case, nickel foam is stable only if the applied potential is more negative than this value, as the Ni^{2+} released into solution is redeposited in the electrode ($Ni^{2+} + 2e^- \rightarrow Ni^0$). This feature of nickel foam could have important implications in the work presented in Chapter 6.

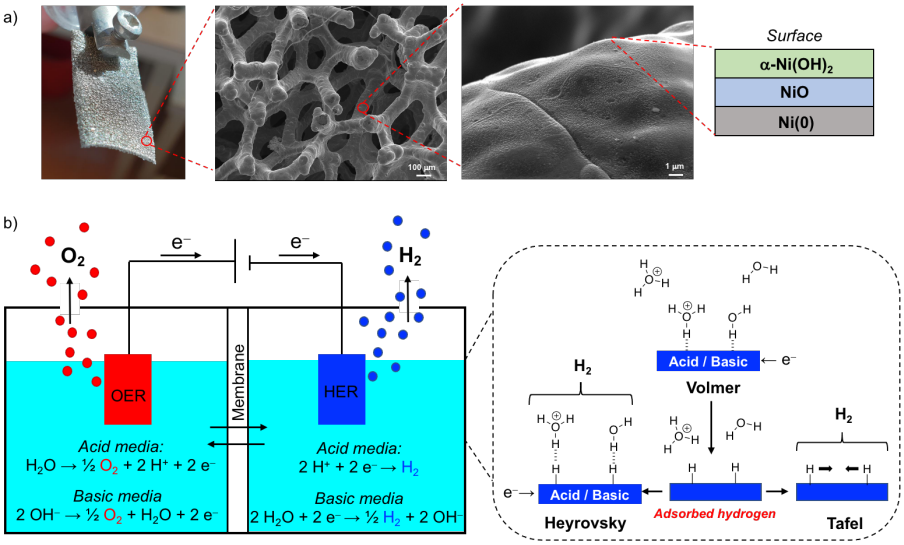

Figure 14. (a) Images of Ni foam and layered surface structure. SEM pictures collected by Dr Gurpreet Kaur; (b) Schematic representation of the water splitting process in a divided cell. Mechanisms involved in the formation of hydrogen adapted from the literature.[143,144]

1.5. Aim of this thesis

The aim of this thesis is the development of heterogeneous catalytic and electrocatalytic reactions based on the use of porous materials, with an emphasis on using MOFs as supports for transition metal catalysts. The reactions selected include heterogeneous C–C bond-forming and hydrogenation reactions catalyzed by palladium supported on MOFs, as well as heterogeneous reactions using earth abundant metal catalysts. In parallel, and intimately related, understanding reaction mechanisms is at the center of attention of our investigations. Important consideration is devoted to the study of catalyst speciation in ligandless systems, the relationship between the size and activity of nanoparticles, as well of the structure of reactive intermediates. Other aspects such as catalyst deactivation and regeneration are also addressed.

2. Synthesis and characterization of Pd NPs on MIL-101-NH_2(Cr) and MIL-88B-NH_2(Cr)

Among the MIL-101 metal analogues (Sc, Ti, V, Cr, Mn, Fe and Al), MIL-101(Cr) is one of the most stable and studied MOFs.[145] This Chapter describes the synthesis of the Cr(III)-based Pd@MOF catalysts used for the projects that are presented in this thesis, as well as their characterization.

The pristine MIL-101(Cr) is synthesized following the original procedure reported by Férey and co-workers,[45] rendering the MOF as a pale green solid in 86% yield (Figure 15). MIL-101-NH_2(Cr) is obtained *via* post-synthetic modification (PSM) of MIL-101(Cr), following a modified procedure from Stock and co-workers.[146] The first PSM step consists of a nitration of MIL-101(Cr) using a H_2SO_4/HNO_3 mixture at 0 ºC, affording MIL-101-NO_2(Cr) as a light green powder in 88% yield (Figure 15). Then, the -NO_2 groups are reduced using $SnCl_2$ in ethanol at 70 ºC, providing MIL-101-NH_2(Cr) as a green powder in quantitative yield. The resulting solid is loaded with palladium(II) following a solution impregnation procedure. MIL-101-NH_2(Cr) is dispersed in a dichloromethane solution containing $PdCl_2(CH_3CN)_2$ and the mixture is stirred for 16 h at r.t. Pd(II)@MIL-101-NH_2(Cr) is obtained as a light brown powder in quantitative yield. By ICP-OES, it was determined that Pd and Cr are present in 7.7 and 12.4 wt%, respectively, indicating a Pd/Cr ratio of 1:3. Therefore, the molecular formula can be expressed as [$PdCr_3F(H_2O)_2O(ATA)_3$], with one Pd per chromium cluster.

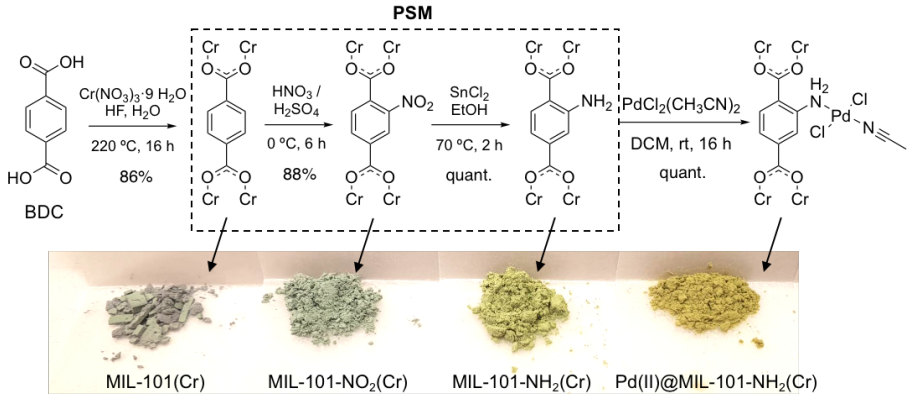

Figure 15. Synthesis of Pd(II)@MIL-101-NH_2(Cr).

MIL-88B-NH_2(Cr) can be obtained *via* a direct synthesis from 2-aminoterephthalic acid under solvothermal conditions, affording an intense green powder in 90% yield (Figure 16).[146] Following a solution impregnation procedure developed by our group,[57] MIL-88B-NH_2 was suspended in a methanol solution containing Na_2PdCl_4 for 72 h, affording Pd(II)@MIL-88B-NH_2(Cr) as a light green powder in quantitative yield (Figure 16).[57] The resulting catalyst was characterized by PXRD and ICP-OES, showing Pd and Cr in 7.4 and 13.6 wt% respectively (Pd/Cr = 1:4). Therefore, the molecular formula for this catalyst could be expressed as $[Pd_{0.75}Cr_3F(H_2O)_2O(ATA)_3]$, being in this case less than one Pd per chromium cluster.

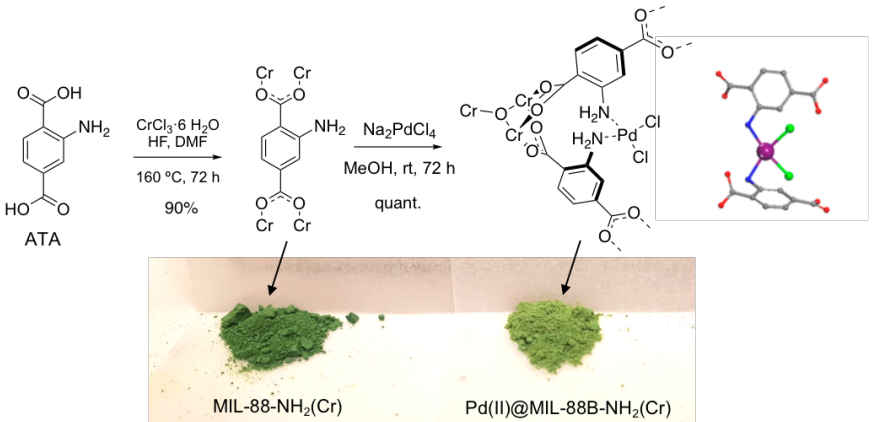

Figure 16. Synthesis of Pd(II)@MIL-88B-NH_2. 3D representation adapted from the literature.[57]

The analysis of both Pd(II)@MIL materials by X-ray absorption spectroscopy (XAS) revealed different coordination environments for the Pd(II) centers as a consequence of the different network features.[57] In the rigid MIL-101-NH_2(Cr), each Pd(II) is coordinated by one linker molecule, whereas in the flexible MIL-88B-NH_2(Cr) two neighbouring linkers can come close enough to coordinate the same Pd(II) center in a *cis* fashion, thereby "locking" the network in a semi-open form.[57]

The last step towards the synthesis of the supported NPs entails the reduction of the abovementioned Pd(II) complexes using ethanolic solutions of sodium borohydride (Figure 17). Analysis by ICP-OES revealed a Pd and Cr content of 7.3 and 10.8 wt% respectively for Pd@MIL-101-NH_2(Cr), whereas these values were 7.8 and 14.1 wt% for Pd@MIL-88B-NH_2(Cr). Commonly, the NP sizes obtained with this method oscillates between 1 - 3 nm and they are distributed both on the surface and within the MOF matrix.

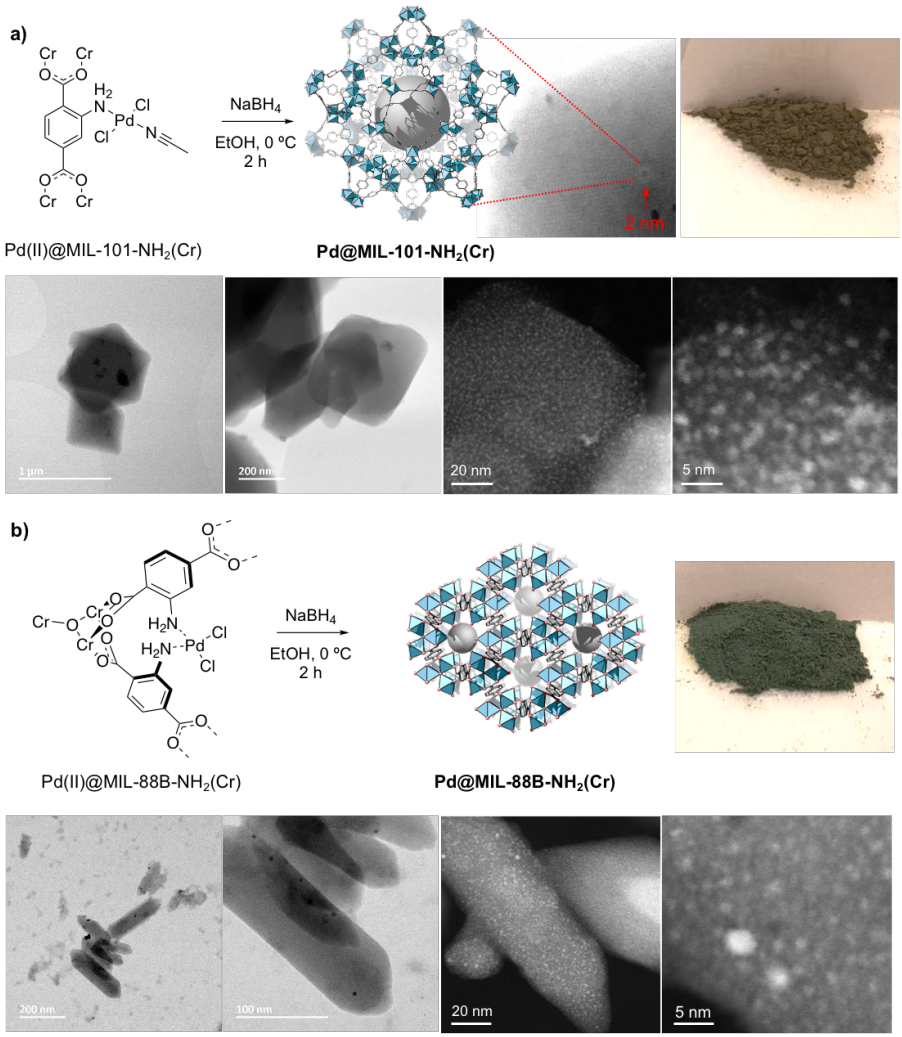

Figure 17. Synthesis of Pd NPs supported on MIL-101-NH_2(Cr) (a) and MIL-88B-NH_2(Cr) (b).[54,146] The corresponding BF- and HAADF-STEM images are shown below each reaction scheme (data collected by Dr Cheuk-Wai Tai).

The materials were characterized by PXRD (Figure 18), showing that the frameworks remained crystalline after the synthesis of Pd NPs, as suggested by the STEM images. The yields and the data collected by STEM, ICP-OES and PXRD agreed with the results previously obtained in the group.

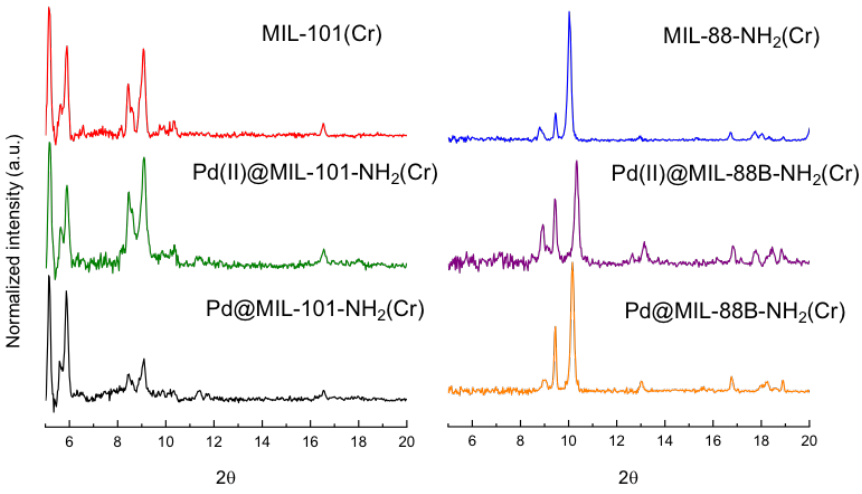

Figure 18. PXRD patterns of MIL-101(Cr) (left) and MIL-88B(Cr) (right) derivatives.

3. Palladium speciation in the ligandless Suzuki-Miyaura reaction (Paper I)

3.1. Background and aim of the project

Catalytic ligandless systems have attracted a widespread attention not only due to their simplicity, but also because they have proven to be highly effective at extremely low palladium loadings (*e.g.* ppms or ppbs). [147–153] The high turn-over numbers (TON) reached by these low metal loadings (up to 10^7) has raised important interest into understanding the reason for such efficiency. Revealing the composition and morphology of the species responsible for this exceptional catalytic activity has been very challenging, to a large extent due to their low concentration and their dynamic character.[63,154] In 2019, Polynski and Ananikov reported a theoretical investigation exploring pathways leading to the stabilization of Pd intermediates in solution, where different structures were proposed (Figure 19).[155] With the exception of Pd(II) dimers, to the best of our knowledge, trimeric and tetrameric structures of this kind have not been characterized before, and therefore very little is known about their reactivity.

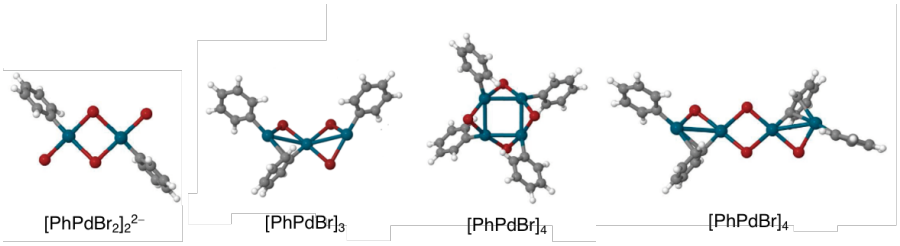

Figure 19. Selected examples of ligandless structures proposed by DFT calculations. Palladium is represented with blue spheres, bromides in red.[155]

Our previous studies on the Suzuki-Miyaura reaction showed that Pd@MIL-101-NH_2 is a very active catalyst under ambient conditions. For example, highly functionalized aryl halides and aryl boronic acids reacted to give quantitative yields of cross-coupled biaryls (Figure 20).[55] In contrast, palladium nanoparticles of identical characteristics immobilized in other materials have been reported to require very harsh conditions for the cross-coupling of simple substrates. [68,156–160] In the work presented in this chapter, we aimed to understand the reactivity of Pd@MIL-101-NH_2 by studying palladium speciation from these systems by techniques such as ESI-MS in combination with DFT calculations.

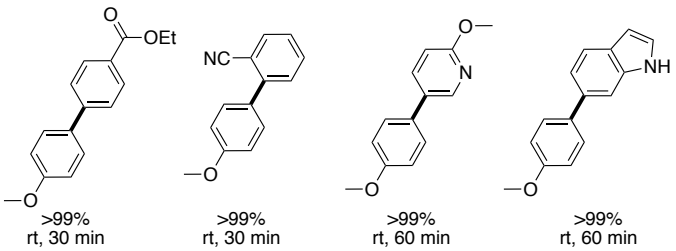

Figure 20. Examples of cross-coupling products obtained using Pd@MIL-101-NH_2(Cr) (1 mol%) reported by our group.[55]

3.2. Detection of reaction intermediates

Considering the numerous literature reports where it was demonstrated that nanocatalysts operate *via* leaching/redeposition pathways, we started our investigations by studying the activity of filtrates from Suzuki-Miyaura cross-coupling reactions mediated by Pd@MIL-101-NH_2(Cr) (2.4 nm average NP size). As electrophiles, we chose to work with aryl bromides and iodides since oxidative addition to Pd(0) is facile, in contrast to that of analogous aryl chlorides.[161,162] 4-Bromobenzotrifluoride **1a** and 4-iodobenzotrifluoride **1a'** were chosen as model substrates, together with phenylboronic acid (**2a**), for studying the coupling mediated by Pd@MIL-101-NH_2(Cr) as catalyst.

The reaction profiles were obtained by following the reaction by ^{1}H NMR spectroscopy (Figure 21a), and the reaction of aryl bromide **1a** showed that a yield of 94% of **3a** is obtained after only 60 min. Interestingly, the yields were much lower for the iodide substrate **1a'** (only 35% yield **3a** in 60 min). This was unexpected, as aryl iodides are excellent electrophiles in Suzuki-Miyaura cross-couplings.[163] The catalytic activity of the filtrates from both reactions was analyzed after 60 minutes as shown in Figure 21b. Upon filtration, the filtrate was added over a new load of reactants without additional Pd@MIL-101-NH_2(Cr) (*i.e.* **1a** or **1a'**, **2a** and KF) and the mixture was left to react for another 60 min. Analysis of the reaction with aryl bromide **1a** (filtrate A) indicated that the palladium remaining in solution afforded **3a** in 90% yield, similar to that obtained in the presence of Pd@MIL-101-NH_2(Cr) (94%). Filtrate A was analyzed by ICP-OES, revealing a very low Pd concentration of 0.1 ppm. This suggested the presence of highly active species in solution (TON = $5.3 \cdot 10^4$) and that the palladium remaining in the MOF support was to a great extent a reservoir of such species. In contrast, the accumulated yield of **3a** when using aryl iodide **1a'** (18%) indicated that filtrate B was inactive, as

the second load of reactants was not consumed. The presence of Pd in filtrate A was also confirmed by STEM, showing crystalline Pd NPs of 4.8 nm average size together with Pd clusters (<1 nm), whereas no MOF crystals could be observed (Figure 21c).

To further assess the nature of the species in solution we turned into electrospray ionization mass spectrometry (ESI-MS). When the filtrate A was analyzed by ESI-MS in the positive ion mode, no species containing palladium were found. However, a series aryl-containing Pd species were observed in the negative ion mode, in the region between *m/z* values of 400 and 1450 (**4a**–**7a**, Figure 22). Adducts **4a**–**7a** were assigned as oxidative addition complexes containing between 1 to 4 palladium atoms, being tetramer **4a** the base peak of the spectrum (Figure 22).

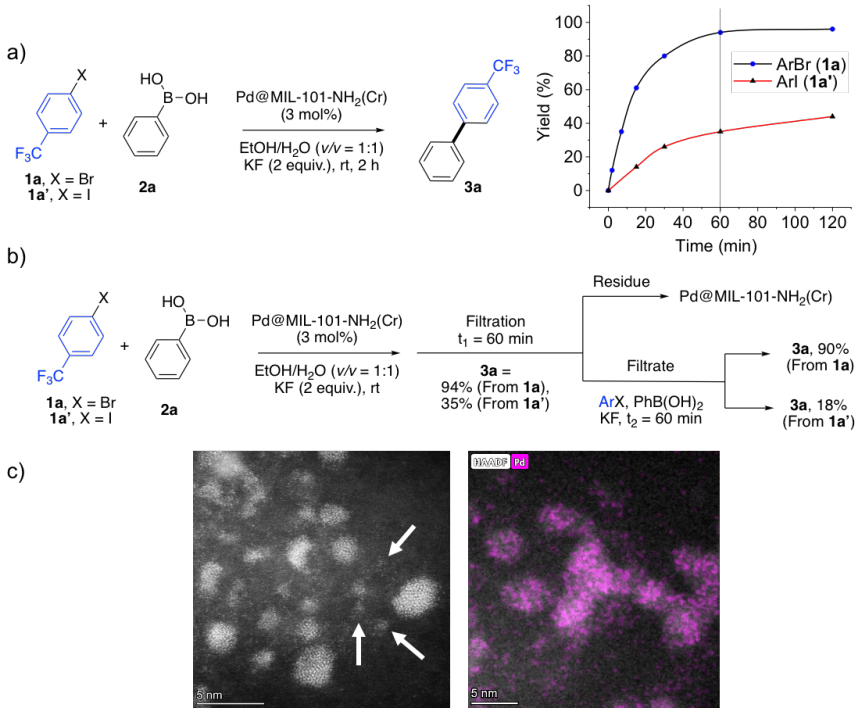

Figure 21. (a) Model Suzuki-Miyaura reaction and kinetic profiles for aryl bromide and iodide **1a** and **1a'**; (b) Filtration experiments. Yields were determined by ^{1}H NMR spectroscopy using an internal standard, yields after filtration are based on the total amount of ArX added; (c) HAADF-STEM image of Pd NPs and clusters in Filtrate A. EDX elemental mapping of Pd overlaid of HAADF image (right).

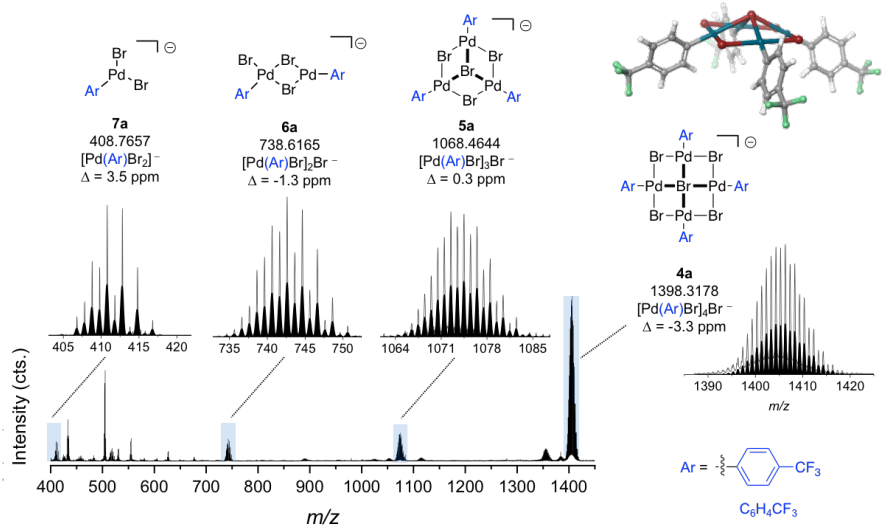

Figure 22. Identified adducts in filtrate A (t = 30 min), indicating measured mass (monoisotopic), formula, and error. Inset shows obtained (grey) and simulated (black) isotopic patterns. 3D structures of **4a** from DFT calculations are shown.

The structure of tetramer **4a** was optimized by Prof. Ahlquist using density functional theory (DFT) (Figure 22). These calculations showed that each palladium(II) center has a geometry close to square planar. The Gibbs free energy at standard state of the species **4a**–**7a** was calculated, and a significant driving force for each step was disclosed (Figure 23). Since intermediates **4a**–**7a** are negatively charged, and the reactions are performed in aqueous media, H_2O ligands were used for the complexes, one for monomer $[ArPdBr_2(OH_2)]^-$ (**7a**) and two for the neutral $[ArPdBr(OH_2)_2]$ were chosen as reference. As Pd–OH_2 bonds will be broken in every step and replaced by Pd–Br bridges, which are weak bonds, it was found that the bonding enthalpy is not the driving force for formation of the higher oligomers **4a** and **5a**. We therefore looked into the two components of the change in Gibbs free energy, the entropic contribution ($-T\Delta S$) and the enthalpic contribution (ΔH). For every step there is an unfavorable enthalpic change, except from trimer **5a** to tetramer **4a** which is slightly exothermic. However, due to the release of coordinated water molecules the entropic contribution favors every step significantly. The stability of the complexes therefore arises from entropy rather than from enthalpy. This may have significant impact on the reactivity, as described below. Tetramer **4a** is the most stable oxidative addition adduct, which was also the base peak in the HRMS experiments.

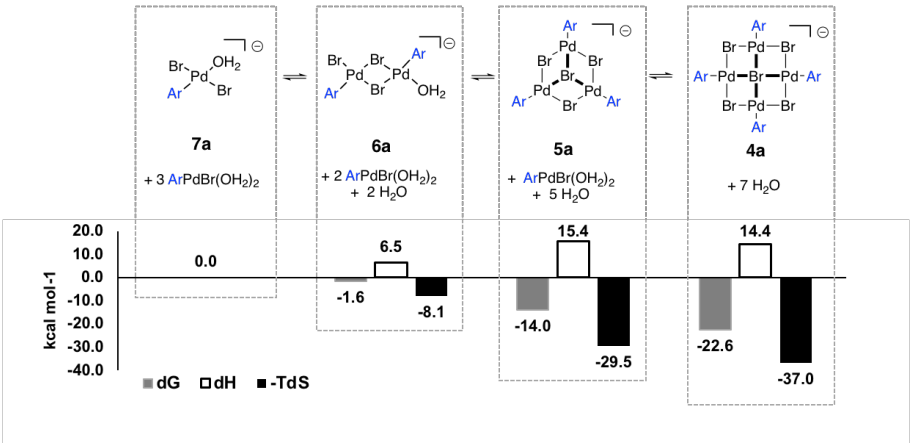

Figure 23. Oligomerization of oxidative addition intermediates and Gibbs free energy change for the equilibrium species involved in the formation of tetramer **4a**. Optimized structures for monomeric and dimeric oxidative addition intermediates found by MS (note that for both monomer and dimer, H_2O has been considered for coordinatively saturated Pd centers).

In the case of the reaction with aryl iodide **1a'** (filtrate B), ESI(−)-MS analysis was performed 15 min after the outset, and it also revealed the formation of tetrameric (**4a'**) and trimeric (**5a'**) adducts. However, in this case monomer **7a'** was found to be major species (Figure 4a, top). After 120 minutes, **4a'** and **5a'** were consumed and the mass spectrum was dominated by monomer **7a'** and a series of palladium anionic iodide salts with formulas $[Pd_2I_4]_n^-$ (n = 1 or 2) and $[Pd_2I_n]^-$ (n = 3 or 5) (Figure 24b). The latter ones have been previously detected (EXAFS) and isolated from other reactions, and due to their high stability they have been considered to be off-cycle species.[108,164] The presence of these inactive forms of Pd agreed well with the sluggish kinetics in the reaction of **1a'** and the lack of catalytic activity of the corresponding filtrate (Figure 21b). This is also in agreement with previous work by Ananikov and co-workers, who pointed out that in dynamic systems there are factors beyond the ease of oxidative addition (iodides > bromides) to assess the efficiency of a process, such as the stabilization of Pd(II) and Pd(0) intermediates by halides.[163] Even if aryl iodides undergo a faster oxidative addition, iodide anions exert a greater stabilization on Pd(II) than bromides, thereby "trapping" these species as inert salts.

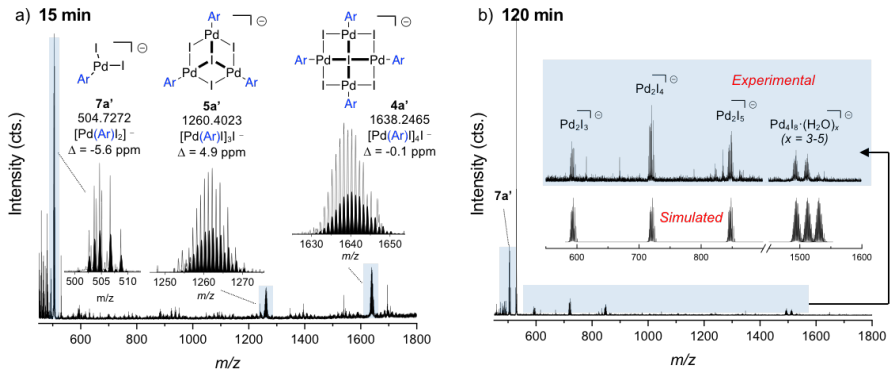

Figure 24. Identified adducts in filtrate B, indicating measured mass (monoisotopic), formula, and error. Ar = $C_6H_4CF_3$

When the profiles of the reaction between **1a** and **2a** (Figure 25 and Figure 20a) was compared with the evolution of Pd species over time, as detected by ESI(–)-MS, it was observed that the formation of tetramer **4a** as major oxidative addition species occurred within just 2 min (12% yield of **3a**; for kinetic profile, see top plot; for **4a** abundance, bottom plot). The fast formation of **4a** reflects that upon oxidative addition, the oligomerization process is favored, what was in agreement with the DFT data (*vide supra,* Figure 23). During the first 30 min of the reaction, the relative abundance of **4a** experienced a boost that correlated with an increase of the yield of **3a** (from 12 to 80%). After 80% yield of **3a** had been achieved, the abundance of **4a** decreased, which correlates with a diminished concentration of the electrophile (*e.g.* **1a**). Interestingly, the abundance of **4a** remains relatively constant after 60 min, when the yield of **3a** is 96%, even after t = 120 min. A possible reason for this could be the depletion of the concentration of boronic acid **2a** in the reaction mixture. Under the reaction conditions, part of the boronic acid can form borates or boroxines that are reported to be worse transmetallation partners.[165] Further, protodemetallation steps may also result in a consumption of the boronic acid reagent. To test this hypothesis, an extra equiv. of **2a** and 2 equiv. of potassium fluoride were added to the reaction mixture at t = 125 min, and allowed to react for additional 10 min (*i.e.* t = 135 min). After this time, **4a** was consumed and a yield of **3a** of 99% was reached.

When using $Pd(OAc)_2$ as the catalyst instead of Pd@MIL-101-NH_2(Cr), the anionic intermediates showed in Figure 22 were also detected. Pd@MIL-101-NH_2(Cr) showed a slightly higher activity after 30 min than $Pd(OAc)_2$, which could be ascribed to the better stabilization of Pd species by the support.

It is important to comment that the reaction catalyzed by $Pd(OAc)_2$ formed Pd(0) aggregates that precipitated in a late stage of the reaction and were visible to the naked eye. These large aggregates are a common cause of catalyst deactivation. This was not the case for the Pd@MOF catalyst, which suggests that the MOF plays an important role in the stabilization of Pd NPs and thereby increasing the lifetime of the catalyst in the reaction mixture. This agrees with the fact that Pd@MIL-101-NH_2(Cr) can be recycled and reused for several runs.[54]

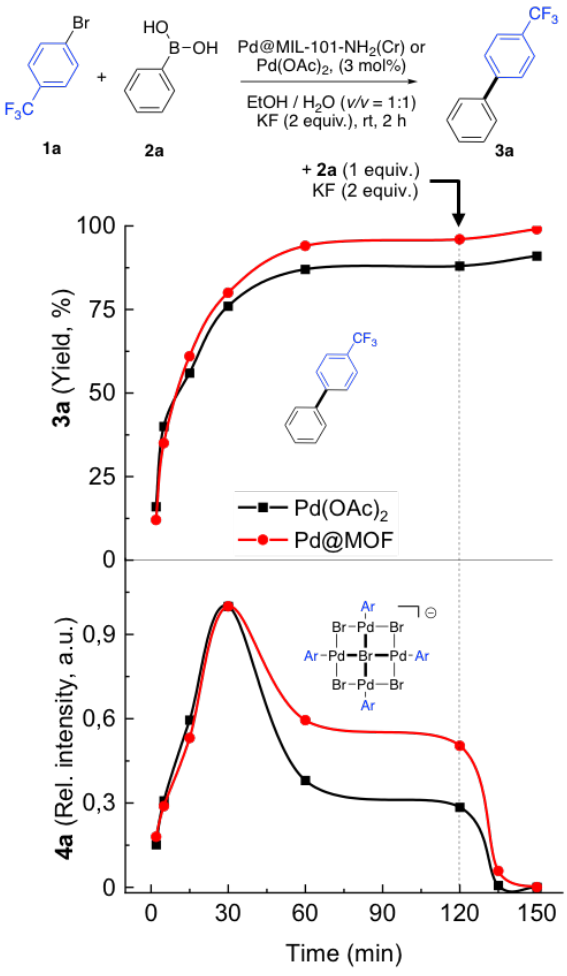

Figure 25. Comparison between the kinetic profiles of the Suzuki-Miyaura reaction using Pd@MOF and $Pd(OAc)_2$ and correlation with the abundance of **4a** determined by ESI(–)-MS versus time.

At this point, we speculated whether the consumption of tetramer **4a** took place as such or if it broke into monomers, such as **7a**, prior to transmetallation. We initially considered this possibility, however the results discussed above suggested a more active role for **4a**. In this regard, the strength of the bonds to be broken (monomer *versus* tetramer) could play a key role when it comes to assessing the reactivity of these species. Since the driving force of tetramer **4a** was not bonding enthalpy, and therefore it could be expected that the bonds to break during the transmetallation are weaker. To the best of our knowledge, species akin to tetramer **4a** have never been characterized before due to their transient character and low concentration. Demonstrating that tetrameric complexes could be important species in the transmetallation step would provide with a better understanding of dynamic systems, and therefore we focused our attention in shedding light on this matter.

3.3. Theoretical investigation on the reactivity of tetrameric palladium complex 4a

The reactivity of tetramer **4a** was investigated by density functional theory (DFT) calculations. The calculations, performed by Prof. Ahlquist, were run simultaneously to our experimental investigations. The results presented here are a selection of the calculations that are supported by our experimental results. As the use of fluoride bases in combination with boronic acids typically generates borate species, fluorodihydroxy(phenyl)borate (**2a'**) was used as reactant (Figure 26). The transmetallation is initiated by borate **2a'** entering from below the plane, and coordinates to one of the four Pd centers, this results in formation of a Pd–O bond. Importantly, the bond between the same Pd atom and the central bromide is broken during the process. Since this central bromide is coordinated with three additional Pd centers, the bond-breaking step is very facile, with an activation energy of 7.9 kcal/mol, and a reaction free energy of –1.0 kcal/mol (**Int1**). Next, the second Pd–Br bond is replaced by a π-phenyl interaction, through a small activation free energy of only 1.9 kcal/mol, and a reaction free energy of –2.0 kcal/mol (**Int2**). In the next step, the Pd–C sigma bond is formed, *i.e.* the key step in the transmetallation, yielding **Int3**. The barrier is only 10.0 kcal/mol relative to the reacting intermediate (**Int 2**). The step is plausibly facilitated by the very low trans influence of the bridging bromide, and the reaction, leading to a Pd(II) species with two aryl groups, is highly exergonic (–15 kcal/mol). In this same step, $BF(OH)_2$ spontaneously de-coordinates from Pd, and it is replaced by a Pd–Br bond. Species

related to the pre-transmetallation intermediates (**Int1** or **Int2**) were not detected by ESI(−)-MS. Since no strong bonds at the palladium cluster are being broken, the transmetallation is very facile. As the Pd–Br interaction decreases at the reacting palladium center, the remaining Pd–Br interactions are strengthened at the spectator Pd sites, leading to very low activation energies. The unfavorable enthalpy of formation showed in Figure 23 thereby makes tetramer **4a** very susceptible to react (due to the weak bonds to break). However, even if it breaks easily, it still forms in substantial amounts due to the entropic increase in its formation. Tetramer **4a** forms due to the coordination properties of bromides, and to the absence of stronger σ-donor ligands. In case of homogenous systems involving phosphines or carbenes, the strong interactions with palladium minimize its aggregation but, on the other hand, the formation of reactive species requires ligand dissociation steps that in some cases can be rate-determining.[166,167]

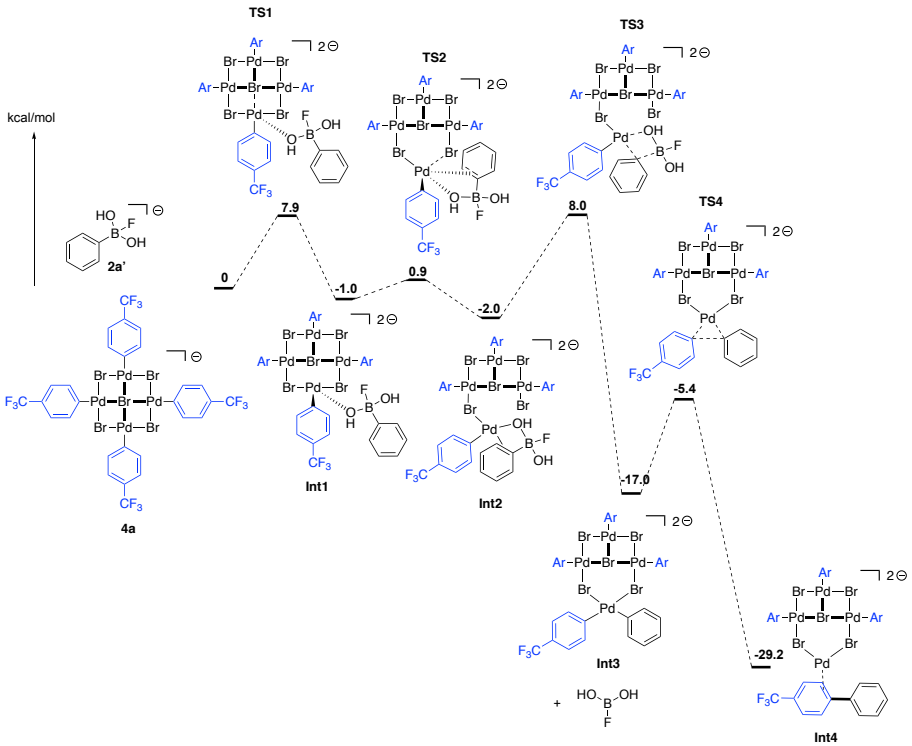

Figure 26. Energy profile for the transmetallation and reductive elimination steps from **4a**.

Reductive elimination of two aryl groups from Pd(II) would be the next step towards formation of the biaryl product. Here we found a low activation

energy of 11.6 kcal/mol, leading to a Pd(0) containing species with the product coordinated (**Int4**). The calculations of the transmetallation step on monomer **7a** resulted in a barrier of 25 kcal/mol, which suggests that this process would be much easier on species such as **4a**.

The substituents of the boronic acid did not affect the detection of tetrameric species, as it is not involved in the stabilization of the anion. However, we observed that electron-withdrawing groups (EWGs) on the aryl halide were needed to detect **4a** (*i.e.* such as *p*-CF_3 on **1a**). Other aryl bromides that allowed the detection of anionic tetramers were those substituted in the *para* position with F (**1b**), SF_5 (**1c**), OCF_3 (**1d**), SCF_3 (**1e**) and SO_2CF_3 (**1f**) (Figure 27). For these substrates, tetrameric intermediates **4a-f** could be detected by ESI(–)-MS. On the other hand, with neutral or electron-rich aryl bromides, palladium tetramers could not be detected (Figure 27, **1g-i**).

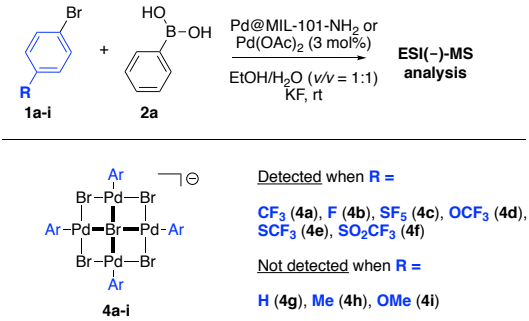

Figure 27. Scope of aryl halides tested for the detection of **4a**.

The stability of tetrameric oxidative addition intermediates containing EDGs was assessed by means of DFT calculations as in Figure 23 for the case of the *p*-bromotoluene (**1h**). The results showed that the formation of oxidative addition tetramer **4h** is still thermodynamically favored (ΔG = –15 kcal/mol), however it is less stable than **4a** (*i.e.* for **4a**, ΔG = –22.6 kcal/mol, Figure 23). This may explain why adducts such as **4h** could not be detected by ESI(–)-MS. This supported our initial hypothesis regarding the use of suitable electronics on the starting material to stabilize anionic intermediates. We are also aware that in "cocktail"-type systems, multiple mechanistic pathways are possible and the choice of electronics might favor some of them versus others. However, the results from MS and DFT investigations suggested that the formation of tetrameric oxidative addition complexes could play an important role in the transmetallation step.

3.4. Conclusions and outcome

We have shown that in ligandless Suzuki-Miyaura reactions (*i.e.* those in the absence of phosphorus, nitrogen or carbene-functionalized ligands), tetrameric oxidative addition intermediates are formed. This is particularly the case when the reactions involved electron-poor aryl bromides. The weak Pd–Br bonding displayed in the tetramers can explain the facile transmetallation step (10 kcal/mol) at r.t., while that of an oxidative addition monomer was found to be significantly higher (25 kcal/mol).

Aryl iodides also give rise to analogous tetrameric adducts, however the higher stabilization of off-cycle Pd(II) iodide species resulted in catalytic efficiencies that were significantly lower to those achieved in reactions involving aryl bromides. These studies contribute to understanding of the very high reactivity of Pd@MIL-101-NH_2(Cr) catalyst in Suzuki-Miyaura cross-couplings.

Some of the remaining questions in this work concerns the isolation and unambiguous determination of the structure of tetramer **4a**. If the isolation of stable forms of these ligandless species could be accomplished, this could be of vital importance for the future development of new and better phosphine-free catalysts that can be applied at ppms or ppbs levels for more sustainable processes.

4. Investigating catalyst activation and deactivation in the Mizoroki-Heck reaction catalyzed by Pd(II)@MIL-101-NH_2(Cr) (Paper II)

4.1. Background and aim of the project

The *in situ* monitoring of reactions is essential to understand any catalytic process, yet this task is remarkably challenging when using heterogeneous catalysts. [168] The main goal of this work is the study of Pd evolution in the Mizoroki-Heck reaction catalyzed by Pd(II)@MIL-101-NH_2(Cr). A major part of this work was performed by Yuan, Pascanu and co-workers, who determined the entire "lifetime" evolution of Pd species that were formed during the reaction (Figure 28). The catalytic performance of Pd(II)@MIL-101-NH_2(Cr) was found to be excellent, however, and in contrast to the Suzuki-Miyaura cross-couplings presented in Chapter 3, the catalyst here could not be recycled. The team found that supported Pd(II) complexes were reduced into catalytically active species that, after reaching 90 ºC, gradually converted into clusters of *ca.* 13-20 atoms (< 1 mn).

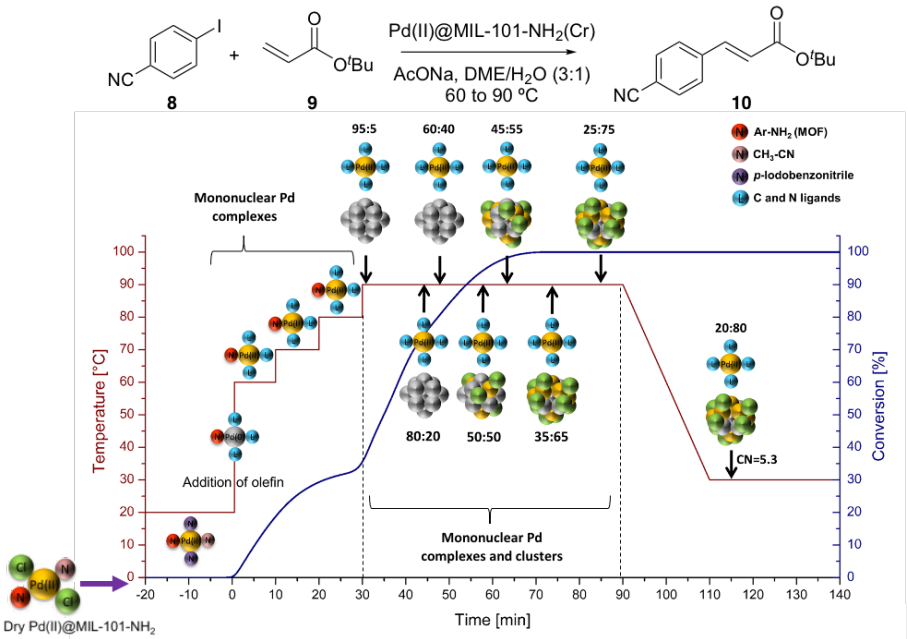

Figure 28. Evolution of Pd species and kinetic profile of the Mizoroki-Heck reaction catalyzed by Pd(II)@MIL-101-NH_2(Cr) determined by Yuan (treatment of EXAFS data), Pascanu (catalysis experiments) and co-workers.[168]

When conversions reached 95% (ca. 60 min), Pd clusters were increasingly covered by chloride anions, which was considered a potential cause of deactivation. The chloride anions originated from the catalyst precursor, $PdCl_2(MeCN)_2$, which was used as the palladium source for the synthesis of Pd(II)@MIL-101-NH_2(Cr). In this thesis, 3 aspects of this work are addressed: Pd(II)@MOF activation, deactivation and the role of the MOF support.

4.2. Formation of Pd(0) species from Pd(II)@MIL-101-NH_2(Cr): Pre-catalyst activation

We anticipated that the pre-catalyst would be reduced in a Wacker-type process, involving Pd(II), *tert*-butylacrylate (**9**) and H_2O, to form *tert*-butyl 3-oxopropanoate (**10a**). When *tert*-butylacrylate was subjected to the reaction conditions in Figure 29a (in the absence of aryl iodide **8**), and the crude was analyzed by ESI(+)-MS, the expected product **10a** (*m/z* 167.07, $M+Na^+$) was not detected (Figure 29a). Instead, the mass spectrum displayed an unknown species at *m/z* 199.0957 that was ascribed to derivatives of **10a**, which was expected to be highly unstable under the reaction conditions. This species was assigned as an acylium cation (**10b**) derived from a Michael adduct (**10c**, Figure 29b). Therefore, it could be proposed that Pd(II) is reduced as proposed in Figure 29c, forming **10c** upon reaction **10a** with *tert*-butylacrylate (**9**).

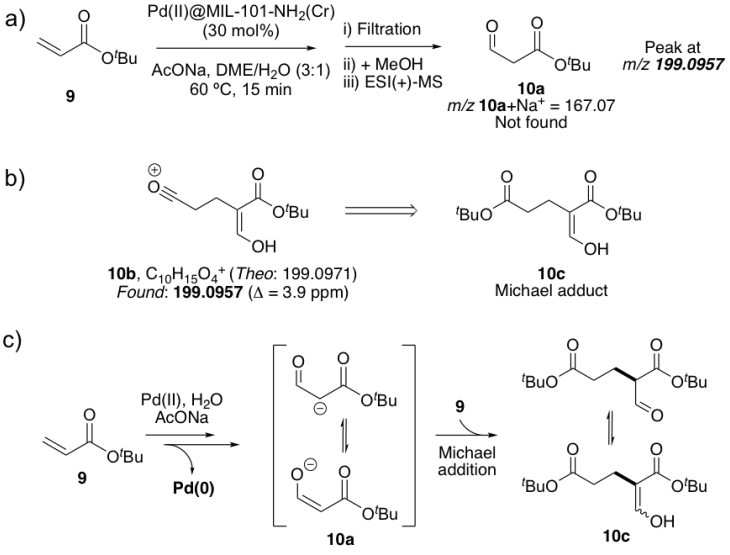

Figure 29. (a) Reduction test and detection of unknown; (b) Proposed structure for the identified cationic adduct and precursor; (c) Proposed mechanism for the formation of the precursor of the specie detected by ESI(+)-MS.

4.3. Catalyst deactivation and importance of the MOF support

Initial recycling experiments performed by Pascanu showed that the Pd@MOF catalyst recovered after the first run suffered a dramatic loss of activity in a second run (21% conversion after 5 h). The work presented in this chapter includes determining whether the remaining Pd(II) complexes in solution are catalytically active when Pd clusters have been poisoned by chlorides (after *ca.* 1 h), and the analysis of the chloride content in the recycled catalyst. To address these questions, a new load of fresh reactants was added to the reaction mixture after 70 min (Figure 30), when a full conversion was achieved and the mixture consisted of *ca.* 40% mononuclear Pd complexes and 60% of poisoned Pd clusters (determined by XAS, Figure 28). After an additional 70 min (total time = 140 min), full conversion of the second load of reactants was achieved. Therefore, the remaining Pd(II) species after 70 min are, albeit differently composed, equally efficient in converting the substrates.

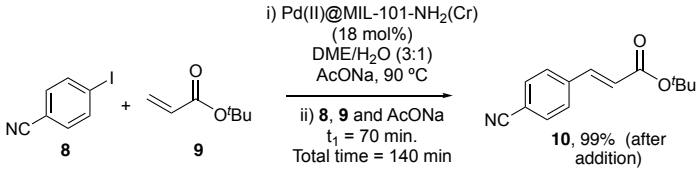

Figure 30. Activity test of remaining Pd(II) complexes in solution.

In a separate experiment, the Pd@MOF catalyst was recovered and the Pd and Cl content was analyzed by ICP-OES. The result showed a significant amount of chloride remaining in the material (1.05 wt%), being the molar ratio Pd/Cl 1.2. This implies that each Pd atom remaining in the recovered material is bound to one chloride anion on average, which was further supported by the EXAFS refinement performed by Yuan.

The detrimental effect of chloride anions in this reaction could not be overcome by the MOF support. However, the effect and benefits of using Pd(II)@MOF was proved by control experiments where commercially available Pd salts (*i.e.* Na_2PdCl_4 and $PdCl_2(CH_3CN)_2$) were used as catalysts, affording the product (**10**) in significantly lower yields (42-43%, Figure 31).

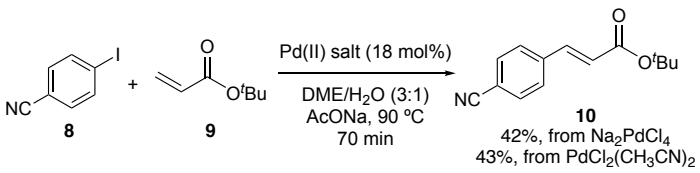

Figure 31. Mizoroki-Heck reaction catalyzed by commercially available Pd salts.

4.4. Conclusions

To conclude, findings from the main authors outlined the whole evolution of Pd species during the Mizoroki-Heck reaction catalyzed by Pd(II)@MOF. Mononuclear Pd complexes were found to dominate at the beginning of the reaction, that then progressively transformed into Pd clusters (13-20 atoms) whose surface was poisoned by coordination of Cl^- ions.

The work presented in this thesis contributed with the detection of species derived from a Wacker oxidation product by ESI(+)-MS, which suggests a possible activation pathway of the Pd(II)@MOF pre-catalyst

The addition of fresh reactants by the time Pd clusters were expected to be poisoned by Cl^- anions proved that remaining Pd(II) species in solution are catalytically active. Finally, the low yields afforded when simple Pd(II) salts were used as catalysts demonstrates the beneficial effects of the MOF support in controlling Pd aggregation.

5. Regeneration of Pd(II)@MIL-88B-NH_2(Cr) for C–C bond forming reactions (Paper III)

5.1. Background and aim of the project

This project started from the observation that Pd(II)@MOF species were reduced extraordinarily fast in the presence of arylboronic acid and base yielding a symmetrical biaryl and Pd(0) particles. Even in the of presence of a support, the aggregation of metal species into particles *via* migration/coalescence or Ostwald ripening is sometimes inevitable.[169] This aggregation often leads to the deactivation of the catalyst. Consequently, the development of protocols that are able to reverse the deactivation process, and thus enabling the recycling of supported metal catalysts, is highly desirable. Diverse strategies have been described in the literature, however the harsh conditions needed are not compatible with hybrid supports such as MOFs (Table 2). In this work, we explored the ability of MIL-88B-NH_2(Cr) to mediate the aggregation of Pd catalysts in the homocoupling of arylboronic acids (see Figure 32 for literature examples). One of the main goals of this work includes the development of a method to redisperse and regenerate supported Pd catalysts.[170]

Table 2. Examples of redispersive strategies for sintered Pd catalysts.

Entry	*Strategy*	*Conditions*	*Ref.*
1	Oxidation/reduction	i) Air, 430 ºC, 16 h ii) H_2, 400 ºC, 16 h	171,172
2	Oxychlorination	i) O_2, 350-500 ºC, 2 h ii) Cl_2, 350 ºC, 1 h	173
3	Calcination	Air, 700 ºC, 1 h	174
4	Chemical oxidation	Conc. HNO_3, 80-120 ºC, 6 h	175

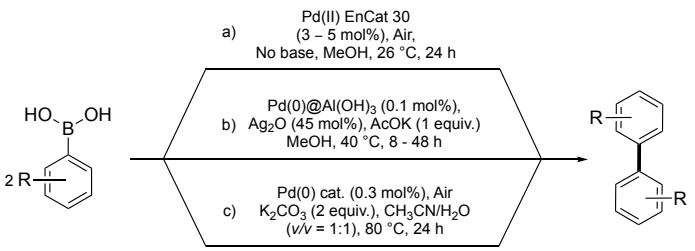

Figure 32. Heterogeneous methods for the homocoupling of boronic acids.[176–178]

5.2. Optimization of reaction conditions

The project was initiated by the optimization of the reaction conditions for the homocoupling of boronic acids. When *p*-tolylboronic acid (**11a**) was subjected to similar conditions to those reported by our group for the Suzuki-Miyaura reaction,[54] but in the absence of an aryl halide, 44% yield of the symmetric biaryl product (**12a**) was obtained (Table 3, entry 1) together with 5% of *p*-cresol (**13a**). When the same reaction was performed under an oxygen atmosphere, full conversion was obtained within 1 h, and a 72% yield of biaryl **12a** was isolated (entry 2). Lower catalyst loadings (0.1 mol%) gave a similar result (entry 4, 69%, TON = 909) after 2 h (entry 3). Lowering the amount of Cs_2CO_3 to 25 mol% under otherwise identical reaction conditions, afforded full conversion as well and a 71% yield of **12a** was obtained after 2 h at r.t. (entry 4). In the absence of base, formation of **12a** was not observed (entry 5). Under an argon atmosphere and using degassed solvents, no product formation was observed either (not shown). The formation of the phenol side-product (**13a**) under aerobic conditions was previously described in the literature.[179] Detailed mechanistic investigations by Adamo and co-workers suggested that formation of 1 equiv. of hydrogen peroxide as responsible for the formation this side-product.

Table 3. Optimization of the reaction conditions.

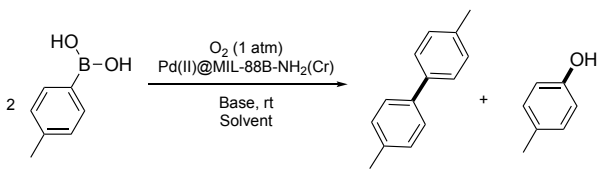

11a **12a** **13a**

Entry	*Cat. (mol%)*	*Solvent (v/v)*	*Base (equiv.)*	*Conv. (%)*	*Yield 12a[a] / 13[d] (%)*
1[b]	0.4	EtOH/H_2O (1:1)	Cs_2CO_3 (1)	67	44 / 5
2	0.4	EtOH/H_2O (1:1)	Cs_2CO_3 (1)	>99	72 / 21
3[c]	0.1	EtOH/H_2O (1:1)	Cs_2CO_3 (1)	>99	69 / 24
4[c]	**0.1**	**EtOH/H_2O (1:1)**	**Cs_2CO_3 (0.25)**	**>99**	**71 / 22**
5[c]	0.1	EtOH/H_2O (1:1)	-	-	Traces / -

Unless otherwise noted: **11a** (2 mmol), Pd(II)@MIL-88B-NH_2 (9.2 wt% Pd), O_2 (1 atm), rt, 1 h. (a) Isolated yields; (b) Under air. (c) 2 h. (d) Yields determined against an internal standard by ^{1}H NMR spectroscopy; volatile under reduced pressure.

5.3. Substrate scope and limitations

With the optimized conditions in hand, a series of substrates were evaluated. First, the homocoupling of *para*-substituted phenylboronic acids with EDGs was investigated (**12a**-**12f**). Good to excellent yields (67 - 91%) were obtained in remarkably short times (2 - 3 h) with the exception of diamine **12e** (21% yield). The method tolerated benzylic alcohols delivering **12d** in good yield (67%) without any observed oxidation side-products. Furthermore, trimethylsilyl substituted substrate **11f** was selectively coupled through the C–B bond,[180] affording biaryl **12f** in good yield (81%). Biphenyl **12g** was obtained in 78% yield after 2 h.

Halide substituted arylboronic acids were also tolerated and compounds **12h** and **12i** were formed in good yields (71 and 65% respectively). Substrates having electron-withdrawing groups at the para position were also evaluated. Those bearing aldehyde, trifluoromethyl, nitrile and ester functional groups gave **12j**-**12m** in moderate-good yields (52 - 66%) in reaction times between 2 and 4 h.

Arylboronic substrates **11n** and **11o** bearing EDG in the *meta* position delivered the corresponding biaryls in 72 and 64% yields respectively. Polysubstituted and polyaromatic substrates were tolerated, and products **12p**-**12u** were isolated in good to excellent yields (57 - 98%).

Remarkably, the majority of the products were obtained by filtration without involving additional purification; the elemental analysis of one of the products isolated in this way (**12a**) showed very high purity: [Calc. (Found)] C 92.26 (92.08), H 7.74 (7.92).

The efficiency of the method was investigated on a gram-scale (5.7 g, 41 mmol) using *p*-tolylboronic acid **11a**, affording total of 2.53 g (70% yield) of **12a**, when only 12 mol% of base was used (Figure 33).

Table 4. Substrate scope and limitations

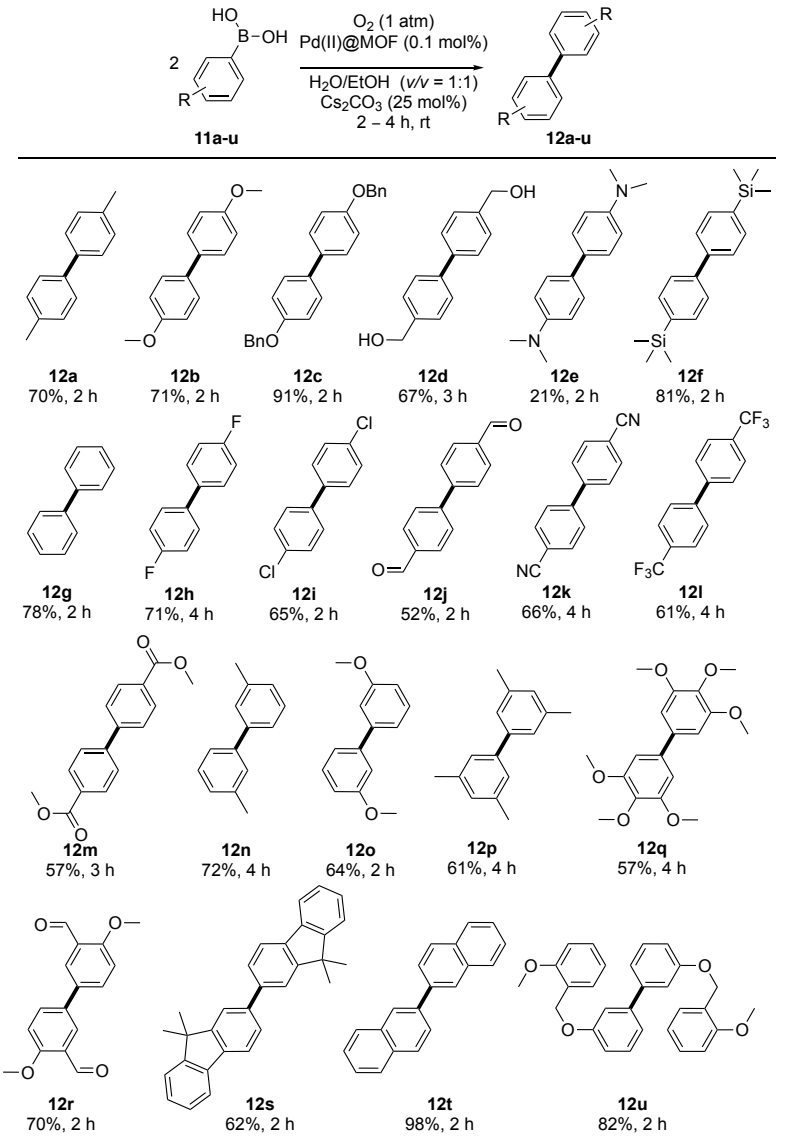

Reaction conditions: $ArB(OH)_2$ (2 mmol), Pd(II)@MIL-88B-NH_2(Cr) 9.2 wt% (0.1 mol%), O_2 (1 atm), Cs_2CO_3 (25 mol%), rt, 2-4 h. Isolated yields.

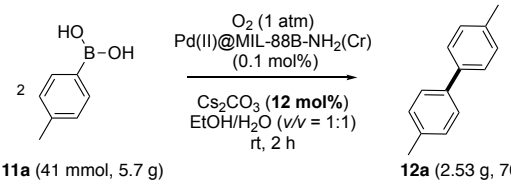

Figure 33. Gram-scale homocoupling of *p*-tolylboronic acid.

5.4. Recyclability and catalyst regeneration

The recyclability of Pd(II)@MIL-88B-NH_2 was evaluated in the homocoupling reaction of *p*-tolylboronic acid for five consecutive runs. Analysis by XRPD of the recovered catalyst revealed that its structure remained after five reaction runs (Figure 34a) at the base loading of 25 mol%. In previous work by our group, carbonates were found to produce severe structural damage in MIL-101(Cr)-based MOFs when higher loadings were used.[56] Slight changes were detected in both 2Θ values of several diffraction peaks, which has been previously reported for this framework, and ascribed to its breathing behaviour.[48]

The activity of the catalyst was retained only until the second run, affording a yield of 70% (Figure 34b, blue bars). The product yields obtained in further runs showed a dramatic decrease, from 30% in run 3 to 7% in run 5. ICP-OES analysis showed that the Pd/Cr ratio in the fresh catalyst (run 0, Figure 14b, orange bars) decreased from 0.63 to 0.48 in the recovered composite after 2 runs (Figure 34b, orange bars). The Pd/Cr ratio is essentially kept afterwards (*i.e.* 0.47 after run 5), which suggested that the loss of catalytic activity might be due to the deactivation of the catalyst due to Pd aggregation rather than leaching.

Indeed, the STEM analysis of the recovered catalyst after 1 run (Figure 34c) showed the formation of homogeneously dispersed Pd NPs of 2.6 nm average size within and on the surface of the MOF matrix. After the second cycle, bigger NPs were observed (4.9 nm average size). After the 5th run the particle distribution turned into big agglomerates of Pd (44 nm average size) with partial crystalline character, coexisting with some remaining smaller particles (Figure 34c). As PXRD data showed (Figure 34a), the STEM images supported a correct preservation of the MIL-88B-NH_2 morphology at the end of the process.

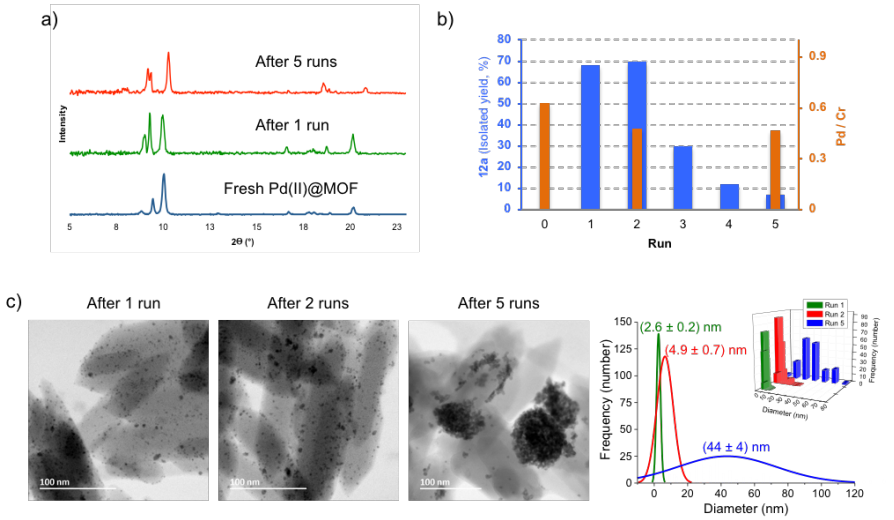

Figure 34. (a) XRPD patterns of the fresh (dark blue) and recovered materials; (b) Recycling experiments on a 4 mmol scale. Isolated yields (left axis, blue bars) and Pd/Cr ratio in the recovered catalyst after 5 runs; (c) BF-STEM images of the recovered Pd@MIL-88B-NH_2 catalyst and change in particle size distribution.

For the oxidative coupling reported here, it is therefore plausible that the reduction and aggregation of Pd(0) species into large particles is the main deactivation pathway.[181,182] To overcome this problem, we envisioned the possibility of restoring the activity of the catalyst by redispersion of the inactive particles using an oxidant under mild reaction conditions. To the best of our knowledge, this has not been attempted before on MOF-supported catalysts.

For this part of the investigation, we chose a Pd(0) surrogate catalyst, Pd@MIL-101-NH_2(Cr), with well-defined crystalline NPs (38.0 nm average size). When this catalyst was used in the homocoupling reaction, a similar result to that of Pd@MIL-88B-NH_2 after five runs was obtained (14%, Table 5, entry 1). Various oxidants were *ex situ* screened on the Pd@MIL-101-NH_2(Cr) composite, and the resulting materials were subsequently tested for catalytic activity (Table 5). Upon treatment with benzoyl peroxide (BPO) in ethanol for 5 h, the catalyst partially recovered its activity, and gave **12a** in 48% yield (Table 4, entry 2). When using nitric acid as regenerant at r.t. for 5 h, 58% of **12a** was obtained (entry 3). The treatment of the catalyst with sulfuric acid or hydrogen peroxide caused the collapse of the crystalline structure (entries 4 and 5), however it remained intact after using aqua regia affording 24% yield of the desired biaryl product. The use of benzoquinone, (diacetoxy)iodobenzene, peracetic acid, Oxone®, potassium peroxodisulfate

($K_2S_2O_8$) and *tert*-butylhydroperoxide in the presence of acetic acid as proton source did not succeed in restoring the catalytic activity (entries 7-12). However, when the two latter ones were used in 2 M HCl at r.t. for 2 h, 68 and 69% yields of **12a** were isolated, whose result was identical that of the fresh Pd(II)@MOF catalyst. STEM analysis confirmed a successful redispersion of the initial NPs into small nanoclusters, keeping the morphology of the support intact (Figure 35).

When these conditions were applied to the deactivated Pd@MIL-88B-NH_2(Cr) after 2 runs the results were reproducible, obtaining 70% yield after treatment with ^{t}BuOOH and 72% with $K_2S_2O_8$ (entries 15 and 16). Interestingly, we found that the activity of $K_2S_2O_8$-regenerated catalysts was kept for only one additional. The amount used of oxidant could be lowered from 20 to 5 equiv. (*versus* palladium), keeping the same efficiency (entry 17), without affecting the MOF structure significantly.

Surprisingly, when applying the same conditions in entry 17 to Pd on charcoal (Pd/C), the catalyst obtained after redispersion was poorly active, affording only 13% yield of **12a** (entry 18). This suggests an active role of the MOF support in the stabilization of the Pd species resulting after redispersion.

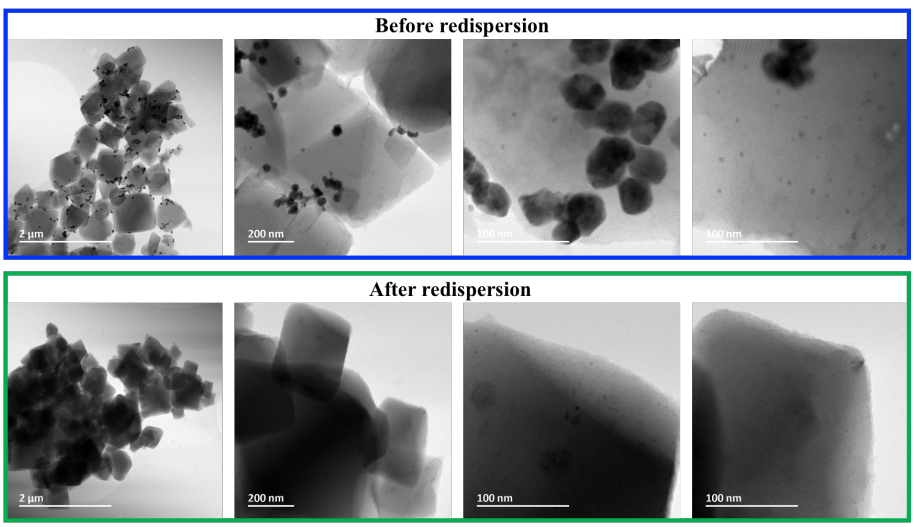

Figure 35. BF-STEM images of Pd@MIL-101-NH_2 before (top) and after (bottom) oxidative redispersion.

Table 5. Oxidant screening and activity of the regenerated Pd@MOF composites

Entry	*Catalyst*	*Oxidant (equiv.)*[a]	*Conditions*	*12a (%)*
1	Pd@MIL-101-NH_2(Cr)	none	-	14
2	Pd@MIL-101-NH_2(Cr)	BPO (20)	EtOH, 5 h	(48)
3	Pd@MIL-101-NH_2(Cr)	HNO_3 conc.	5 h	(58)
4	Pd@MIL-101-NH_2(Cr)	H_2SO_4 conc.	5 h	-
5	Pd@MIL-101-NH_2(Cr)	H_2O_2 (20)	H_2O/AcOH, 5 h	-
6	Pd@MIL-101-NH_2(Cr)	Aqua regia	5 h	(24)
7	Pd@MIL-101-NH_2(Cr)	BQ (20)	AcOH, 5 h	(18)
8	Pd@MIL-101-NH_2(Cr)	$PhI(OAc)_2$ (20)	H_2O/AcOH, 5 h	Traces
9	Pd@MIL-101-NH_2(Cr)	CH_3CO_3H (20)	H_2O/AcOH, 5 h	(17)
10	Pd@MIL-101-NH_2(Cr)	Oxone (20)	H_2O/AcOH, 5 h	(14)
11	Pd@MIL-101-NH_2(Cr)	^{t}BuOOH (20)	H_2O/AcOH, 5 h	(37)
12	Pd@MIL-101-NH_2(Cr)	$K_2S_2O_8$ (20)	H_2O/AcOH, 5 h	(45)
13	Pd@MIL-101-NH_2 (Cr)	^{t}BuOOH (20)	HCl 2M, 2 h	68
14	Pd@MIL-101-NH_2(Cr)	$K_2S_2O_8$ (10)	HCl 2M, 2 h	69
15	Pd@MIL-88B-NH_2(Cr)[b]	^{t}BuOOH (20)	HCl 2M, 2 h	70
16	Pd@MIL-88B-NH_2(Cr)[b]	$K_2S_2O_8$ (10)	HCl 2M, 2 h	72
17	**Pd@MIL-88B-NH_2(Cr)[b]**	**$K_2S_2O_8$ (5)**	**HCl 2M, 2 h**	**70**
18	Pd/C	$K_2S_2O_8$ (5)	HCl 2M, 2 h	13

Oxidant screening reactions were performed under sonication. After redispersion, catalytsts were tested under the following conditions: 2 mmol **11a**, catalyst (0.1 mol%), Cs_2CO_3 (25 mol%), 50% EtOH (0.2 M), rt, 2 h. (a) Versus palladium. (b) Deactivated Pd@MIL-88B-NH_2(Cr) obtained after 2 reaction runs; Isolated yields. In parenthesis, yields determined by ^{1}H NMR spectroscopy using an internal standard.

We then applied the optimized catalyst redispersion procedure in a new recyclability test (runs 1'- 6'; Figure 36, green bars) under the conditions presented (Table 5, entry 17; Figure 36a). After two new runs (1' and 2'), the deactivated catalyst was subjected to oxidative conditions (Figure 36a, Ox_1), and a 71 % yield of **12a** was obtained in run 3', *versus* 30% obtained in run 3 without oxidation treatment (blue bars in the same plot). Interestingly, the redispersed catalyst after run 2' displayed the same efficiency for an additional run (69% yield in run 4' *versus* 12% in run 4), after which product yield again decreased to 38% in run 5'. The recovered catalyst after run 5' was subjected to a second redispersion (Ox_2), obtaining a yield of 71% of biaryl **12a** in a sixth run (6').

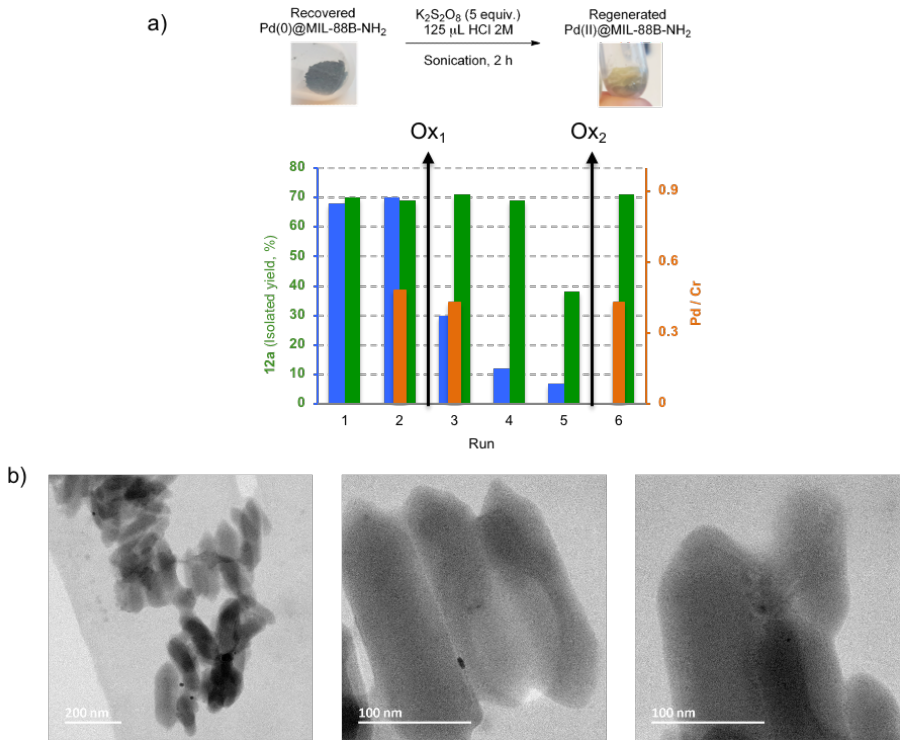

Figure 36. (a) Ex situ oxidative regeneration of the Pd(II)@MOF catalyst and new recycling experiments on a 4 mmol scale (green). Regeneration of the catalyst was performed after runs 2' and 5' (green arrows; yields obtained using the deactivated catalyst are kept in blue for easier comparison). Pd/Cr ratio in the catalyst before and after oxidative regenerations (orange) are represented in the right axis; (b) BF-STEM images of the Pd@MIL-88B-NH_2(Cr) catalyst after 5 reaction runs and the second oxidation step (Ox_2), prior to run 6'.

The evolution of the supported palladium species after the oxidative treatments was monitored using STEM, showing that the number of Pd(0) particles was dramatically reduced (Figure 34c *versus* Figure 36b), and a correct preservation of the MIL-88B-NH_2(Cr) morphology. The Pd load of the framework was analyzed by ICP-OES after runs 2', 3', and 6'. From run 2' to 3' (after Ox_1), a slight decrease of in the Pd/Cr ratio was detected (10%, Figure 36a, orange bars), but the same ratio was retained after run 6' (0.43). The repetition of this deactivation-reactivation sequence strengthens the hypothesis that the amount of catalytically active Pd(II) precursors decreases critically after two runs to form inactive Pd(0) particles where the reoxidation by oxygen is very limited.

5.5. Conclusions

Pd(II) complexes supported on MIL-88B-NH_2(Cr) showed good catalytic activity in the homocoupling of arylboronic acids under mild conditions, and in short reaction times. Diverse biaryls were obtained and easily isolated in moderate to excellent yields, and it was possible to scale up the reaction tenfold with the same efficiency.

The catalyst showed a decreased performance after two runs. We ascribed this behaviour to the progressive reduction of Pd(II) into Pd(0) particles of crescent size, where the aerobic oxidation to form catalytically active Pd(II) is increasingly difficult. The presence of Pd(II) probed to be essential; after being subjected to oxidative conditions, the inactive Pd particles could be redispersed and the catalytic activity restored. This procedure was successfully applied twice, showing a good tolerance for the crystalline structure of MIL-88B-NH_2(Cr).

The STEM analysis of the catalyst showed that small particles could be stabilized by the MOF matrix after the first reaction runs. We believe that, beyond a passive support, the MOF could increase catalyst lifetime by avoiding, to some extent, the formation of *in situ* generated inactive particles and clusters.

6. Electrocatalytic semireduction of alkynes on nickel foam (Paper IV)

6.1. Background and aim of the project

As it was mentioned in the introduction (section 1.4), Ni foam is a well-known catalyst for the HER.[183] The initial goal of this work was developing a hydrogenation protocol using electrochemically generated hydrogen from a Ni foam electrocatalyst and Pd@MIL-101-NH_2(Cr) as hydrogenation catalyst (Figure 37). In the very first attempts, using 2-cyclohexenone (**14**) as model substrate, a 76% of cyclohexanone **15** was obtained in 2 h together with a 20% of an unexpected phenol side-product (**15'**).

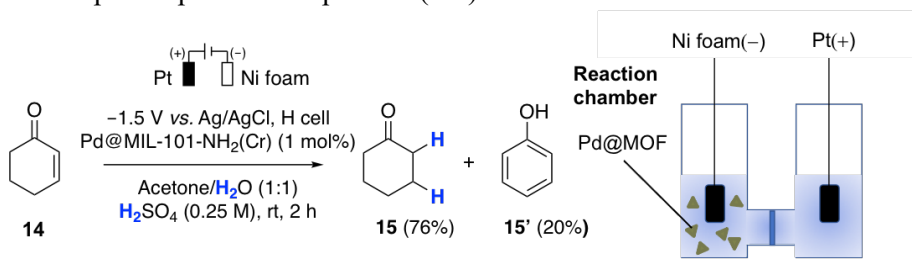

Figure 37. Initial electrochemical hydrogenation experiments.

To get a better understanding on the system, a series of control experiments were conducted. When the reaction was performed using the same Ni foam electrode in absence of the Pd@MOF catalyst, 57% of **15** was obtained (no phenol observed, Figure 38a). When the recycled Ni foam (denoted Pd@Ni foam) was subjected to the hydrogenation of 2-cyclohexenone using a hydrogen balloon, quantitative yields of the hydrogenated product (**15**) was obtained after 16 h (no potential applied; Figure 38b). However, only traces of the product were obtained when a fresh nickel foam was used over the same reaction time (Figure 38c). These three experiments confirmed that after 1 reaction with Pd@MOF in suspension a Pd-Ni alloy is formed, which is catalytically active under a hydrogen atmosphere (no applied potential needed). Furthermore, it demonstrated that a fresh Ni foam is inactive under a hydrogen atmosphere. Surprisingly, when the reaction was performed with a fresh Ni foam under electrochemical conditions and no Pd@MOF added (Figure 38d), a 90% of **15** was obtained. This result was a breakthrough, as it suggested that this transformation could be carried out using a commercially available catalyst based on an earth-abundant metal.

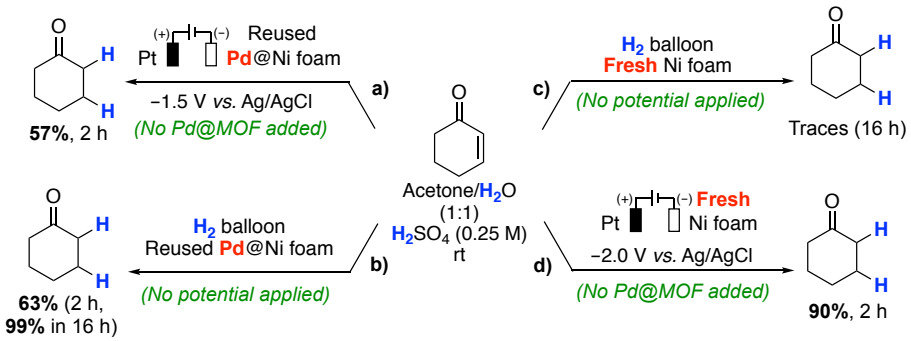

Figure 38. Control experiments in the hydrogenation of 2-cyclohexenone (**14**). Yields determined by ^{1}H NMR spectroscopy using an internal standard.

Taking this interesting result into consideration, we decided to investigate if other functional groups that are typically reduced under palladium catalysis, such as alkynes, were compatible with the method. Subjecting diphenylacetylene (**16**) to similar reaction conditions using bare carbon cloth (CC) as counterelectrode, afforded *Z*-stilbene (**17**) selectively (*E*/*Z* = 10:1), in a promising 31% yield, along with a 3% of *E*-stilbene (**18**), and 10% of the over-hydrogenated product (**19**, 1,2-diphenylethane; Figure 39). Given the potential of this stereoselective olefin synthesis using first-row transition metals, we focused on exploring the scope of this transformation.

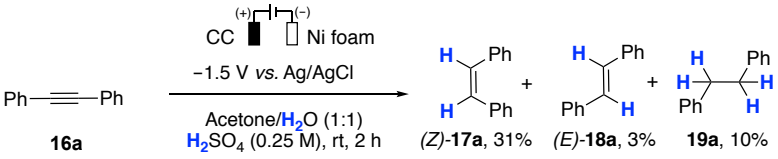

Figure 39. Electrochemical hydrogenation of diphenylacetylene.

6.2. Optimization of reaction conditions

From the starting conditions (Figure 39 and Table 6 entry 1), 48% of **17a** was obtained when the reaction time was extended to 6 h, however, together with large amounts of **19a** (32%, entry 2). The reaction was sensitive to the concentration of sulfuric acid, as when using 0.13 M instead of 0.25 M (entry 3), 29% of **17a** was obtained, with only 2% of alkane **19a** (5-fold less than in entry 1). When sulfuric acid was replaced by NBu_4BF_4 as electrolyte (entry 4) only traces of **17a** were obtained. Increasing the potential to –2.0 V and –2.5 V in H_2SO_4 (0.13 M), provided **17a** in 51% and 64% within 2 h (entries 5 and 6 respectively). When the reaction time was increased to 4 h at –2.5 V, the desired Z-alkene **17a** was obtained in 76% yield, with a very high selectivity *Z*/*E* = 19:1 (entry 7).

Other well-known catalysts for HER described in the literature, such as cobalt phosphide (CoP),[184] cobalt phosphosulfide (CoPS)[185] and nickel-molybdenum alloy (Ni-Mo),[186] were investigated for the same transformation. Interestingly, they were all outperformed by the commercially available Ni foam (entries 8-10). Bare carbon cloth was also used as cathode, affording only 2% of **17a** (entry 11). Notably, all the alternative cathodes that were tested including CC (entries 8-11) evolved amounts of hydrogen gas that were noticeable to the naked eye, as in the case of Ni foam. However, even if all of them were able to produce hydrogen, only the nickel foam was able to catalyze this reaction. A full optimization table can be found in Paper IV.

The reaction profile under conditions in entry 7 showed that **17a** is consumed upon depletion of the concentration of the starting material **16a**, forming the over-hydrogenated product **19a** (Figure 40).

Table 6. Optimization of the reaction conditions.

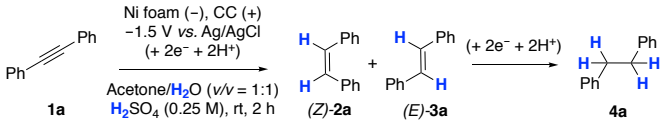

Entry	*Deviation from initial conditions*	*Conv. (%)*	*Yield 17a / 18a / 19a (%)*	*Z/E*
1	none	44	31 / 3 / 10	10:1
2	6 h	87	48 / 7 / 32	7:1
3	H_2SO_4 (0.13 M)	33	29 / 2 / 2	15:1
4	NBu_4BF_4 (0.25 M)	-	traces	-
5	H_2SO_4 (0.13 M), –2.0 V	59	51 / 3 / 5	19:1
6	H_2SO_4 (0.13 M), –2.5 V	78	64 / 4 / 10	16:1
7	**H_2SO_4 (0.13 M), –2.5 V, 4 h**	**94**	**76 / 4 / 13**	**19:1**
8	CoP@CC (–)	4	3 / 1 / -	3:1
9	CoPS@CC (–)	-	n.r.	-
10	Ni-Mo (–)	33	23 / 3 / 7	8:1
11	CC (–)	4	2 / 2 / -	1:1

Reactions were performed in a divided cell using 0.4 mmol **16a** in 25 mL of solvent mixture (in each chamber). Conversion, yields and *Z/E* ratios were determined by ^{1}H NMR spectroscopy using an internal standard.

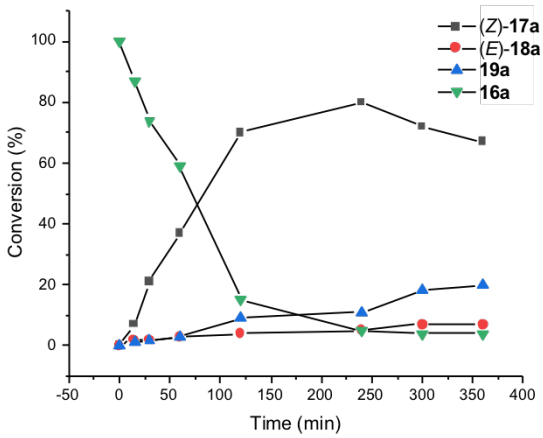

Figure 40. Kinetic profile for the semihydrogenation reaction under optimal conditions (Table 6, entry 7).

6.3. Scope and limitations

We then investigated the reaction scope (Table 7). Substituted diphenylacetylene derivatives (R=Ar, R'=Ph) having EDGs at the *para* position on one of the aryl groups gave *Z*-alkenes **17b** (*p*-OCH_3) and **17c** (*p*-CH_2OH) in 80% and 83% yield respectively, and with high stereoselectivity (*Z/E* up to 18:1).

Fluorinated derivatives **16d** (*p*-OCF_3) and **16e** (*p*-CF_3) were reduced in 70% and 51% yield. Importantly, acetyl-substituted diphenylacetylene (**16f**) was reduced chemoselectively, giving **17f** in 55% yield. In the case of the NO_2-containing substrate **16g**, only the quantitative cathodic reduction of the NO_2 group was observed (*i.e.* **17g** was not detected).

Diphenylacetylene **16h** with a F substituent at the *meta* position gave **17h** in good yield (74%). Halides such as Cl and Br on **16i** and **16j** were very well tolerated, and **17i** and **17j** formed in 71% and 75% yield respectively. Other substrates with *ortho* substituents, *o*-F (**16k**) and *o*-Br (**16l**) afforded the corresponding *Z*-alkenes in good yields (73% and 80% respectively).

Naphthalene derivative **17m** was obtained in 75% yield with a *Z/E* = 20:1. Reduction of poly-chlorinated and fluorinated aromatics (2,4-dichlorophenyl and pentafluorophenyl) **16n** and **16o** worked well, giving synthetically useful yields (67 and 71%). The efficiency of the system for the reduction of heterocyclic-containing alkynes was tested by reducing 3-thiophenylethynyl pyridine **16p**, providing **17p** in 70% yield with a *Z/E* ratio of 20:1. Polysubstituted derivative **17q** was obtained in modest yield (45%), whereas propargylic alcohol **16r** was efficiently reduced to (*Z*)-**17r** in outstanding yield and selectivity (92%, *Z/E* = 20:1). Gratifingly, the cyano group was unaltered during the process. This provides access to important functionalized aromatic building blocks that can be further functionalized.

Ester groups on **16s** and **16t**, and on aliphatic **16u** were tolerated, giving **17s - u** in 73%, 72% and 62% yield respectively. Remarkably, in the case of 4-iodopheyl acrylate (**16t**) protodehalogenation did not occur, which is a common cause for by-product formation when using Pd catalysts.[187]

The method also works well on aliphatic alkynes (R, R' = alkyl), as exemplified with **17v - y**. (*Z*)-Bicyclo[6.1.0]non-4-en-9-ylmethanol (**17v**) was ob-

tained in 73% isolated yield after selective hydrogenation of the corresponding strained cyclooctyne also carrying a primary alcohol. (*Z*)-Dec-5-en-1-ol (**17w**) was obtained in 91% yield. Aliphatic aldehyde **16x** was chemoselectively semihydrogenated, affording **17x** in 69% yield along with only 15% of alcohol **17w**. Oleic acid (**17y**) was obtained upon reduction of unprotected stearolic acid in 81% yield.

In general, terminal aliphatic alkynes (R=Ar, R'=H) are reduced easily under these conditions, as exemplified by **16z**, **16aa**, **16ab**, **16ac** and **16ad**. To the best of our knowledge, there are only two semireduction methods in the literature that are compatible with aryl iodides,[188,189] which makes the herein presented method an excellent alternative when a high chemoselectivity is required. More complex molecules such as ethynylestradiol (**16ad**) could also be semihydrogenated, giving **17ad** in 58% yield.

Table 7. Scope and limitations

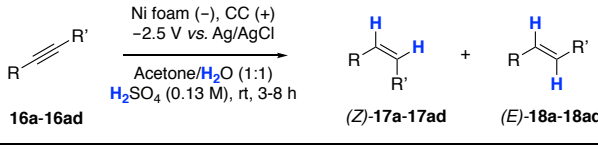

16a-16ad *(Z)*-**17a-17ad** + *(E)*-**18a-18ad**

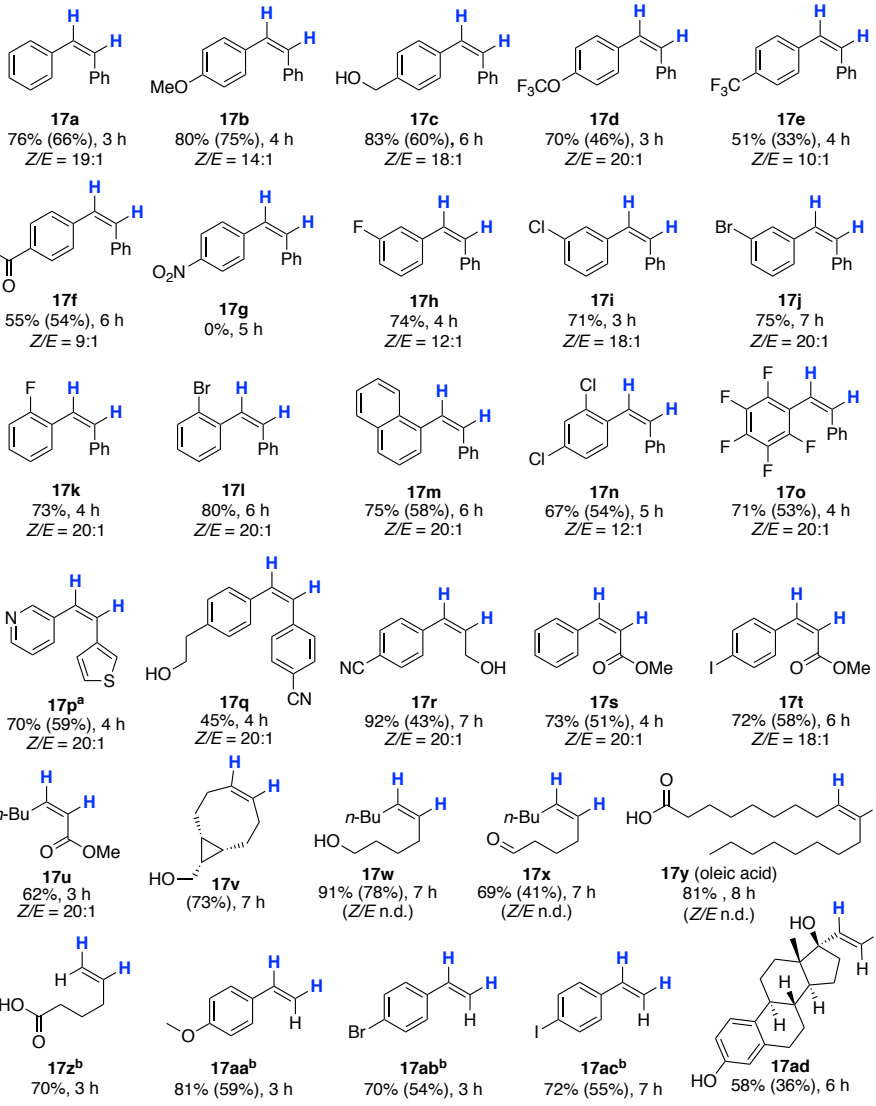

17a
76% (66%), 3 h
Z/*E* = 19:1

17b
80% (75%), 4 h
Z/*E* = 14:1

17c
83% (60%), 6 h
Z/*E* = 18:1

17d
70% (46%), 3 h
Z/*E* = 20:1

17e
51% (33%), 4 h
Z/*E* = 10:1

17f
55% (54%), 6 h
Z/*E* = 9:1

17g
0%, 5 h

17h
74%, 4 h
Z/*E* = 12:1

17i
71%, 3 h
Z/*E* = 18:1

17j
75%, 7 h
Z/*E* = 20:1

17k
73%, 4 h
Z/*E* = 20:1

17l
80%, 6 h
Z/*E* = 20:1

17m
75% (58%), 6 h
Z/*E* = 20:1

17n
67% (54%), 5 h
Z/*E* = 12:1

17o
71% (53%), 4 h
Z/*E* = 20:1

17p[a]
70% (59%), 4 h
Z/*E* = 20:1

17q
45%, 4 h
Z/*E* = 20:1

17r
92% (43%), 7 h
Z/*E* = 20:1

17s
73% (51%), 4 h
Z/*E* = 20:1

17t
72% (58%), 6 h
Z/*E* = 18:1

17u
62%, 3 h
Z/*E* = 20:1

17v
(73%), 7 h

17w
91% (78%), 7 h
(*Z*/*E* n.d.)

17x
69% (41%), 7 h
(*Z*/*E* n.d.)

17y (oleic acid)
81% , 8 h
(*Z*/*E* n.d.)

17z[b]
70%, 3 h

17aa[b]
81% (59%), 3 h

17ab[b]
70% (54%), 3 h

17ac[b]
72% (55%), 7 h

17ad
58% (36%), 6 h

Unless otherwise indicated: alkyne (0.4 mmol), acetone/H_2O (25 mL, *v*/*v* = 1:1), H_2SO_4 (0.13 M), Ni foam cathode (1 cm^2). a) H_2SO_4 0.25 M; b) H_2SO_4 0.06 M. Yields and *Z*/*E* ratios were determined by ^1H NMR spectroscopy using an internal standard. Isolated yields indicated in parenthesis.

6.4. Applications: isotopic labeling

To obtain deuterated alkenes, deuterium gas (D_2) and a metal catalyst (normally, palladium) or superstoichiometric amounts strong reductants are typically used.[135,190–193] As a milder and more benign alternative we were interested in investigating if Ni foam could be used for the synthesis of D-labeled *Z*-alkenes. Using a mixture of non-deuterated acetone (C_3H_6O) and a deuterated sulfuric acid solution (D_2SO_4 in D_2O) in a 1:1 ratio (*v*/*v*) afforded (*Z*)-1-bromo-2-(2-phenylvinyl-1,2-d_2)benzene (**20l**-[D_2]) as the major product with an 87% of deuterium incorporation. The remaining material was identified as a mixture of partially deuterated and hydrogenated products, (**20l'-20l''**)-[D_1] and **17l** respectively (Figure 41a). We initially believed that proton scrambling from acetone would be slow enough to not affect the result (pK_a = 20), but given the long reaction times it could be a potential reason for the high proton incorporation observed.

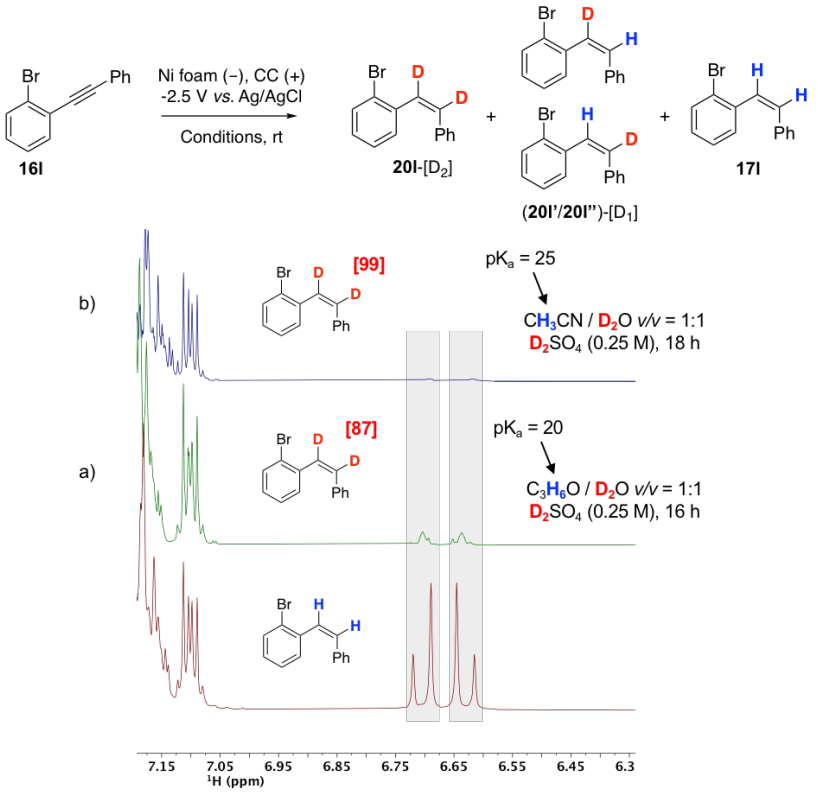

Figure 41. Preliminary deuteration experiments and ^{1}H NMR spectra of the reaction products, including hydrogenated **17l** for comparison (bottom).

To test this hypothesis, acetone was replaced by acetonitrile ($pK_a = 25$) and **20l**-[D_2] was obtained in 70% yield and 99% deuterium incorporation after18 h. The scope of the deuteration reactions was similar to that of the hydrogenations shown in Table 7. Deuterated arylacetylene derivatives **20a**-[D_2]-**20k**-[D_2] were obtained in good to high yields (53-86%, Table 8). In all cases, the deuterium content was higher than 95%, as determined by ^{1}H NMR spectroscopy. Remarkably, oleic acid-9,10-*d*$_2$ (**20k**-[D_2]) could be synthesized in 81% isolated yield and 95% deuterium incorporation.

Table 8. Library of deuterated *Z*-alkenes

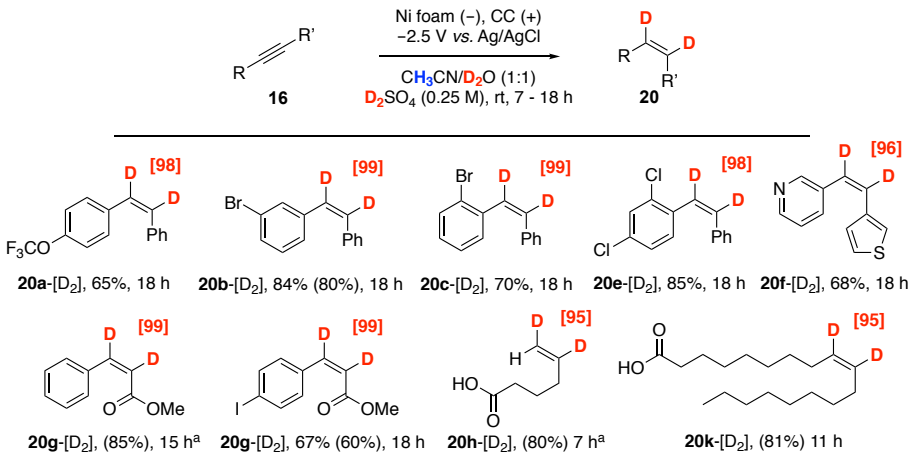

Unless otherwise indicated: 0.4 mmol alkyne, CH_3CN/H_2O (25 mL, *v*/*v* = 1:1), H_2SO_4 (0.25 M), Ni Foam cathode (1 cm^2). (a) H_2SO_4 (0.13 M); Yields were determined by ^{1}H NMR spectroscopy using an internal standard. Isolated yields indicated in parenthesis. Deuterium incorporations were determined by ^{1}H NMR spectroscopy and are indicated in brackets.

6.5. Mechanistic studies and recyclability

As the protonation of Ni foam was reported to be a slow step in the formation of adsorbed hydrogen or deuterium species, deuterations were expected to be significantly slower than hydrogenations.[142,194–196] This was illustrated in a H/D competition experiment where a mixture 1:1 of H_2SO_4 and D_2SO_4 solutions were used (in combination with CH_3CN, Figure 42a). The mixture of products was analyzed by HRMS and a ratio H/D of 4.7 was determined, suggesting a faster formation of Ni-H* than Ni-D* species (or faster H incorporation). Importantly, the ^{1}H NMR spectrum showed the same H content in both C_α and C_β (86%, Figure 42a), suggesting that both H atoms are transferred to the alkyne from the Ni foam surface (*i.e.* the ratio of Ni-H*/Ni-

D* is *ca.* 4.7), therefore ruling out protodemetallation pathways. When the deuteration of diphenylacetylene was performed under a hydrogen atmosphere, a 94% of deuterium incorporation in **20l**-[D_2] was obtained after 1 h, suggesting that the evolved gas does not undergo dissociative adsorption on the Ni foam surface (Figure 42b). This was further supported by experiments in absence of electricity and under a hydrogen atmosphere, where only 7% of **17a** was formed even after heating at 60 ºC for 14 h (Figure 42c), which is in agreement with the control experiments discussed at the beginning of this chapter (Figure 38). This demonstrates that Ni foam is active for the hydrogenation reaction only under electrochemical conditions and that H^+ or D^+ are the only source of adsorbed hydrogen (see also Table 6, entry 4).

The trapping of adsorbed hydrogen (H*) using *tert*-butanol (*t*-BuOH) [197–199] suggested that Ni-H* could be catalytically active species, as a significant decrease in the yield of **17a** was observed in presence of the scavenger in the same reaction time (from 64% to 34% in 2 h, Figure 42d).

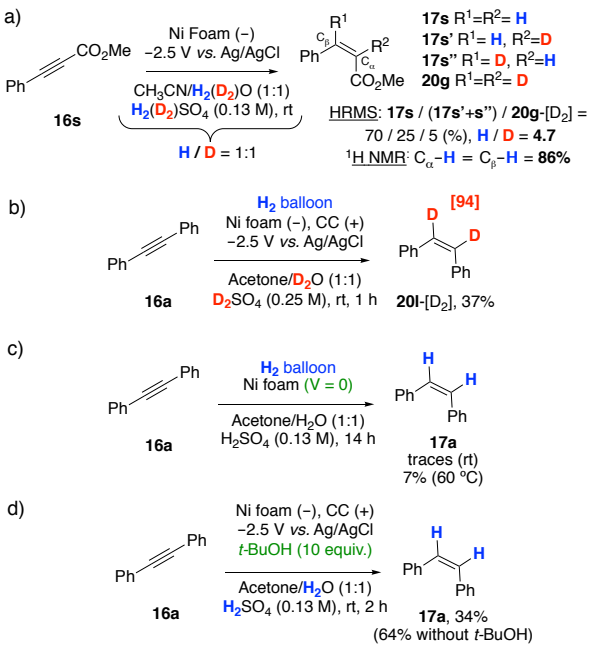

Figure 42. Control experiments on the nickel-catalyzed semireduction of alkynes.

Finally, the recyclability of the Ni foam was investigated for 14 cycles in 2 h reactions, using diphenylacetylene as model substrate (Figure 43). Gratifyingly, the Ni foam electrode showed excellent recyclability during the 14 runs,

delivering the desired *Z*-alkene in 54 ± 9% with the same selectivity. During the first 11 runs, the Ni foam electrode was washed in between experiments with HCl 0.5 M and water under sonication, in order to clean the electrode surface.[200] Interestingly, the Ni foam performed equally well when no washing was performed (between runs 12 and 14), suggesting that under the reaction conditions the electrode surface might be activated in the presence of sulfuric acid. Scanning electron microscopy (SEM) images were collected to analyze the morphology of the fresh Ni foam as obtained from the supplier (both un-washed and washed), after 10 (washed) and 14 runs (unwashed) (Figure 44). The commercially available electrode showed a dramatic change in the surface after treatment with HCl 0.5 M that can be correlated with the formation of α-$Ni(OH)_2$ species (Figure 44, a and b).[200] After 10 cycles, the surface resembles to that of the fresh Ni foam after acid treatment, suggesting that the structure of the electrode is unaltered after multiple cycles (Figure 44c). However, when the Ni foam is recycled for additional three runs without washing, the surface shows some additional material (Figure 44d). This could be ascribed to the deposition of sulfate salts formed during the reaction and that were proved to not compromise the performance of the material (Figure 43).

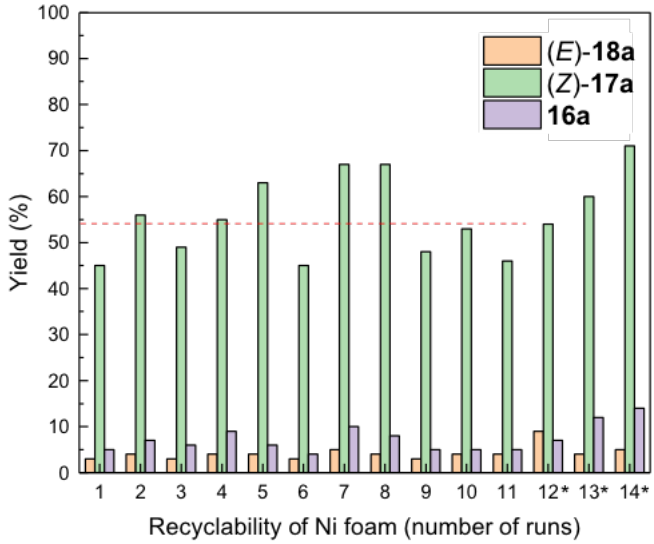

Figure 43. Recyclability of the Ni Foam electrode. Runs where the catalyst was not washed are marked with (*). Most of the recycling experiments were performed by Dr Gurpreet Kaur.

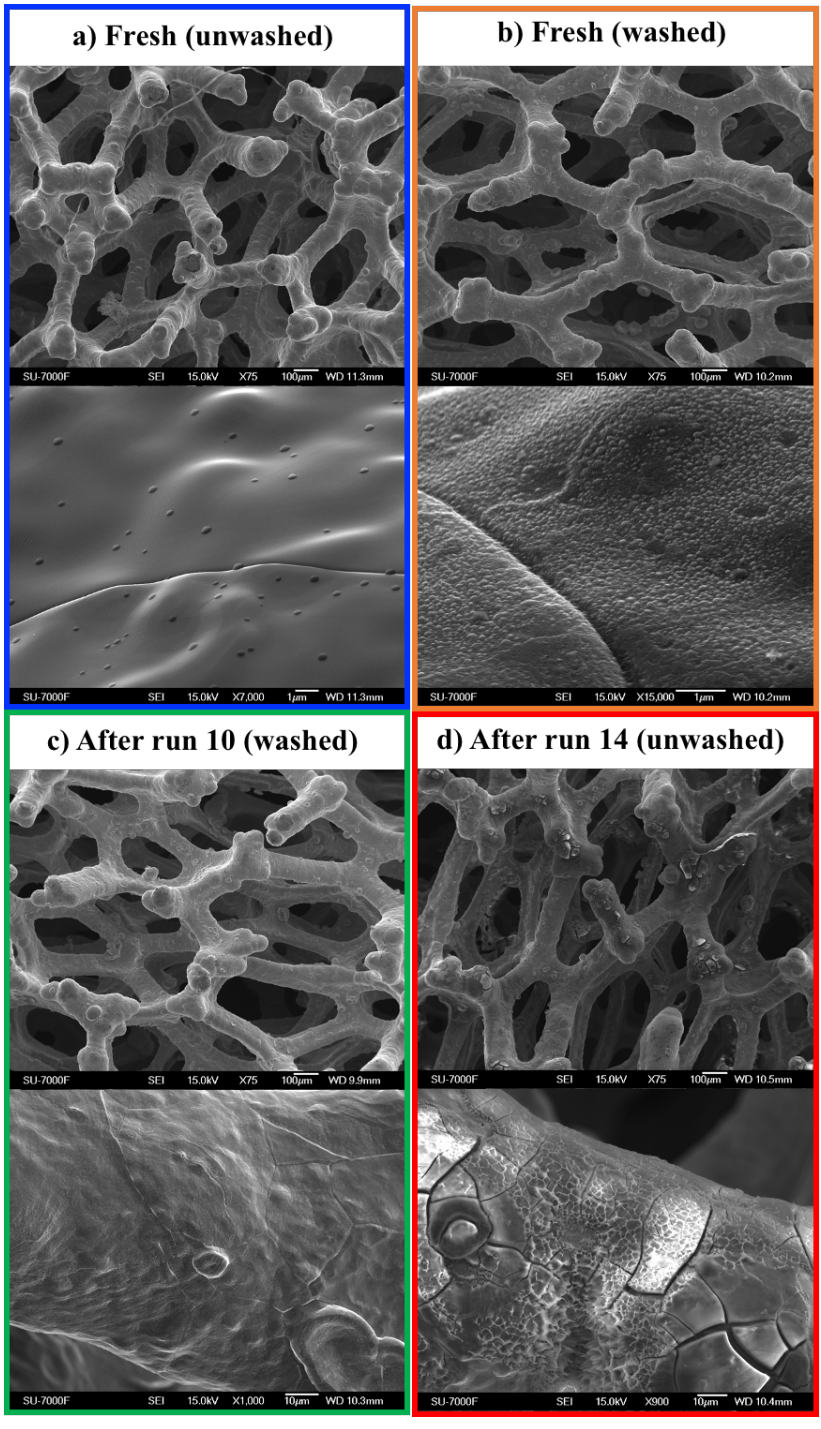

Figure 44. SEM images of Ni foam at different stages of the recyclability study. collected by Dr Gurpreet Kaur

6.6. Conclusions and outcome

To conclude, continuing efforts in increasing the use earth-abundant resources for the reduction of organic compounds have motivated the work in this final chapter.

A straightforward strategy for the selective semireduction of alkynes was successfully developed using a commercially available Ni foam and H_3O^+ as sole hydrogen source under very mild conditions (rt, air). Notably, it was demonstrated that Ni foam not only can be used to obtain a variety of *Z*-alkenes with very high chemo- and stereoselectivity in short reaction times, but it can also be used to obtain deuterium-labeled derivatives that otherwise are cumbersome to obtain. Furthermore, recyclability tests proved the robustness of this catalysts after being used 14 times without loss of its catalytic properties.

Some of the remaining challenges include a better understanding of the reaction mechanism under acidic conditions. This might help to elucidate factors governing the selectivity towards the semihydrogenated product, as in some cases considerable amounts of over-hydrogenated side-products were observed.

However, even if relatively high potentials were applied, the outcome presented in this work greatly compensates the electricity input and set a precedent in the future development of more and better catalysts based on earth-abundant elements.

7. Concluding remarks

The work presented in this doctoral thesis covers multiple aspects of heterogeneous transition-metal catalysis, and has provided new methods for the synthesis of organic building blocks as well as mechanistic understanding.

The results presented in Chapter 3 shows that formation of oxidative addition tetramers may play an important role in the Suzuki-Miyaura reaction, providing a pathway *via* a very facile transmetallation step. We are aware that in ligandless systems, there might be endless possible combinations in the evolution of a metal precursor to form highly active species. Many of these are currently unknown, and the most reactive ones might be extremely challenging to characterize. However, this work has shed some light in one of those species, whose reactivity agrees with the efficiency commonly reported for ligandless systems.

In Chapter 4, the reasons that led to catalyst deactivation in the Mizoroki-Heck reaction were addressed. Chlorides were found to have a very detrimental effect when binding to Pd clusters, as the strong interaction was responsible for the deactivation of the catalyst. However, the work presented here demonstrated that residual Pd complexes in solution could still be catalytically active, as well as the beneficial effects of the MOF support.

Chapter 5 also deals with deactivation processes but with a different and very extended origin to the one presented in Chapter 3: particle aggregation. In this work, a practical procedure for the regeneration of supported active Pd species was developed. Compared to other protocols in the literature, the presented method is applicable to hybrid supports such as MOFs.

In Chapter 6, an electrochemical method for the semihydrogenation of alkynes was presented, using a commercially available nickel foam catalyst in acidic water. The method enabled by this very robust and recyclable catalyst proved to be effective with a wide variety of functionalized alkynes and suitable for the synthesis of isotopically labeled derivatives. This work highlights the potential of using electrochemistry tools for the sustainable synthetic strategies.

8. Appendix A: Author's contributions

Paper I. Design and execution of all the experimental work with BMM, with the exception of the STEM (CWT) and DFT calculations (MSGA), however, exerted an important role in the development and scientific discussions about these topics. Wrote most of the manuscript and supporting information with BMM.

Paper II. Contributed with the activation and deactivation studies, as well as understanding the process by which the active palladium species is formed *in situ*. Wrote a minor part of the manuscript and the supporting information.

Paper III. Performed most of the reactions, including the optimization studies and the reaction scope. Together with SC, synthesized and characterized the catalysts. Developed the oxidative method for the regeneration of the catalyst. Wrote the manuscript and most of the supporting information with BMM.

Paper IV. Developed the catalytic method using the nickel foam after initial findings by ASM, optimized both hydrogenation and deuteration conditions and synthesized the majority of the starting materials and hydrogenated products. Contributed to the purification of some of the final compounds. Participated in the recyclability study. Wrote the manuscript with BMM and small parts of the supporting information.

9. Appendix B: reprint permissions

Permissions to reprint the following publications were obtained from the respective publishers:

Paper II. Yuan, N.; Pascanu, V.; Huang, Z.; Valiente, A.; Heidenreich, N.; Leubner, S.; Inge, A. K.; Gaar, J.; Stock, N.; Persson, I.; Martín-Matute, B.; Zou, X. *J. Am. Chem. Soc.* **2018**, *140*, 8206–8217.

Paper III. Valiente, A.; Carrasco, S.; Sanz-Marco, A.; Tai, C. W.; Bermejo Gómez, A.; Martín-Matute, B. *ChemCatChem* **2019**, *11*, 3933–3940.

Paper IV. Valiente, A.; Martínez-Pardo, P.; Kaur, G.; Johansson, J. M.; Martín-Matute, B. *Accepted for publication in ChemSusChem. DOI: 10.1002/cssc.202102221*

Permissions to reprint parts of figures 4, 8b, 8c, 16 and 19 were obtained from the respective publishers:

Figure 4. Biswas, S.; Couck, S.; Grzywa, M.; Denayer, J. F. M.; Volkmer, D.; Van Der Voort, P. *Eur. J. Inorg. Chem.* **2012**, 2481–2486.

Figure 8b. Yunker, L. P. E.; Ahmadi, Z.; Logan, J. R.; Wu, W.; Li, T.; Martindale, A.; Oliver, A. G.; McIndoe, J. S. *Organometallics* **2018**, *37*, 4297–4308.

Figure 8c. Kolter, M.; Böck, K.; Karaghiosoff, K.; Koszinowski, K. *Angew. Chem. Int. Ed.* **2017**, *56*, 13244–13248.

Figure 16. Pascanu, V.; Bermejo Gómez, A.; Ayats, C.; Platero-Prats, A. E.; Carson, F.; Su, J.; Yao, Q.; Pericàs, M. A.; Zou, X.; Martín-Matute, B. *ACS Catal.* **2015**, *5*, 472–479.

Figure 19. Polynski, M. V.; Ananikov, V. P. *ACS Catal.* **2019**, *9*, 3991–4005.

10. Acknowledgements

I would like to express my most sincere gratitude to:

First and foremost, Prof. Belen Martín-Matute, for accepting me in the group and giving me the chance to live this experience that has been so important in my life as a chemist and as a person. Thank you for believing in me and for all the support that I received during these years.

Prof. Inmaculada Robina, because you identified and endorsed a potential in me that others dismissed and, thanks to you I got to know about the one that eventually became my group.

Prof. Mimi Hii, for accepting as faculty opponent of this PhD defense.

Dr Antonio Bermejo Gómez, for all the support that I got from you not only at the beginning of my adventure in Stockholm, but also the times that you came back to the group.

Dr Nicklas Selander and Prof. Kálmán Szabó for their interest in my thesis and the helpful comments.

Prof. Mårten Ahlquist for the continuous collaboration that led to an important part of the work that I present in this thesis.

Dr Cheuk-Wai Tai, for the countless STEM images that you collected and were so important for the development of the research that I performed.

Prof. Xiaodong Zou and Prof. Ingmar Persson, for their help and discussions in our projects and synchrotron activities. Prof. Licheng Sun, Dr Oleksander Kravchenko and Hao Yang for their support. Prof. Adam Slabon and Dr Robin Gueret, for their help and advice on our hydrogenation project.

All my project co-workers, because without their help in the lab and their implication this doctoral thesis would not have been possible: Dr Amparo Sanz, Dr Sergio Carrasco, Dr Antonio Bermejo, Dr Gurpreet Kaur, Dr Pablo Martinez, Dr Robin Gueret and Duc Ha Phan.

My beloved friend Julio Milla, for the translation and to my first proof-readers: Beatriz Saavedra, Victor García, Gurpreet Kaur and Pablo Martínez.

Dr Andrew Kentaro, for his help with MOFs and synchrotron planning. To Erik Svensson, for his kind help and tutorials on MOF drawing.

Dr Vlad Pascanu, for guiding me in my first steps in this lab.

Kristina Romare, Martin Roxengren, Jonas Ståhle, Ola Andersson, Sigrid Mattsson and Petra Godin, for their assistance whenever it was needed.

Past and present members of the BMM group, with whom I shared many moments in and out of the lab: Dr Marta Vico, Dr Amparo Sanz, Dr Samuel Martinez, Dr Elis Erbing, Dr Nagaraju Molleti, Dr Antonio Bernejo, Dr Sergio Carrasco, Alba Carretero, Victor Garcia, Dr Pablo Martinez, Dr Gurpreet Kaur, Dr Greco Gonzalez, Manuel Ramirez, Hugo Santalla, Aitor Bermejo, Dr Vlad Pascanu, Dr Elisa Martínez, Dr Beatriz Saavedra, Majken Raeder, Dr Aditya Dharanipragada, Maria Obieta, Aya Ismael, Mathias Salomon, Pedro Tortajada, Dr Martin Pauze, Dr Kenji Kopf, Duc Ha Phan, Erik Weis and Alexandru Postole.

Past and present members of the department, with whom I also shared parties and trips: Dr Ferran Planas, Dr Marc Montesinos, Marie Deliaval, soon to be Dr Matteo Costantini, Dr Miguel Cortés, Dr Jorge Otero, Dr Alberto Abengózar, Dr Paz Trillo and Dr Tanja Laine.

My good friends in Stockholm: Jasmin Dzanic, Julio Milla, Marko Dombi and Jose Bertikian, for of all the moments we have shared and that have made my time in Stockholm unforgettable. And Alba Carretero, who more than a friend I consider part of my family.

My beloved friends from Spain, whose friendship has been one of my biggest supports all these years: Jesus Prieto, Ines Castaño, Blanca Antón, Javi Romero, Elena Remesal, Lourdes Reguera, Mercedes Reguera, Josema García, la Pillina de Triana, Pilón Elias, Luis Rosa, Chari Marquez and Juanjo Cabrera.

To my aunt Carmen, who I love and admire. Thanks for always being there.

To my parents, José and Rosalía, for the unconditional love and support. Thanks for the education that you gave me, because it made me the person I am today.

Finally, to my dearest Frans, who has been my strongest support since he came into my life. Thanks for being by my side and keep me on my feet during these times. I cannot wait to see what is next ;)

11. References

(1) Berzelius, J. J. *Årsberättelse om framstegen i fysik och kemi*; Norstedt: Stockholm, **1835**.

(2) River, B.; Juniperus, J.; June, O. Catalysis 1. *Nature* **1902**, *65*, 522–526. https://doi.org/10.1038/065522a0.

(3) Laidler, K. J. A Glossary of Terms Used in Chemical Kinetics, Including Reaction Dynamics (IUPAC Recommendations 1996). *Pure Appl. Chem.* **1996**, *68*, 149–192. https://doi.org/10.1351/pac199668010149.

(4) Smil, V. Detonator of the Population Explosion. *Nature* **1999**, *400*, 415. https://doi.org/10.1038/22672.

(5) Erisman, J. W.; Sutton, M. A.; Galloway, J.; Klimont, Z.; Winiwarter, W. How a Century of Ammonia Synthesis Changed the World. *Nat. Geosci.* **2008**, *1*, 636–639. https://doi.org/10.1038/ngeo325.

(6) Barbier, P. Philippe Barbier (1848–1922) and Victor Grignard (1871–1935): Pioneers of Organomagnesium Chemistry. *Georg Thieme Versl. Stuttgart* **2018**, 155–159. https://doi.org/10.1055/s-0037-1609793.

(7) Meijere, A. De; Br, S.; Oestreich, M. *Metal-Catalyzed Cross-Coupling Reactions and More*; de Meijere, A., Bräse, S., Oestreich, M., Eds.; Wiley-VCH Verlag GmbH & Co. KGaA: Weinheim, Germany, **2014**. https://doi.org/10.1002/9783527655588.

(8) Hutchings, G. J.; Catlow, C. R. A.; Hardacre, C.; Davidson, M. G. Catalysis Making the World a Better Place: Satellite Meeting. *Philos. Trans. R. Soc. A Math. Phys. Eng. Sci.* **2016**, *374*. https://doi.org/10.1098/rsta.2015.0358.

(9) Hagen, J. *Industrial Catalysis*; Wiley-VCH Verlag GmbH & Co. KGaA, Weinheim, **2005**. https://doi.org/10.1002/3527607684.

(10) Hartwig, J. F. *Organotransition Metal Chemistry : From Bonding to Catalysis*; University Science Books, **2010**.

(11) Cui, X.; Li, W.; Ryabchuk, P.; Junge, K.; Beller, M. Bridging Homogeneous and Heterogeneous Catalysis by Heterogeneous Single-Metal-Site Catalysts. *Nat. Catal.* **2018**, *1*, 385–397. https://doi.org/10.1038/s41929-018-0090-9.

(12) Crabtree, R. H. Resolving Heterogeneity Problems and Impurity Artifacts in Operationally Homogeneous Transition Metal Catalysts. *Chem. Rev.* **2012**, *112*, 1536–1554. https://doi.org/10.1021/cr2002905.

(13) Schwartz, J. Alkane Activation by Oxide-Bound Organorhodium Complexes. *Acc. Chem. Res.* **1985**, *18*, 302–308. https://doi.org/10.1021/ar00118a004.

(14) Lin, Y.; Finke, R. G. A More General Approach to Distinguishing “Homogeneous” from “Heterogeneous” Catalysis: Discovery of Polyoxoanion- and Bu4N+-Stabilized, Isolable and Redissolvable, High-Reactivity Ir~190–450 Nanocluster Catalysts. *Inorg. Chem.* **1994**, *33*, 4891–4910. https://doi.org/10.1021/ic00100a012.

(15) Zhang, Y.; Fu, D.; Xu, X.; Sheng, Y.; Xu, J.; Han, Y. F. Application of Operando Spectroscopy on Catalytic Reactions. *Curr. Opin. Chem. Eng.* **2016**, *12*, 1–7. https://doi.org/10.1016/j.coche.2016.01.004.

(16) Bayram, E.; Linehan, J. C.; Fulton, J. L.; Roberts, J. A. S.; Szymczak, N. K.; Smurthwaite, T. D.; Özkar, S.; Balasubramanian, M.; Finke, R. G. Is It Homogeneous or Heterogeneous Catalysis Derived from [RhCp *Cl2]2? In Operando XAFS, Kinetic, and Crucial Kinetic Poisoning Evidence for Subnanometer Rh4 Cluster-Based Benzene Hydrogenation Catalysis. *J. Am. Chem. Soc.* **2011**, *133*, 18889–18902. https://doi.org/10.1021/ja2073438.

(17) Batten, S. R.; Champness, N. R.; Chen, X.-M.; Garcia-Martinez, J.; Kitagawa, S.; Öhrström, L.;

O'Keeffe, M.; Paik Suh, M.; Reedijk, J. Terminology of Metal–Organic Frameworks and Coordination Polymers (IUPAC Recommendations 2013). *Pure Appl. Chem.* **2013**, *85*, 1715–1724. https://doi.org/10.1351/PAC-REC-12-11-20.

(18) Kinoshita, Y.; Matsubara, I.; Saito, Y. The Crystal Structure of Bis(Glutaronitrilo)Copper(I) Nitrate. *Bull. Chem. Soc. Jpn.* **1959**, *32*, 1216–1221. https://doi.org/10.1246/bcsj.32.1216.

(19) Kinoshita, Y.; Matsubara, I.; Higuchi, T.; Saito, Y. The Crystal Structure of Bis(Adiponitrilo)Copper(I) Nitrate. *Bull. Chem. Soc. Jpn.* **1959**, *32*, 1221–1226. https://doi.org/10.1246/bcsj.32.1221.

(20) Kinoshita, Y.; Matsubara, I.; Saito, Y. The Crystal Structure of Bis(Succinonitrilo)Copper(I) Nitrate. *Bull. Chem. Soc. Jpn.* **1959**, *32*, 741–747. https://doi.org/10.1246/bcsj.32.741.

(21) Aumüller, A.; Erk, P.; Klebe, G.; Hünig, S.; von Schütz, J. U.; Werner, H.-P. A Radical Anion Salt of 2,5-Dimethyl-N,N′-Dicyanoquinonediimine with Extremely High Electrical Conductivity. *Angew. Chem. Int. Ed.* **1986**, *25*, 740–741. https://doi.org/10.1002/anie.198607401.

(22) Hoskins, B. F.; Robson, R. Infinite Polymeric Frameworks Consisting of Three Dimensionally Linked Rod-like Segments. *J. Am. Chem. Soc.* **1989**, *111*, 5962–5964. https://doi.org/10.1021/ja00197a079.

(23) Hoskins, B. F.; Robson, R. Assembly of Porphyrin Building Blocks into Network Structures with Large Channels. *J. Am. Chem. Soc.* **1990**, *112*, 1546–1554. https://doi.org/10.1021/ja00160a038.

(24) Abrahams, B. F.; Hoskins, B. F.; Michail, D. M.; Robson, R. Assembly of Porphyrin Building Blocks into Network Structures with Large Channels. *Nature* **1994**, *369*, 727–729. https://doi.org/10.1038/369727a0.

(25) Kondo, M.; Yoshitomi, T.; Matsuzaka, H.; Kitagawa, S.; Seki, K. Three-Dimensional Framework with Channeling Cavities for Small Molecules:{[M2(4, 4′-Bpy)3(NO3)4]·xH2O}n(M□ Co, Ni, Zn). *Angew. Chem. Int. Ed.* **1997**, *36*, 1725–1727. https://doi.org/10.1002/anie.199717251.

(26) Kitagawa, S.; Kondo, M. Functional Micropore Chemistry of Crystalline Metal Complex-Assembled Compounds. *Bulletin of the Chemical Society of Japan*. 1998, pp 1739–1753. https://doi.org/10.1246/bcsj.71.1739.

(27) Venkataraman, D.; Gardner, G. B.; Lee, S.; Moore, J. S. Zeolite-like Behavior of a Coordination Network. *J. Am. Chem. Soc.* **1995**, *117*, 11600–11601. https://doi.org/10.1021/ja00151a034.

(28) Gardner, G. B.; Venkataraman, D.; Moore, J. S.; Lee, S. Spontaneous Assembly of a Hinged Coordination Network. *Nature* **1995**, *374*, 792–795. https://doi.org/10.1038/374792a0.

(29) Yaghi, O. M.; Richardson, D. A.; Li, G.; Davis, C. E.; Groy, T. L. Open-Framework Solids with Diamond-Like Structures Prepared from Clusters and Metal-Organic Building Blocks. *MRS Proc.* **1994**, *371*, 15. https://doi.org/10.1557/PROC-371-15.

(30) Yaghi, O. M.; Li, G.; Li, H. Selective Binding and Removal of Guests in a Microporous Metal–Organic Framework. *Nature* **1995**, *378*, 703–706. https://doi.org/10.1038/378703a0.

(31) Yaghi, O. M.; Li, H. Hydrothermal Synthesis of a Metal-Organic Framework Containing Large Rectangular Channels. *J. Am. Chem. Soc.* **1995**, *117*, 10401–10402. https://doi.org/10.1021/ja00146a033.

(32) Li, H.; Eddaoudi, M.; Groy, T. L.; Yaghi, O. M. Establishing Microporosity in Open Metal-Organic Frameworks: Gas Sorption Isotherms for Zn(BDC) (BDC = 1,4-Benzenedicarboxylate) [28]. *J. Am. Chem. Soc.* **1998**, *120*, 8571–8572. https://doi.org/10.1021/ja981669x.

(33) Li, H.; Eddaoudi, M.; O'Keeffe, M.; Yaghi, O. M. Design and Synthesis of an Exceptionally Stable and Highly Porous Metal-Organic Framework. *Nature* **1999**, *402*, 276–279. https://doi.org/10.1038/46248.

(34) Fujita, M.; Washizu, S.; Ogura, K.; Kwon, Y. J. Preparation, Clathration Ability, and Catalysis of a Two-Dimensional Square Network Material Composed of Cadmium(II) and 4, 4′-Bipyridine. *J.*

Am. Chem. Soc. **1994**, *116*, 1151–1152. https://doi.org/10.1021/ja00082a055.

(35) Subramanian, S.; Zaworotko, M. J. Porous Solids by Design:[Zn(4,4′-Bpy)2(SiF6)]N·xDMF, a Single Framework Octahedral Coordination Polymer with Large Square Channels. *Angew. Chem. Int. Ed.* **1995**, *34*, 2127–2129. https://doi.org/10.1002/anie.199521271.

(36) Chui, S. S. Y.; Lo, S. M. F.; Charmant, J. P. H.; Orpen, A. G.; Williams, I. D. A Chemically Functionalizable Nanoporous Material [Cu3(TMA)2 (H2O)3](N). *Science* **1999**, *283*, 1148–1150. https://doi.org/10.1126/science.283.5405.1148.

(37) Furukawa, H.; Cordova, K. E.; O'Keeffe, M.; Yaghi, O. M. The Chemistry and Applications of Metal-Organic Frameworks. *Science* **2013**, *341*, 1230444. https://doi.org/10.1126/science.1230444.

(38) Jiao, L.; Seow, J. Y. R.; Skinner, W. S.; Wang, Z. U.; Jiang, H. L. Metal–Organic Frameworks: Structures and Functional Applications. *Mater. Today* **2019**, *27*, 43–68. https://doi.org/10.1016/j.mattod.2018.10.038.

(39) Lu, W.; Wei, Z.; Gu, Z. Y.; Liu, T. F.; Park, J.; Park, J.; Tian, J.; Zhang, M.; Zhang, Q.; Gentle, T.; Bosch, M.; Zhou, H. C. Tuning the Structure and Function of Metal-Organic Frameworks via Linker Design. *Chem. Soc. Rev.* **2014**, *43*, 5561–5593. https://doi.org/10.1039/c4cs00003j.

(40) Öhrström, L.; Amombo Noa, F. M. *Metal-Organic Frameworks*; ACS In Focus; American Chemical Society: Washington, DC, USA, **2021**. https://doi.org/10.1021/acs.infocus.7e4004.

(41) Bavykina, A.; Kolobov, N.; Khan, I. S.; Bau, J. A.; Ramirez, A.; Gascon, J. Metal-Organic Frameworks in Heterogeneous Catalysis: Recent Progress, New Trends, and Future Perspectives. *Chem. Rev.* **2020**, *120*, 8468–8535. https://doi.org/10.1021/acs.chemrev.9b00685.

(42) Gascon, J.; Corma, A.; Kapteijn, F.; Llabrés I Xamena, F. X. Metal Organic Framework Catalysis: Quo Vadis? *ACS Catal.* **2014**, *4*, 361–378. https://doi.org/10.1021/cs400959k.

(43) Luo, S.; Zeng, Z.; Zeng, G.; Liu, Z.; Xiao, R.; Chen, M.; Tang, L.; Tang, W.; Lai, C.; Cheng, M.; Shao, B.; Liang, Q.; Wang, H.; Jiang, D. Metal Organic Frameworks as Robust Host of Palladium Nanoparticles in Heterogeneous Catalysis: Synthesis, Application, and Prospect. *ACS Appl. Mater. Interfaces* **2019**, *11*, 32579–32598. https://doi.org/10.1021/acsami.9b11990.

(44) Pascanu, V.; González Miera, G.; Inge, A. K.; Martín-Matute, B. Metal-Organic Frameworks as Catalysts for Organic Synthesis: A Critical Perspective. *J. Am. Chem. Soc.* **2019**, *141*, 7223–7234. https://doi.org/10.1021/jacs.9b00733.

(45) Ferey, G.; Mellot-Draznieks, C.; Serre, C.; Millange, F.; Dutour, J.; Surblé, S.; Margiolaki, I. A Chromium Terephthalate-Based Solid with Unusually Large Pore Volumes and Surface Area. *Science* **2005**, *309*, 2040–2042. https://doi.org/10.1126/science.1116275.

(46) Surblé, S.; Serre, C.; Mellot-Draznieks, C.; Millange, F.; Férey, G. A New Isoreticular Class of Metal-Organic-Frameworks with the MIL-88 Topology. *Chem. Commun.* **2006**, No. 3, 284–286. https://doi.org/10.1039/B512169H.

(47) Lebedev, O. I.; Millange, F.; Serre, C.; Van Tendeloo, G.; Férey, G. First Direct Imaging of Giant Pores of the Metal-Organic Framework MIL-101. *Chem. Mater.* **2005**, *17*, 6525–6527. https://doi.org/10.1021/cm051870o.

(48) Serre, C.; Mellot-Draznieks, C.; Surble, S.; Audebrand, N.; Filinchuk, Y.; Ferey, G. Role of Solvent-Host Interactions That Lead to Very Large Swelling of Hybrid Frameworks. *Science* **2007**, *315*, 1828–1831. https://doi.org/10.1126/science.1137975.

(49) Biswas, S.; Couck, S.; Grzywa, M.; Denayer, J. F. M.; Volkmer, D.; Van Der Voort, P. Vanadium Analogues of Nonfunctionalized and Amino-Functionalized MOFs with MIL-101 Topology - Synthesis, Characterization, and Gas Sorption Properties. *Eur. J. Inorg. Chem.* **2012**, No. 15, 2481–2486. https://doi.org/10.1002/ejic.201200106.

(50) Yang, Q.; Xu, Q.; Jiang, H. L. Metal-Organic Frameworks Meet Metal Nanoparticles: Synergistic

Effect for Enhanced Catalysis. *Chem. Soc. Rev.* **2017**, *46*, 4774–4808. https://doi.org/10.1039/c6cs00724d.

(51) Li, H.; Zhu, Z.; Zhang, F.; Xie, S.; Li, H.; Li, P.; Zhou, X. Palladium Nanoparticles Confined in the Cages of MIL-101: An Efficient Catalyst for the One-Pot Indole Synthesis in Water. *ACS Catal.* **2011**, *1*, 1604–1612. https://doi.org/10.1021/cs200351p.

(52) Liu, H.; Li, Y.; Luque, R.; Jiang, H. A Tuneable Bifunctional Water-Compatible Heterogeneous Catalyst for the Selective Aqueous Hydrogenation of Phenols. *Adv. Synth. Catal.* **2011**, *353*, 3107–3113. https://doi.org/10.1002/adsc.201100479.

(53) Huang, Y.; Zheng, Z.; Liu, T.; Lü, J.; Lin, Z.; Li, H.; Cao, R. Palladium Nanoparticles Supported on Amino Functionalized Metal-Organic Frameworks as Highly Active Catalysts for the Suzuki-Miyaura Cross-Coupling Reaction. *Catal. Commun.* **2011**, *14*, 27–31. https://doi.org/10.1016/j.catcom.2011.07.004.

(54) Pascanu, V.; Yao, Q.; Bermejo Gõmez, A.; Gustafsson, M.; Yun, Y.; Wan, W.; Samain, L.; Zou, X.; Martín-Matute, B. Sustainable Catalysis: Rational Pd Loading on MIL-101Cr-NH2 for More Efficient and Recyclable Suzuki-Miyaura Reactions. *Chem. Eur. J.* **2013**, *19*, 17483–17493. https://doi.org/10.1002/chem.201302621.

(55) Pascanu, V.; Hansen, P. R.; Bermejo Gómez, A.; Ayats, C.; Platero-Prats, A. E.; Johansson, M. J.; Pericàs, M.; Martín-Matute, B. Highly Functionalized Biaryls via Suzuki-Miyaura Cross-Coupling Catalyzed by Pd@MOF under Batch and Continuous Flow Regimes. *ChemSusChem* **2015**, *8*, 123–130. https://doi.org/10.1002/cssc.201402858.

(56) Carson, F.; Pascanu, V.; Bermejo-Gómez, A.; Zhang, Y.; Platero-Prats, A. E.; Zou, X.; Martín-Matute, B. Influence of the Base on Pd@MIL-101-NH2(Cr) as Catalyst for the Suzuki-Miyaura Cross-Coupling Reaction. *Chem. Eur. J.* **2015**, *21*, 10896–10902. https://doi.org/10.1002/chem.201500843.

(57) Pascanu, V.; Bermejo Gómez, A.; Ayats, C.; Platero-Prats, A. E.; Carson, F.; Su, J.; Yao, Q.; Pericàs, M. A.; Zou, X.; Martín-Matute, B. Double-Supported Silica-Metal-Organic Framework Palladium Nanocatalyst for the Aerobic Oxidation of Alcohols under Batch and Continuous Flow Regimes. *ACS Catal.* **2015**, *5*, 472–479. https://doi.org/10.1021/cs501573c.

(58) Pascanu, V.; Carson, F.; Solano, M. V.; Su, J.; Zou, X.; Johansson, M. J.; Martín-Matute, B. Selective Heterogeneous C-H Activation/Halogenation Reactions Catalyzed by Pd@MOF Nanocomposites. *Chem. Eur. J.* **2016**, *22*, 3729–3737. https://doi.org/10.1002/chem.201502918.

(59) Vico Solano, M.; González Miera, G.; Pascanu, V.; Inge, A. K.; Martín-Matute, B. Versatile Heterogeneous Palladium Catalysts for Diverse Carbonylation Reactions under Atmospheric Carbon Monoxide Pressure. *ChemCatChem* **2018**, *10*, 1089–1095. https://doi.org/10.1002/cctc.201701439.

(60) Huskić, I.; Pekov, I. V.; Krivovichev, S. V.; Friščić, T. Minerals with Metal-Organic Framework Structures. *Sci. Adv.* **2016**, *2*, 1–8. https://doi.org/10.1126/sciadv.1600621.

(61) Yang, Q.; Yao, F.; Zhong, Y.; Chen, F.; Shu, X.; Sun, J.; He, L.; Wu, B.; Hou, K.; Wang, D.; Li, X. Metal–Organic Framework Supported Palladium Nanoparticles: Applications and Mechanisms. *Part. Part. Syst. Charact.* **2019**, *36*, 1–19. https://doi.org/10.1002/ppsc.201800557.

(62) Trzeciak, A. M.; Augustyniak, A. W. The Role of Palladium Nanoparticles in Catalytic C–C Cross-Coupling Reactions. *Coord. Chem. Rev.* **2019**, *384*, 1–20. https://doi.org/10.1016/j.ccr.2019.01.008.

(63) Eremin, D. B.; Ananikov, V. P. Understanding Active Species in Catalytic Transformations: From Molecular Catalysis to Nanoparticles, Leaching, “Cocktails” of Catalysts and Dynamic Systems. *Coord. Chem. Rev.* **2017**, *346*, 2–19. https://doi.org/10.1016/j.ccr.2016.12.021.

(64) Ananikov, V. P.; Beletskaya, I. P. Toward the Ideal Catalyst: From Atomic Centers to a “Cocktail”

of Catalysts. *Organometallics* **2012**, *31*, 1595–1604. https://doi.org/10.1021/om201120n.

(65) Miyaura, N.; Suzuki, A. Palladium-Catalyzed Cross-Coupling Reactions of Organoboron Compounds. *Chem. Rev.* **1995**, *95*, 2457–2483. https://doi.org/10.1021/cr00039a007.

(66) Hooshmand, S. E.; Heidari, B.; Sedghi, R.; Varma, R. S. Recent Advances in the Suzuki-Miyaura Cross-Coupling Reaction Using Efficient Catalysts in Eco-Friendly Media. *Green Chem.* **2019**, *21*, 381–405. https://doi.org/10.1039/c8gc02860e.

(67) Beletskaya, I. P.; Alonso, F.; Tyurin, V. The Suzuki-Miyaura Reaction after the Nobel Prize. *Coord. Chem. Rev.* **2019**, *385*, 137–173. https://doi.org/10.1016/j.ccr.2019.01.012.

(68) Biffis, A.; Centomo, P.; Del Zotto, A.; Zecca, M. Pd Metal Catalysts for Cross-Couplings and Related Reactions in the 21st Century: A Critical Review. *Chem. Rev.* **2018**, *118*, 2249–2295. https://doi.org/10.1021/acs.chemrev.7b00443.

(69) Johansson Seechurn, C. C. C.; Kitching, M. O.; Colacot, T. J.; Snieckus, V. Palladium-Catalyzed Cross-Coupling: A Historical Contextual Perspective to the 2010 Nobel Prize. *Angew. Chem. Int. Ed.* **2012**, *51*, 5062–5085. https://doi.org/10.1002/anie.201107017.

(70) Lennox, A. J. J.; Lloyd-Jones, G. C. Transmetalation in the Suzuki-Miyaura Coupling: The Fork in the Trail. *Angew. Chem. Int. Ed.* **2013**, *52*, 7362–7370. https://doi.org/10.1002/anie.201301737.

(71) Phan, N. T. S.; Van Der Sluys, M.; Jones, C. W. On the Nature of the Active Species in Palladium Catalyzed Mizoroki-Heck and Suzuki-Miyaura Couplings - Homogeneous or Heterogeneous Catalysis, a Critical Review. *Adv. Synth. Catal.* **2006**, *348*, 609–679. https://doi.org/10.1002/adsc.200505473.

(72) Schmidt, A. F.; Kurokhtina, A. A.; Larina, E. V. Role of a Base in Suzuki-Miyaura Reaction. *Russ. J. Gen. Chem.* **2011**, *81*, 1573–1574. https://doi.org/10.1134/S1070363211070334.

(73) Carrow, B. P.; Hartwig, J. F. Distinguishing between Pathways for Transmetalation in Suzuki-Miyaura Reactions. *J. Am. Chem. Soc.* **2011**, *133*, 2116–2119. https://doi.org/10.1021/ja1108326.

(74) Amatore, C.; Le Duc, G.; Jutand, A. Mechanism of Palladium-Catalyzed Suzuki-Miyaura Reactions: Multiple and Antagonistic Roles of Anionic “Bases” and Their Countercations. *Chem. Eur. J.* **2013**, *19*, 10082–10093. https://doi.org/10.1002/chem.201300177.

(75) Amatore, C.; Jutand, A.; Leduc, G. The Triple Role of Fluoride Ions in Palladium-Catalyzed Suzuki-Miyaura Reactions: Unprecedented Transmetalation from [ArPdFL 2] Complexes. *Angew. Chem. Int. Ed.* **2012**, *51*, 1379–1382. https://doi.org/10.1002/anie.201107202.

(76) Amatore, C.; Jutand, A.; Le Duc, G. Kinetic Data for the Transmetalation/Reductive Elimination in Palladium-Catalyzed Suzuki-Miyaura Reactions: Unexpected Triple Role of Hydroxide Ions Used as Base. *Chem. Eur. J.* **2011**, *17*, 2492–2503. https://doi.org/10.1002/chem.201001911.

(77) Amatore, C.; Jutand, A.; Le Duc, G. Mechanistic Origin of Antagonist Effects of Usual Anionic Bases (OH -, CO 32-) as Modulated by Their Countercations (Na +, Cs +, K +) in Palladium-Catalyzed Suzuki-Miyaura Reactions. *Chem. Eur. J.* **2012**, *18*, 6616–6625. https://doi.org/10.1002/chem.201200516.

(78) Thomas, A. A.; Denmark, S. E. Pre-Transmetalation Intermediates in the Suzuki-Miyaura Reaction Revealed: The Missing Link. *Science* **2016**, *352*, 329–332. https://doi.org/10.1126/science.aad6981.

(79) Olding, A.; Ho, C.; Canty, A.; Lucas, N.; Horne, J.; Bissember, A. C. Synthesis of Arylpalladium(II) Boronates: Confirming the Structure of Pre-transmetalation Intermediates in the Suzuki–Miyaura Reaction Crystallographically. *Angew. Chem. Int. Ed.* **2021**, anie.202104802. https://doi.org/10.1002/anie.202104802.

(80) Belyakov, P. A.; Kadentsev, V. I.; Chizhov, A. O.; Kolotyrkina, N. G.; Shashkov, A. S.; Ananikov, V. P. Mechanistic Insight into Organic and Catalytic Reactions by Joint Studies Using Mass Spectrometry and NMR Spectroscopy. *Mendeleev Commun.* **2010**, *20*, 125–131.

https://doi.org/10.1016/j.mencom.2010.05.001.

(81) Vikse, K. L.; McIndoe, J. S. Mechanistic Insights from Mass Spectrometry: Examination of the Elementary Steps of Catalytic Reactions in the Gas Phase. *Pure Appl. Chem.* **2015**, *87*, 361–377. https://doi.org/10.1515/pac-2014-1118.

(82) Qian, R.; Liao, Y. X.; Guo, Y. L.; Guo, H. ESI-FTICR-MS Studies on Gas Phase Fragmentation Reactions of ArPd(PPh3)2I Complexes. *J. Am. Soc. Mass Spectrom.* **2006**, *17*, 1582–1589. https://doi.org/10.1016/j.jasms.2006.07.009.

(83) Vikse, K. L.; Ahmadi, Z.; Manning, C. C.; Harrington, D. A.; McIndoe, J. S. Powerful Insight into Catalytic Mechanisms through Simultaneous Monitoring of Reactants, Products, and Intermediates. *Angew. Chem. Int. Ed.* **2011**, *123*, 8454–8456. https://doi.org/10.1002/ange.201102630.

(84) Vikse, K. L.; Ahmadi, Z.; Scott McIndoe, J. The Application of Electrospray Ionization Mass Spectrometry to Homogeneous Catalysis. *Coord. Chem. Rev.* **2014**, *279*, 96–114. https://doi.org/10.1016/j.ccr.2014.06.012.

(85) Limberger, J.; Leal, B. C.; Monteiro, A. L.; Dupont, J. Charge-Tagged Ligands: Useful Tools for Immobilising Complexes and Detecting Reaction Species during Catalysis. *Chem. Sci.* **2015**, *6*, 77–94. https://doi.org/10.1039/c4sc02151g.

(86) Aliprantis, A. O.; Canary, J. W. Observation of Catalytic Intermediates in the Suzuki Reaction by Electrospray Mass Spectrometry. *J. Am. Chem. Soc.* **1994**, *116*, 6985–6986. https://doi.org/10.1021/ja00094a083.

(87) Oliveira, F. F. D.; Dos Santos, M. R.; Lalli, P. M.; Schmidt, E. M.; Bakuzis, P.; Lapis, A. A. M.; Monteiro, A. L.; Eberlin, M. N.; Neto, B. A. D. Charge-Tagged Acetate Ligands as Mass Spectrometry Probes for Metal Complexes Investigations: Applications in Suzuki and Heck Phosphine-Free Reactions. *J. Org. Chem.* **2011**, *76*, 10140–10147. https://doi.org/10.1021/jo201990n.

(88) Vikse, K. L.; Henderson, M. A.; Oliver, A. G.; McIndoe, J. S. Direct Observation of Key Intermediates by Negative-Ion Electrospray Ionisation Mass Spectrometry in Palladium-Catalysed Cross-Coupling. *Chem. Commun.* **2010**, *46*, 7412–7414. https://doi.org/10.1039/c0cc02773a.

(89) Yunker, L. P. E.; Ahmadi, Z.; Logan, J. R.; Wu, W.; Li, T.; Martindale, A.; Oliver, A. G.; McIndoe, J. S. Real-Time Mass Spectrometric Investigations into the Mechanism of the Suzuki-Miyaura Reaction. *Organometallics* **2018**, *37*, 4297–4308. https://doi.org/10.1021/acs.organomet.8b00705.

(90) Kolter, M.; Böck, K.; Karaghiosoff, K.; Koszinowski, K. Anionic Palladium(0) and Palladium(II) Ate Complexes. *Angew. Chem. Int. Ed.* **2017**, *56*, 13244–13248. https://doi.org/10.1002/anie.201707362.

(91) Kolter, M.; Koszinowski, K. Second Comes First: Switching Elementary Steps in Palladium-Catalyzed Cross-Coupling Reactions. *Chem. Eur. J.* **2020**, *26*, 12212–12218. https://doi.org/10.1002/chem.202001041.

(92) Leyva-Pérez, A.; Oliver-Meseguer, J.; Rubio-Marqués, P.; Corma, A. Water-Stabilized Three- and Four-Atom Palladium Clusters as Highly Active Catalytic Species in Ligand-Free C-C Cross-Coupling Reactions. *Angew. Chem. Int. Ed.* **2013**, *52*, 11554–11559. https://doi.org/10.1002/anie.201303188.

(93) Yang, C.; Zhang, L.; Lu, C.; Zhou, S.; Li, X.; Li, Y.; Yang, Y.; Li, Y.; Liu, Z.; Yang, J.; Houk, K. N.; Mo, F.; Guo, X. Unveiling the Full Reaction Path of the Suzuki–Miyaura Cross-Coupling in a Single-Molecule Junction. *Nat. Nanotechnol.* **2021**. https://doi.org/10.1038/s41565-021-00959-4.

(94) Astruc, D. Palladium Nanoparticles as Efficient Green Homogeneous and Heterogeneous Carbon-Carbon Coupling Precatalysts: A Unifying View. *Inorg. Chem.* **2007**, *46*, 1884–1894. https://doi.org/10.1021/ic062183h.

(95) Heck, K. F.; Nolley, J. P. Palladium-Catalyzed Vinylic Hydrogen Substitution Reactions with Aryl, Benzyl, and Styryl Halides. *J. Org. Chem.* **1972**, *37*, 2320–2322. https://doi.org/10.1021/jo00979a024.

(96) Heck, R. F. Arylation, Methylation, and Carboxyalkylation of Olefins by Group VIII Metal Derivatives. *J. Am. Chem. Soc.* **1968**, *90*, 5518–5526. https://doi.org/10.1021/ja01022a034.

(97) Mizoroki, T.; Mori, K.; Ozaki, A. Arylation of Olefin with Aryl Iodide Catalyzed by Palladium. *Bull. Chem. Soc. Jpn.* **1971**, *44*, 581–581. https://doi.org/10.1246/bcsj.44.581.

(98) Kikukawa, K.; Yamane, T.; Takagi, M.; Matsuda, T. Reaction of Co-Ordinated Phosphines: Arylation of Olefins by Palladium(II) Acetate and Triarylphosphine. *J. Chem. Soc. Chem. Commun.* **1972**, *0*, 695. https://doi.org/10.1039/c39720000695.

(99) Amatore, C.; Carré, E.; Jutand, A.; M'Barki, M. A.; Meyer, G. Evidence for the Ligation of Palladium(0) Complexes by Acetate Ions: Consequences on the Mechanism of Their Oxidative Addition with Phenyl Iodide and PhPd(OAc)(PPh3)2 as Intermediate in the Heck Reaction. *Organometallics* **1995**, *14*, 5605–5614. https://doi.org/10.1021/om00012a029.

(100) Amatore, C.; Jutand, A. Anionic Pd(0) and Pd(II) Intermediates in Palladium-Catalyzed Heck and Cross-Coupling Reactions. *Acc. Chem. Res.* **2000**, *33*, 314–321. https://doi.org/10.1021/ar980063a.

(101) Amatore, C.; Azzabi, M.; Jutand, A. Role and Effects of Halide Ions on the Rates and Mechanisms of Oxidative Addition of Iodobenzene to Low-Ligated Zerovalent Palladium Complexes Pd0(PPh3)2. *J. Am. Chem. Soc.* **1991**, *113*, 8375–8384. https://doi.org/10.1021/ja00022a026.

(102) Amatore, C.; Jutand, A.; M'Barki, M. A. Evidence of the Formation of Zerovalent Palladium from Pd(OAc)2 and Triphenylphosphine. *Organometallics* **1992**, *11*, 3009–3013. https://doi.org/10.1021/om00045a012.

(103) Jeffery, T. On the Efficiency of Tetraalkylammonium Salts in Heck Type Reactions. *Tetrahedron* **1996**, *52*, 10113–10130. https://doi.org/10.1016/0040-4020(96)00547-9.

(104) Jeffery, T.; David, M. [Pd/Base/QX] Catalyst Systems for Directing Heck-Type Reactions. *Tetrahedron Lett.* **1998**, *39*, 5751–5754. https://doi.org/10.1016/S0040-4039(98)01135-6.

(105) Beletskaya, I. P.; Cheprakov, A. V. Heck Reaction as a Sharpening Stone of Palladium Catalysis. *Chem. Rev.* **2000**, *100*, 3009–3066. https://doi.org/10.1021/cr9903048.

(106) Reetz, M. T.; Westermann, E.; Lohmer, R.; Lohmer, G. A Highly Active Phosphine-Free Catalyst System for Heck Reactions of Aryl Bromides. *Tetrahedron Lett.* **1998**, *39*, 8449–8452. https://doi.org/10.1016/S0040-4039(98)01967-4.

(107) de Vries, A. H. M.; Mulders, J. M. C. A.; Mommers, J. H. M.; Henderickx, H. J. W.; de Vries, J. G. Homeopathic Ligand-Free Palladium as a Catalyst in the Heck Reaction. A Comparison with a Palladacycle. *Org. Lett.* **2003**, *5*, 3285–3288. https://doi.org/10.1021/ol035184b.

(108) De Vries, J. G. A Unifying Mechanism for All High-Temperature Heck Reactions. the Role of Palladium Colloids and Anionic Species. *Dalt. Trans.* **2006**, No. 3, 421–429. https://doi.org/10.1039/b506276b.

(109) Fernandes, T. D. A.; Gontijo Vaz, B.; Eberlin, M. N.; Da Silva, A. J. M.; Costa, P. R. R. Palladium-Catalyzed Tandem Heck-Lactonization from o-Iodophenols and Enoates: Synthesis of Coumarins and the Study of the Mechanism by Electrospray Ionization Mass Spectrometry. *J. Org. Chem.* **2010**, *75*, 7085–7091. https://doi.org/10.1021/jo1010922.

(110) Evans, J.; O'Neill, L.; Kambhampati, V. L.; Rayner, G.; Turin, S.; Genge, A.; Dent, A. J.; Neisius, T. Structural Characterisation of Solution Species Implicated in the Palladium-Catalysed Heck Reaction by Pd K-Edge X-Ray Absorption Spectroscopy: Palladium Acetate as a Catalyst Precursor. *J. Chem. Soc. Dalt. Trans.* **2002**, No. 10, 2207–2212. https://doi.org/10.1039/b200617k.

(111) Reimann, S.; Stötzel, J.; Frahm, R.; Kleist, W.; Grunwaldt, J. D.; Baiker, A. Identification of the

Active Species Generated from Supported Pd Catalysts in Heck Reactions: An in Situ Quick Scanning EXAFS Investigation. *J. Am. Chem. Soc.* **2011**, *133*, 3921–3930. https://doi.org/10.1021/ja108636u.

(112) Oger, C.; Balas, L.; Durand, T.; Galano, J. M. Are Alkyne Reductions Chemo-, Regio-, and Stereoselective Enough to Provide Pure (Z)-Olefins in Polyfunctionalized Bioactive Molecules? *Chem. Rev.* **2013**, *113*, 1313–1350. https://doi.org/10.1021/cr3001753.

(113) Elsevier, C. J.; de Vries, J. G. *The Handbook of Homogeneous Hydrogenation*; Wiley-VCH, Weinheim, **2006**. https://doi.org/10.1002/9783527619382.

(114) Lindlar, H. Ein Neuer Katalysator Für Selektive Hydrierungen. *Helv. Chim. Acta* **1952**, *35*, 446–450. https://doi.org/10.1002/hlca.19520350205.

(115) Chinchilla, R.; Nájera, C. Chemicals from Alkynes with Palladium Catalysts. *Chem. Rev.* **2014**, *114*, 1783–1826. https://doi.org/10.1021/cr400133p.

(116) Delgado, J. A.; Benkirane, O.; Claver, C.; Curulla-Ferré, D.; Godard, C. Advances in the Preparation of Highly Selective Nanocatalysts for the Semi-Hydrogenation of Alkynes Using Colloidal Approaches. *Dalt. Trans.* **2017**, *46*, 12381–12403. https://doi.org/10.1039/c7dt01607g.

(117) Molnár, Á.; Sárkány, A.; Varga, M. Hydrogenation of Carbon-Carbon Multiple Bonds: Chemo-, Regio- and Stereo-Selectivity. *J. Mol. Catal. A Chem.* **2001**, *173*, 185–221. https://doi.org/10.1016/S1381-1169(01)00150-9.

(118) Reina, A.; Favier, I.; Pradel, C.; Gómez, M. Stable Zero-Valent Nickel Nanoparticles in Glycerol: Synthesis and Applications in Selective Hydrogenations. *Adv. Synth. Catal.* **2018**, *360*, 3544–3552. https://doi.org/10.1002/adsc.201800786.

(119) Rai, R. K.; Awasthi, M. K.; Singh, V. K.; Barman, S. R.; Behrens, S.; Singh, S. K. Aqueous Phase Semihydrogenation of Alkynes over Ni-Fe Bimetallic Catalysts. *Catal. Sci. Technol.* **2020**, *10*, 4968–4980. https://doi.org/10.1039/d0cy01153c.

(120) Thiel, N. O.; Kaewmee, B.; Tran Ngoc, T.; Teichert, J. F. A Simple Nickel Catalyst Enabling an E-Selective Alkyne Semihydrogenation. *Chem. Eur. J.* **2020**, *26*, 1597–1603. https://doi.org/10.1002/chem.201903850.

(121) Murugesan, K.; Bheeter, C. B.; Linnebank, P. R.; Spannenberg, A.; Reek, J. N. H.; Jagadeesh, R. V.; Beller, M. Nickel-Catalyzed Stereodivergent Synthesis of E- and Z-Alkenes by Hydrogenation of Alkynes. *ChemSusChem* **2019**, *12*, 3363–3369. https://doi.org/10.1002/cssc.201900784.

(122) Ramirez, B. L.; Lu, C. C. Rare-Earth Supported Nickel Catalysts for Alkyne Semihydrogenation: Chemo- And Regioselectivity Impacted by the Lewis Acidity and Size of the Support. *J. Am. Chem. Soc.* **2020**, *142*, 5396–5407. https://doi.org/10.1021/jacs.0c00905.

(123) Konnerth, H.; Prechtl, M. H. G. Selective Partial Hydrogenation of Alkynes to (Z)-Alkenes with Ionic Liquid-Doped Nickel Nanocatalysts at near Ambient Conditions. *Chem. Commun.* **2016**, *52*, 9129–9132. https://doi.org/10.1039/c6cc00499g.

(124) Murugesan, K.; Alshammari, A. S.; Sohail, M.; Beller, M.; Jagadeesh, R. V. Monodisperse Nickel-Nanoparticles for Stereo- and Chemoselective Hydrogenation of Alkynes to Alkenes. *J. Catal.* **2019**, *370*, 372–377. https://doi.org/10.1016/j.jcat.2018.12.018.

(125) Böldl, M.; Fleischer, I. Homogeneous Nickel-Catalyzed Hydrogenations. In *Homogeneous Hydrogenation with Non-Precious Catalysts*; Wiley, **2019**; pp 63–86. https://doi.org/10.1002/9783527814237.ch3.

(126) Decker, D.; Drexler, H. J.; Heller, D.; Beweries, T. Homogeneous Catalytic Transfer Semihydrogenation of Alkynes-an Overview of Hydrogen Sources, Catalysts and Reaction Mechanisms. *Catal. Sci. Technol.* **2020**, *10*, 6449–6463. https://doi.org/10.1039/d0cy01276a.

(127) Chen, T.; Xiao, J.; Zhou, Y.; Yin, S.; Han, L. B. Nickel-Catalyzed (E)-Selective Semihydrogenation of Internal Alkynes with Hypophosphorous Acid. *J. Organomet. Chem.* **2014**,

749, 51–54. https://doi.org/10.1016/j.jorganchem.2013.09.023.

(128) Richmond, E.; Moran, J. Ligand Control of E/Z Selectivity in Nickel-Catalyzed Transfer Hydrogenative Alkyne Semireduction. *J. Org. Chem.* **2015**, *80*, 6922–6929. https://doi.org/10.1021/acs.joc.5b01047.

(129) Wen, X.; Shi, X.; Qiao, X.; Wu, Z.; Bai, G. Ligand-Free Nickel-Catalyzed Semihydrogenation of Alkynes with Sodium Borohydride: A Highly Efficient and Selective Process for: Cis -Alkenes under Ambient Conditions. *Chem. Commun.* **2017**, *53*, 5372–5375. https://doi.org/10.1039/c7cc02140b.

(130) Shi, Z.; Li, N.; Lu, H.-K.; Chen, X.; Zheng, H.; Yuan, Y.; Ye, K.-Y. Recent Advances in the Electrochemical Hydrogenation of Unsaturated Hydrocarbons. *Curr. Opin. Electrochem.* **2021**, *28*, 100713. https://doi.org/10.1016/j.coelec.2021.100713.

(131) Sherbo, R. S.; Delima, R. S.; Chiykowski, V. A.; MacLeod, B. P.; Berlinguette, C. P. Complete Electron Economy by Pairing Electrolysis with Hydrogenation. *Nat. Catal.* **2018**, *1*, 501–507. https://doi.org/10.1038/s41929-018-0083-8.

(132) Li, B.; Ge, H. Highly Selective Electrochemical Hydrogenation of Alkynes: Rapid Construction of Mechanochromic Materials. *Sci. Adv.* **2019**, *5*, eaaw2774. https://doi.org/10.1126/sciadv.aaw2774.

(133) Wu, Y.; Liu, C.; Wang, C.; Lu, S.; Zhang, B. Selective Transfer Semihydrogenation of Alkynes with H2O (D2O) as the H (D) Source over a Pd-P Cathode. *Angew. Chem. Int. Ed.* **2020**, *59*, 21170–21175. https://doi.org/10.1002/anie.202009757.

(134) Atzrodt, J.; Derdau, V.; Fey, T.; Zimmermann, J. The Renaissance of H/D Exchange. *Angew. Chem. Int. Ed.* **2007**, *46*, 7744–7765. https://doi.org/10.1002/anie.200700039.

(135) Kurimoto, A.; Sherbo, R. S.; Cao, Y.; Loo, N. W. X.; Berlinguette, C. P. Electrolytic Deuteration of Unsaturated Bonds without Using D2. *Nat. Catal.* **2020**, *3*, 719–726. https://doi.org/10.1038/s41929-020-0488-z.

(136) Ling, Y.; Wu, Y.; Wang, C.; Liu, C.; Lu, S.; Zhang, B. Selenium Vacancy Promotes Transfer Semihydrogenation of Alkynes from Water Electrolysis. *ACS Catal.* **2021**, *11*, 9471–9478. https://doi.org/10.1021/acscatal.1c02316.

(137) Chaudhari, N. K.; Jin, H.; Kim, B.; Lee, K. Nanostructured Materials on 3D Nickel Foam as Electrocatalysts for Water Splitting. *Nanoscale* **2017**, *9*, 12231–12247. https://doi.org/10.1039/c7nr04187j.

(138) Siwek, K. I.; Eugénio, S.; Santos, D. M. F.; Silva, M. T.; Montemor, M. F. 3D Nickel Foams with Controlled Morphologies for Hydrogen Evolution Reaction in Highly Alkaline Media. *Int. J. Hydrogen Energy* **2019**, *44*, 1701–1709. https://doi.org/10.1016/j.ijhydene.2018.11.070.

(139) Lu, J.; Xiong, T.; Zhou, W.; Yang, L.; Tang, Z.; Chen, S. Metal Nickel Foam as an Efficient and Stable Electrode for Hydrogen Evolution Reaction in Acidic Electrolyte under Reasonable Overpotentials. *ACS Appl. Mater. Interfaces* **2016**, *8*, 5065–5069. https://doi.org/10.1021/acsami.6b00233.

(140) Lambers, E. S.; Dykstal, C. N.; Seo, J. M.; Rowe, J. E.; Holloway, P. H. Room-Temperature Oxidation of Ni(110) at Low and Atmospheric Oxygen Pressures. *Oxid. Met.* **1996**, *45*, 301–321. https://doi.org/10.1007/BF01046987.

(141) Visscher, W.; Barendrecht, E. Absorption of Hydrogen in Reduced Nickel Oxide. *J. Appl. Electrochem.* **1980**, *10*, 269–274. https://doi.org/10.1007/BF00726096.

(142) Muralidharan, V.; Veerashanmugamani, M.; Paruthimalkalaignan, G.; Arulraj, I. Mechanism of Corrosion of Pure Nickel in Sulphuric Acid Solutions. *Bull. Electrochem.* **1985**, *1*, 241–244.

(143) Wei, J.; Zhou, M.; Long, A.; Xue, Y.; Liao, H.; Wei, C.; Xu, Z. J. Heterostructured Electrocatalysts for Hydrogen Evolution Reaction Under Alkaline Conditions. *Nano-Micro Lett.* **2018**, *10*, 1–15.

https://doi.org/10.1007/s40820-018-0229-x.

(144) Gonçalves, J. M.; Martins, P. R.; Araki, K.; Angnes, L. Recent Progress in Water Splitting and Hybrid Supercapacitors Based on Nickel-Vanadium Layered Double Hydroxides. *J. Energy Chem.* **2021**, *57*, 496–515. https://doi.org/10.1016/j.jechem.2020.08.047.

(145) Zorainy, M. Y.; Gar Alalm, M.; Kaliaguine, S.; Boffito, D. C. Revisiting the MIL-101 Metal–Organic Framework: Design, Synthesis, Modifications, Advances, and Recent Applications. *J. Mater. Chem. A* **2021**, *9*, 22159–22217. https://doi.org/10.1039/d1ta06238g.

(146) Bernt, S.; Guillerm, V.; Serre, C.; Stock, N. Direct Covalent Post-Synthetic Chemical Modification of Cr-MIL-101 Using Nitrating Acid. *Chem. Commun.* **2011**, *47*, 2838–2840. https://doi.org/10.1039/c0cc04526h.

(147) Liu, C.; Zhang, Y.; Liu, N.; Qiu, J. A Simple and Efficient Approach for the Palladium-Catalyzed Ligand-Free Suzuki Reaction in Water. *Green Chem.* **2012**, *14*, 2999–3003. https://doi.org/10.1039/c2gc36098e.

(148) Alimardanov, A.; Schmieder-Van De Vondervoort, L.; De Vries, A. H. M.; De Vries, J. G. Use of "Homeopathic" Ligand-Free Palladium as Catalyst for Aryl-Aryl Coupling Reactions. *Adv. Synth. Catal.* **2004**, *346*, 1812–1817. https://doi.org/10.1002/adsc.200404210.

(149) Xu, L.; Liu, F. Y.; Zhang, Q.; Chang, W. J.; Liu, Z. L.; Lv, Y.; Yu, H. Z.; Xu, J.; Dai, J. J.; Xu, H. J. The Amine-Catalysed Suzuki–Miyaura-Type Coupling of Aryl Halides and Arylboronic Acids. *Nat. Catal.* **2021**, *4*, 71–78. https://doi.org/10.1038/s41929-020-00564-z.

(150) Avanthay, M.; Bedford, R.; Begg, C.; Böse, D.; Clayden, J.; Davis, S.; Eloi, J.C.; Goryunov, G.P.; Hartung, I.V.; Heeley, J.; Khaikin, K.A.; Kitching, M.; Krieger, J.; Kulyabin, P.S.; Lennox, A.; Nolla-Saltiel, R.; Pridmore, N.E.; Rowsell, B.J.S.; Sparkes, H. J. Amine-Catalysed Suzuki–Miyaura-Type Coupling? The Identification and Isolation of the Palladium Culprits. *ChemRxiv* **2021**. https://doi.org/10.26434/chemrxiv.14237288.v1.

(151) Novák, Z.; Adamik, R.; Csenki, J. T.; Béke, F.; Gavaldik, R. Curse or Blessing ? Influence of Impurities on Cross-Coupling — Guideline for Elucidating Catalysts. *ChemRxiv* **2021**, 1–17.

(152) Diallo, A. K.; Ornelas, C.; Salmon, L.; Aranzaes, J. R.; Astruc, D. "Homeopathic" Catalytic Activity and Atom-Leaching Mechanism in Miyaura-Suzuki Reactions under Ambient Conditions with Precise Dendrimer-Stabilized Pd Nanoparticles. *Angew. Chem. Int. Ed.* **2007**, *46*, 8644–8648. https://doi.org/10.1002/anie.200703067.

(153) Deraedt, C.; Astruc, D. "homeopathic" Palladium Nanoparticle Catalysis of Cross Carbon-Carbon Coupling Reactions. *Acc. Chem. Res.* **2014**, *47*, 494–503. https://doi.org/10.1021/ar400168s.

(154) Kashin, A. S.; Ananikov, V. P. Catalytic C-C and C-Heteroatom Bond Formation Reactions: In Situ Generated or Preformed Catalysts? Complicated Mechanistic Picture behind Well-Known Experimental Procedures. *J. Org. Chem.* **2013**, *78*, 11117–11125. https://doi.org/10.1021/jo402038p.

(155) Polynski, M. V.; Ananikov, V. P. Modeling Key Pathways Proposed for the Formation and Evolution of "Cocktail"-Type Systems in Pd-Catalyzed Reactions Involving ArX Reagents. *ACS Catal.* **2019**, *9*, 3991–4005. https://doi.org/10.1021/acscatal.9b00207.

(156) Verho, O.; Nagendiran, A.; Johnston, E. V.; Tai, C. W.; Bäckvall, J. E. Nanopalladium on Amino-Functionalized Mesocellular Foam: An Efficient Catalyst for Suzuki Reactions and Transfer Hydrogenations. *ChemCatChem* **2013**, *5*, 612–618. https://doi.org/10.1002/cctc.201200247.

(157) Tao, X.; Long, R.; Wu, D.; Hu, Y.; Qiu, G.; Qi, Z.; Li, B.; Jiang, R.; Xiong, Y. Anchoring Positively Charged Pd Single Atoms in Ordered Porous Ceria to Boost Catalytic Activity and Stability in Suzuki Coupling Reactions. *Small* **2020**, *16*, 1–11. https://doi.org/10.1002/smll.202001782.

(158) Li, Y.; Xu, L.; Xu, B.; Mao, Z.; Xu, H.; Zhong, Y.; Zhang, L.; Wang, B.; Sui, X. Cellulose Sponge

Supported Palladium Nanoparticles as Recyclable Cross-Coupling Catalysts. *ACS Appl. Mater. Interfaces* **2017**, *9*, 17155–17162. https://doi.org/10.1021/acsami.7b03600.

(159) Wang, Y.; Liao, J.; Xie, Z.; Zhang, K.; Wu, Y.; Zuo, P.; Zhang, W.; Li, J.; Gao, Z. Zeolite-Enhanced Sustainable Pd-Catalyzed C-C Cross-Coupling Reaction: Controlled Release and Capture of Palladium. *ACS Appl. Mater. Interfaces* **2020**, *12*, 11419–11427. https://doi.org/10.1021/acsami.9b18110.

(160) Song, K.; Liu, P.; Wang, J.; Tan, B.; Li, T. Highly Active Palladium Nanoparticles Immobilized on Knitting Microporous Organic Polymers as Efficient Catalysts for Suzuki–Miyaura Cross-Coupling Reaction. *J. Porous Mater.* **2016**, *23*, 725–731. https://doi.org/10.1007/s10934-016-0127-x.

(161) Anjali, B. A.; Suresh, C. H. Interpreting Oxidative Addition of Ph-X (X = CH3, F, Cl, and Br) to Monoligated Pd(0) Catalysts Using Molecular Electrostatic Potential. *ACS Omega* **2017**, *2*, 4196–4206. https://doi.org/10.1021/acsomega.7b00745.

(162) McMullin, C. L.; Jover, J.; Harvey, J. N.; Fey, N. Accurate Modelling of Pd(0) + PhX Oxidative Addition Kinetics. *Dalt. Trans.* **2010**, *39*, 10833–10836. https://doi.org/10.1039/c0dt00778a.

(163) Galushko, A. S.; Prima, D. O.; Burykina, J. V.; Ananikov, V. P. Comparative Study of Aryl Halides in Pd-Mediated Reactions: Key Factors beyond the Oxidative Addition Step. *Inorg. Chem. Front.* **2021**, *8*, 620–635. https://doi.org/10.1039/d0qi01133a.

(164) Carrow, B. P.; Hartwig, J. F. Ligandless, Anionic, Arylpalladium Halide Intermediates in the Heck Reaction. *J. Am. Chem. Soc.* **2010**, *132*, 79–81. https://doi.org/10.1021/ja909306f.

(165) Lennox, A. J. J.; Lloyd-Jones, G. C. Selection of Boron Reagents for Suzuki-Miyaura Coupling. *Chem. Soc. Rev.* **2014**, *43*, 412–443. https://doi.org/10.1039/c3cs60197h.

(166) McMullin, C. L.; Fey, N.; Harvey, J. N. Computed Ligand Effects on the Oxidative Addition of Phenyl Halides to Phosphine Supported Palladium(0) Catalysts. *Dalt. Trans.* **2014**, *43*, 13545–13556. https://doi.org/10.1039/c4dt01758g.

(167) Barrios-landeros, F.; Hartwig, J. F. Distinct Mechanisms for the Oxidative Addition of Chloro- , Bromo- , and Iodoarenes to a Bisphosphine Palladium (0) Complex with Hindered Ligands. **2005**, *3*, 6944–6945.

(168) Yuan, N.; Pascanu, V.; Huang, Z.; Valiente, A.; Heidenreich, N.; Leubner, S.; Inge, A. K.; Gaar, J.; Stock, N.; Persson, I.; Martín-Matute, B.; Zou, X. Probing the Evolution of Palladium Species in Pd@MOF Catalysts during the Heck Coupling Reaction: An Operando X-Ray Absorption Spectroscopy Study. *J. Am. Chem. Soc.* **2018**, *140*, 8206–8217. https://doi.org/10.1021/jacs.8b03505.

(169) Hansen, T. W.; Delariva, A. T.; Challa, S. R.; Datye, A. K. Sintering of Catalytic Nanoparticles: Particle Migration or Ostwald Ripening? *Acc. Chem. Res.* **2013**, *46*, 1720–1730. https://doi.org/10.1021/ar3002427.

(170) Valiente, A.; Carrasco, S.; Sanz-Marco, A.; Tai, C. W.; Bermejo Gómez, A.; Martín-Matute, B. Aerobic Homocoupling of Arylboronic Acids Catalyzed by Regenerable Pd(II)@MIL-88B-NH2(Cr). *ChemCatChem* **2019**, *11*, 3933–3940. https://doi.org/10.1002/cctc.201900556.

(171) Heinrichs, B.; Noville, F.; Schoebrechts, J. P.; Pirard, J. P. Palladium-Silver Sol-Gel Catalysts for Selective Hydrodechlorination of 1,2-Dichloroethane into Ethylene: IV. Deactivation Mechanism and Regeneration. *J. Catal.* **2003**, *220*, 215–225. https://doi.org/10.1016/j.jcat.2003.07.006.

(172) Homeyer, S. T.; Sachtler, W. M. H. Oxidative Redispersion of Palladium and Formation of PdO Particles in NaY. *Appl. Catal.* **1989**, *54*, 189–202. https://doi.org/10.1016/S0166-9834(00)82364-7.

(173) C. Feeley, O.; Sachtler, W. M. H. Redispersion of Palladium in Y-Zeolites by Chlorine. *Appl. Catal.* **1991**, *75*, 93–103. https://doi.org/10.1016/S0166-9834(00)83126-7.

(174) Peterson, E. J.; DeLaRiva, A. T.; Lin, S.; Johnson, R. S.; Guo, H.; Miller, J. T.; Kwak, J. H.; Peden, C. H. F.; Kiefer, B.; Allard, L. F.; Ribeiro, F. H.; Datye, A. K. Low-Temperature Carbon Monoxide Oxidation Catalysed by Regenerable Atomically Dispersed Palladium on Alumina. *Nat. Commun.* **2014**, *5*. https://doi.org/10.1038/ncomms5885.

(175) Zhang, L.; Wang, B.; Ding, Y.; Wen, G.; Hamid, S. B. A.; Su, D. Disintegrative Activation of Pd Nanoparticles on Carbon Nanotubes for Catalytic Phenol Hydrogenation. *Catal. Sci. Technol.* **2016**, *6*, 1003–1006. https://doi.org/10.1039/c5cy02165k.

(176) Yamamoto, Y.; Suzuki, R.; Hattori, K.; Nishiyama, H. Base- and Phosphine-Free Palladium-Catalyzed Homocoupling of -Arylboronic Acid Derivatives under Air. *Synlett* **2006**, *2006*, 1027–1030. https://doi.org/10.1055/s-2006-939071.

(177) Li, X.; Li, D.; Bai, Y.; Zhang, C.; Chang, H.; Gao, W.; Wei, W. Homocoupling Reactions of Terminal Alkynes and Arylboronic Compounds Catalyzed by in Situ Formed Al(OH)3-Supported Palladium Nanoparticles. *Tetrahedron* **2016**, *72*, 6996–7002. https://doi.org/10.1016/j.tet.2016.09.035.

(178) Sable, V.; Maindan, K.; Kapdi, A. R.; Shejwalkar, P. S.; Hara, K. Active Palladium Colloids via Palladacycle Degradation as Efficient Catalysts for Oxidative Homocoupling and Cross-Coupling of Aryl Boronic Acids. *ACS Omega* **2017**, *2*, 204–217. https://doi.org/10.1021/acsomega.6b00326.

(179) Adamo, C.; Amatore, C.; Ciofini, I.; Jutand, A.; Lakmini, H. Mechanism of the Palladium-Catalyzed Homocoupling of Arylboronic Acids: Key Involvement of a Palladium Peroxo Complex. *J. Am. Chem. Soc.* **2006**, *128*, 6829–6836. https://doi.org/10.1021/ja0569959.

(180) Shibata, M.; Ito, H.; Itami, K. Oxidative Homocoupling Reaction of Aryltrimethylsilanes by Pd/ o -Chloranil Catalysis. *Chem. Lett.* **2017**, *46*, 1701–1704. https://doi.org/10.1246/cl.170723.

(181) Molnár, Á. Efficient, Selective, and Recyclable Palladium Catalysts in Carbon-Carbon Coupling Reactions. *Chem. Rev.* **2011**, *111*, 2251–2320. https://doi.org/10.1021/cr100355b.

(182) Chen, J.; Zhang, Q.; Wang, Y.; Wan, H. Size-Dependent Catalytic Activity of Supported Palladium Nanoparticles for Aerobic Oxidation of Alcohols. *Adv. Synth. Catal.* **2008**, *350*, 453–464. https://doi.org/10.1002/adsc.200700350.

(183) Oshchepkov, A. G.; Braesch, G.; Bonnefont, A.; Savinova, E. R.; Chatenet, M. Recent Advances in the Understanding of Nickel-Based Catalysts for the Oxidation of Hydrogen-Containing Fuels in Alkaline Media. *ACS Catal.* **2020**, *10*, 7043–7068. https://doi.org/10.1021/acscatal.0c00101.

(184) Zhang, C.; Huang, Y.; Yu, Y.; Zhang, J.; Zhuo, S.; Zhang, B. Sub-1.1 Nm Ultrathin Porous CoP Nanosheets with Dominant Reactive {200} Facets: A High Mass Activity and Efficient Electrocatalyst for the Hydrogen Evolution Reaction. *Chem. Sci.* **2017**, *8*, 2769–2775. https://doi.org/10.1039/C6SC05687C.

(185) Chang, J.; Ouyang, Y.; Ge, J.; Wang, J.; Liu, C.; Xing, W. Cobalt Phosphosulfide in the Tetragonal Phase: A Highly Active and Durable Catalyst for the Hydrogen Evolution Reaction. *J. Mater. Chem. A* **2018**, *6*, 12353–12360. https://doi.org/10.1039/c8ta03951h.

(186) McKone, J. R.; Sadtler, B. F.; Werlang, C. A.; Lewis, N. S.; Gray, H. B. Ni-Mo Nanopowders for Efficient Electrochemical Hydrogen Evolution. *ACS Catal.* **2013**, *3*, 166–169. https://doi.org/10.1021/cs300691m.

(187) Nakao, R.; Rhee, H.; Uozumi, Y. Hydrogenation and Dehalogenation under Aqueous Conditions with an Amphiphilic-Polymer-Supported Nanopalladium Catalyst. *Org. Lett.* **2005**, *7*, 163–165. https://doi.org/10.1021/ol047670k.

(188) Semba, K.; Fujihara, T.; Xu, T.; Terao, J.; Tsuji, Y. Copper-Catalyzed Highly Selective Semihydrogenation of Non-Polar Carbon-Carbon Multiple Bonds Using a Silane and an Alcohol. *Adv. Synth. Catal.* **2012**, *354*, 1542–1550. https://doi.org/10.1002/adsc.201200200.

(189) Ilies, L.; Yoshida, T.; Nakamura, E. Iron-Catalyzed Chemo- and Stereoselective

Hydromagnesiation of Diarylalkynes and Diynes. *J. Am. Chem. Soc.* **2012**, *134*, 16951–16954. https://doi.org/10.1021/ja307631v.

(190) Han, M.; Ding, Y.; Yan, Y.; Li, H.; Luo, S.; Adijiang, A.; Ling, Y.; An, J. Transition-Metal-Free, Selective Reductive Deuteration of Terminal Alkynes with Sodium Dispersions and EtOD- D1. *Org. Lett.* **2018**, *20*, 3010–3013. https://doi.org/10.1021/acs.orglett.8b01036.

(191) Alonso, F.; Yus, M. Hydrogenation of Alkynes with Hydrated Nickel Chloride, Lithium and a Catalytic Amount of Naphthalene. *Tetrahedron Lett.* **1997**, *38*, 149–152. https://doi.org/10.1016/S0040-4039(96)02239-3.

(192) Rowbotham, J. S.; Ramirez, M. A.; Lenz, O.; Reeve, H. A.; Vincent, K. A. Bringing Biocatalytic Deuteration into the Toolbox of Asymmetric Isotopic Labelling Techniques. *Nat. Commun.* **2020**, *11*, 1–7. https://doi.org/10.1038/s41467-020-15310-z.

(193) Atzrodt, J.; Derdau, V.; Kerr, W. J.; Reid, M. Deuterium- and Tritium-Labelled Compounds: Applications in the Life Sciences. *Angew. Chem. Int. Ed.* **2018**, *57*, 1758–1784. https://doi.org/10.1002/anie.201704146.

(194) Krishtalik, L. I. Kinetic Isotope Effect in the Hydrogen Evolution Reaction. *Electrochim. Acta* **2001**, *46*, 2949–2960. https://doi.org/10.1016/S0013-4686(01)00526-6.

(195) Jaksic, M. M.; Johansen, B.; Tunold, R. Electrochemical Behaviour of Iridium in Alkaline and Acidic Solutions of Heavy and Regular Water. *Int. J. Hydrogen Energy* **1994**, *19*, 321–335. https://doi.org/10.1016/0360-3199(94)90064-7.

(196) Salomon, M.; Conway, B. E. Reaction Rate and Separation Factor Isotope Effects in the Hydrogen Evolution Reaction. *Ber. Bunsenges. Phys. Chem.* **1965**, *69*, 669–674. https://doi.org/10.1002/bbpc.19650690804.

(197) Liu, H.; Han, J.; Yuan, J.; Liu, C.; Wang, D.; Liu, T.; Liu, M.; Luo, J.; Wang, A.; Crittenden, J. C. Deep Dehalogenation of Florfenicol Using Crystalline CoP Nanosheet Arrays on a Ti Plate via Direct Cathodic Reduction and Atomic H. *Environ. Sci. Technol.* **2019**, *53*, 11932–11940. https://doi.org/10.1021/acs.est.9b04352.

(198) Liu, C.; Zhang, A. Y.; Pei, D. N.; Yu, H. Q. Efficient Electrochemical Reduction of Nitrobenzene by Defect-Engineered TiO2-x Single Crystals. *Environ. Sci. Technol.* **2016**, *50*, 5234–5242. https://doi.org/10.1021/acs.est.6b00730.

(199) Yang, L.; Chen, Z.; Cui, D.; Luo, X.; Liang, B.; Yang, L.; Liu, T.; Wang, A.; Luo, S. Ultrafine Palladium Nanoparticles Supported on 3D Self-Supported Ni Foam for Cathodic Dechlorination of Florfenicol. *Chem. Eng. J.* **2019**, *359*, 894–901. https://doi.org/10.1016/j.cej.2018.11.099.

(200) Abdullah, M. I.; Hameed, A.; Zhang, N.; Islam, M. H.; Ma, M.; Pollet, B. G. Ultrasonically Surface-Activated Nickel Foam as a Highly Efficient Monolith Electrode for the Catalytic Oxidation of Methanol to Formate. *ACS Appl. Mater. Interfaces* **2021**, *13*, 30603–30613. https://doi.org/10.1021/acsami.1c06258.